Administrative unit: **University of Padova**

Department: **Land, Environment, Agriculture and Forestry (LEAF)**

PhD Program: **Land, Environment, Resources and Health (LERH)**

Batch: XXX

RUNOFF GENERATION IN A FORESTED PRE-ALPINE CATCHMENT: HYPOTHESIS TESTING BY MEANS OF ISOTOPIC AND GEOCHEMICAL TRACERS

Thesis financially supported by CARIPARO Foundation

PhD Program Coordinator: Prof. Davide Matteo Pettenella

Supervisor: Prof. Marco Borga

Co-supervisor: Dr. Ilja van Meerveld

PhD candidate: Dr. Luisa Pianezzola

UNIVERSITÀ
DEGLI STUDI
DI PADOVA

Sede Amministrativa: **Università degli Studi di Padova**

Dipartimento: **Territorio e Sistemi Agro-Forestali (TESAF)**

CORSO DI DOTTORATO DI RICERCA: **Land, Environment, Resources, Health (LERH)**

Ciclo: XXX

GENERAZIONE DI DEFLUSSO IN UN BACINO PREALPINO FORESTATO: IPOTESI TESTATE PER MEZZO DI TRACCIANTI ISOTOPICI E GEOCHIMICI

Tesi redatta con il contributo finanziario della Fondazione CARIPARO

Coordinatore: Prof. Davide Matteo Pettenella

Supervisore: Prof. Marco Borga

Co-supervisore: Dr. Ilja van Meerveld

Dottorando: Dr. Luisa Pianezzola

ABSTRACT

Understanding of the complex runoff generation mechanisms is important for water management and to predict the effects of land use and climate change on streamflow. In particular, the mechanisms through which precipitation becomes streamflow and the spatio-temporal variability of the runoff components is still unclear. The integrated use of isotopic and geochemical tracers, combined with hydrometric data, has proven to be a useful method to investigate hydrological processes in small catchments. In this study, we used stable isotopes of water, major ions and electrical conductivity as tracers together with hydrometric data to i) compare the response of the water table and soil moisture to the streamflow response during rainfall-runoff events, ii) analyze the spatial and temporal variability in tracer signature (stable isotopes of water, EC and major ions) of different end members contributing to stream runoff, iii) assess how the main event characteristics (total rainfall amount, intensity and antecedent wetness conditions) affect the event water contribution to stream runoff, and iv) investigate how the use of different tracers affects the results of the two-component hydrograph separation.

The hydrometric and tracer data was analyzed for 15 rainfall-runoff events between September 2015 and October 2016 during different wetness conditions in a small catchment in the Italian pre-Alps. Continuous measurements for streamflow, precipitation, air temperature, shallow groundwater levels at six locations in different parts of the catchment (riparian, bottom of the hillslope, mid hillslope and upper hillslope), soil moisture at four locations along a riparian-hillslope transect were available for the study period. Samples for isotopic and geochemical analysis were taken from precipitation, stream, shallow groundwater, soil water at 5 locations (riparian at 10 cm and 20 cm depth; mid hillslope at 10 cm and 30 cm depth; upper hillslope at 30 cm depth). Electrical conductivity was measured directly in the field using a portable meter. Isotopic composition and ion concentrations were determined in the laboratory of Legnaro (Dip. TESAF, University of Padova) by laser absorption spectroscopy and ion-chromatography, respectively.

Mixing plot analysis shows that precipitation, near-surface riparian soil water and shallow groundwater are the main contributors to runoff. Two-component hydrograph separation showed that new water contributions increase with increasing rainfall amount and intensity and decrease with increasing antecedent wetness conditions. During events with high rainfall intensity with dry antecedent conditions, the new water fraction was high, especially in the initial phase of the event and near the streamflow peak, suggesting that streamflow is

mainly generated by direct channel precipitation and saturated overland flow in the riparian zone. With increasing wetness conditions, pre-event water dominated runoff, suggesting the development of subsurface stormflow and an increasing contribution from groundwater pools located in different parts of the catchment. In the middle and at the end of large events in wet periods, the new water fraction in streamflow increased due to the expansion of the saturated area near the stream and flow through shallow soil layers. Differences in the event water fractions computed using isotopes, EC or major ions, suggest an ionic enrichment of rainfall due to the accumulation of ions in the ephemeral portion of the stream and the soil surface.

RIASSUNTO

Negli ultimi decenni e' aumentato sempre di piu' l'interesse nel meglio comprendere i complessi processi idrologici. In particolare, i meccanismi attraverso cui la precipitazione controlla i processi di generazione di deflusso superficiale e la variabilita' spaziale e temporale delle componenti di deflusso sono attualmente ancora poco chiari. L'uso integrato dei traccianti isotopici e geochimici, abbinato ai dati idrometrici, si sta dimostrando uno strumento efficace e sempre piu' utilizzato per studiare i sistemi idrologici e i meccanismi di generazione di deflusso superficiale e sottosuperficiale. In questo studio, gli isotopi stabili dell'acqua, la conducibilita' elettrica e gli ioni sono stati utilizzati come traccianti insieme ai dati idrometrici al fine di i) analizzare la risposta della falda e dell'umidita' del suolo rispetto alla risposta del torrente durante gli eventi di afflusso-deflusso ii) analizzare la variabilita' spaziale e temporale dei traccianti (isotopi stabili dell'acqua, EC e ioni) nelle diverse componenti di deflusso superficiale iii) valutare il controllo esercitato dalle principali caratteristiche dell'evento sui processi di generazione di deflusso superficiale e ii) verificare come l'uso di diversi traccianti influenza i risultati ottenuti dalla separazione dell'idrogramma a due componenti.

Per questo studio, sono stati analizzati i dati idrometrici e dei traccianti ricavati da 15 eventi di pioggia campionati durante diverse condizioni di umidita' del suolo nel periodo che va da settembre 2015 ad ottobre 2016 in un piccolo bacino nelle prealpi italiane. Durante questo periodo sono stati misurati in continuo il livello del torrente, la precipitazione, la temperatura dell'aria, il livello della falda in 6 punti posti in diverse parti del bacino (zona riparia, zona di basso versante, versante) e l'umidita' del suolo in 4 punti disposti lungo un transetto dal torrente al versante. Inoltre sono stati raccolti a scala di evento campioni di acqua per l'analisi isotopica e geochimica dalla pioggia, dal torrente, dalla falda e dal suolo in 5 punti a diverse profondita' (nella zona riparia a 10 cm e 20 cm di profondita'; nella zona a meta' versante a 10 cm e 30 cm di profondita'; nella parte alta del versante a 30 cm di profondita'). La conducibilita' elettrica e' stata misurata direttamente in campo utilizzando un conduttimetro. Le concentrazioni isotopiche e ioniche sono state misurate nel laboratorio di Legnaro (Dip. TESAF, Universita' degli Studi di Padova) rispettivamente tramite spettroscopia laser e cromatografia ionica.

L'analisi EMMA rivela che la precipitazione, l'acqua di suolo nella zona riparia e la falda superficiale sono le principali componenti che contribuiscono all'evento di piena. La tecnica di separazione dell'idrogramma a due componenti rivela che il contributo di acqua nuova al

torrente aumenta con l'aumentare della pioggia totale e dell'intensita' di pioggia mentre diminuisce durante condizioni di umidita' antecedente l'evento umide. Durante gli eventi che avvengono in condizioni di umidita' secche e che sono caratterizzati da elevate intensita' di pioggia, l'acqua nuova contribuisce al torrente in maggior misura, soprattutto nelle fasi iniziali dell'evento e in prossimita' del picco di portata, indicando che l'acqua nuova proviene principalmente dalla pioggia incanalata direttamente nel torrente e dal deflusso superficiale che si forma nella zona riparia. Con l'aumento delle condizioni di umidita', l'acqua vecchia (di pre-evento) inizia a contribuire maggiormente al torrente, indicando uno sviluppo della connessione sottosuperficiale durante l'evento ed un maggior contributo di acqua di falda proveniente da diverse parti nel bacino. Nella fase intermedia e finale di eventi avvenuti durante periodi umidi e caratterizzati da elevate quantita' di pioggia, aumenta la componente di acqua nuova nel torrente, aumento dovuto all'espansione della zona satura vicino al torrente. Le differenze riscontrate nel calcolo della componente di acqua nuova usando i traccianti isotopici e geochimici suggeriscono che la pioggia viene arricchita in ioni prima di essere incanalata nel torrente a causa dell'accumulo di ioni nella zona effimera del torrente e negli strati superficiali del suolo.

SUMMARY

FIGURE INDEX

TABLE INDEX

1 INTRODUCTION

1.1 Water cycle and runoff generation processes

The hydrological cycle, or water cycle, indicates all phenomena related to water and its natural movement between atmosphere, land and oceans. During this movement the water passes from gaseous state, to liquid state or solid states thanks to the solar energy and gravitational forces.

Figure 1 represents water fluxes in hydrological cycle. The hydrologic cycle starts from the evaporation of water from the surface water bodies (oceans, lakes, rivers). Once evaporated, water rise upwards in the atmosphere, it cools and it condenses to form clouds. Thanks to the movements of air masses around the globe, the clouds move for long distances until they return to the surface as precipitation. A part of precipitation is immediately intercepted by the canopy of trees and returns to the atmosphere by evaporation. The precipitation that passes over the canopy is called "throughfall", and it is the water that takes place physically inside the soil profile (Kirkby and Chorley, 1967). Throughfall falls on the soil surface directly or indirectly flowing along the branches and trunk of the trees (stremflow). The part of throughfall depends both on the structural characteristics of tree populations (species composition, age, density, vertical profile, coverage) and on the intensity and duration of the event (Iovino, 2009). Higher intensity and duration of rainfall event, greater throughfall. Once precipitation reaches the ground, a portion of the water evaporates back into the atmosphere, some water remains in surface and flow as surface runoff conforming to gradient lines, some water infiltrates into the ground in depth and it becomes groundwater. Groundwater can be stored in depth for long period of time. Some groundwater is absorbed by the roots of the plants and it is released back into the atmosphere through plant transpiration. Some groundwater seeps back into the lakes, rivers, and streams. Finally, surface runoff reaches the oceans, where the cycle begins again.

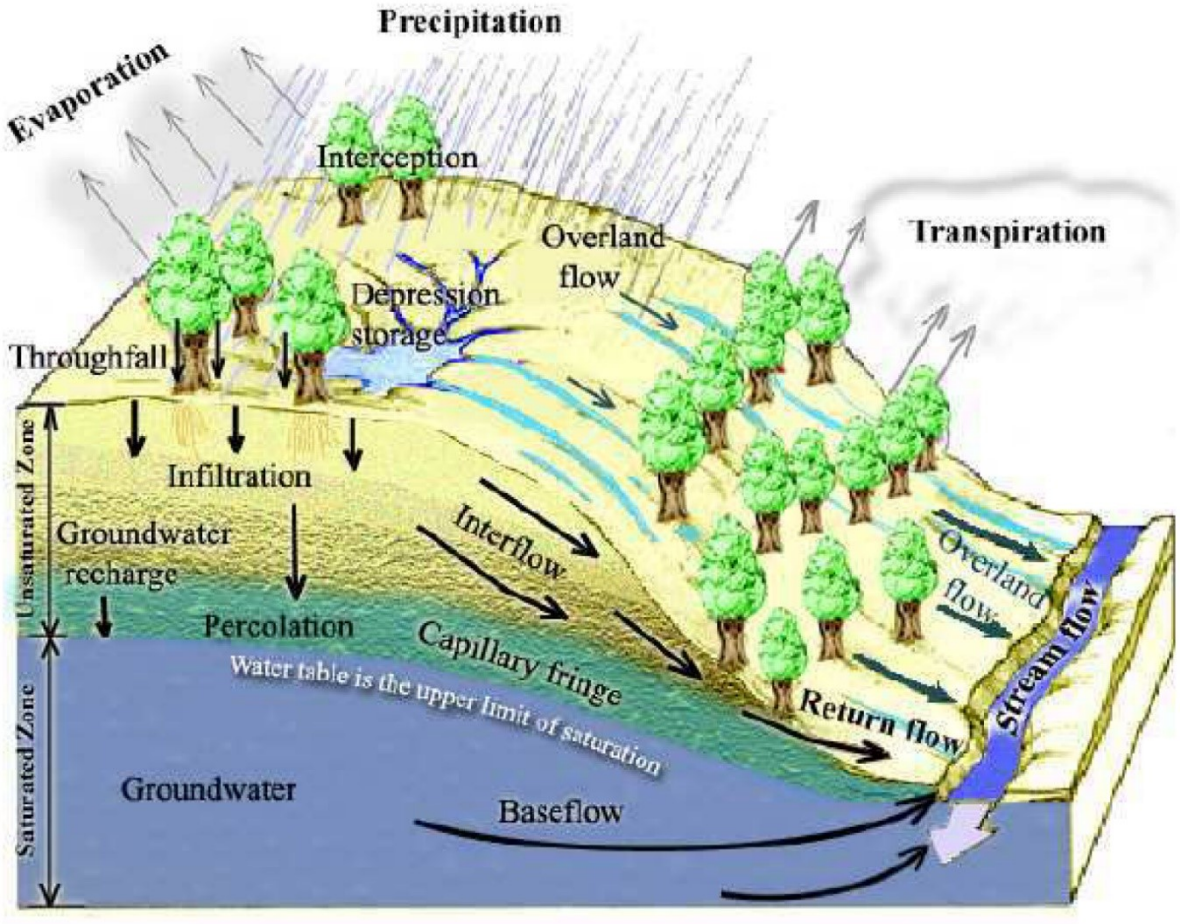

Figure 1: Physical processes involved in runoff generation (Tarboton, 2003).

In this framework, water moves through transpiration, evaporation, precipitation and becomes the main channel to transfer solar energy between ecosystems. The movement of water in the atmosphere affects the distribution of rainfall. The distribution of water resources affects life and survival of all living beings. Water is the primary resource that enables life on our planet. Oceans are the most important reservoir of water, representing 97% of water available on Earth surface. Also important are polar icecaps and continental glaciers that contain 2% of water available on Earth surface. Other reserves of water are in the soil, lakes and rivers, in the atmosphere and into the groundwater (difficult to estimate).

The residence time of water, that is the time during which water lies within a water body (aquifer, lake, river, etc.) before continuing around the hydrological cycle, may vary from days for shallow gravel aquifers to millions of years for deep aquifers with very low values for hydraulic conductivity. The residence time of water in rivers is a few days, while in large lakes the residence time of water ranges up to several decades.

Mountainous catchments are characterized by high spatial and temporal variability of hydrologic responses due to be highly heterogeneous. Here, different landscape units including forest, meadows and wetlands are often part of the same basin and the role of topography, soil depth, geology and land use has a significant impact on runoff generation processes.

Despite decades of increasingly more intensive study, storm runoff generation remains a controversial topic, and specifically where the complexity of the landscape is high, such as in mountainous basins. Streamflow is generated mainly by processes operating beyond the permanent stream channel, but the relative importance of surface versus subsurface flow and of rapid throughflow (via soil macropores) versus translatory flow mechanisms is still not clear.

Since Hewlett (U.S. Forest Service, 1961) developed his theory on the variable source area, different assumptions have been made on runoff generation in humid vegetated zones (Figure 2). All these assumptions presuppose that quasi-uniform runoff generation occurred at large scale during rainfall-runoff events in humid vegetated catchment can not only originate via hortonian overland flow (Horton, 1933; Freeze, 1974). Figure 2 summarizes the most important studies that investigated the variable source area hypothesis and showed field evidence for each mechanism involved in runoff generation. All these mechanisms are characterized by a specific variable source area of runoff generation that it is not constant in time but it expands and contracts at event and seasonal scale. The main factors that control spatial and temporal variability of each variable source area are the nature of storm event, antecedent wetness conditions of the catchment, soil physical properties, watershed topography and hydrology (Kennedy et al., 1986), groundwater level, environmental conditions, vegetation cover, land uses such as agriculture, urbanization, reforestation. In particular, the impact of land uses and climate changes on water balance and on availability of water resources is a widely debated topic in the field of environmental and hydrological sciences. Consequently, the response of the catchment during the events is strictly correlated with the conformation of each variable source (Pearce et al., 1986).

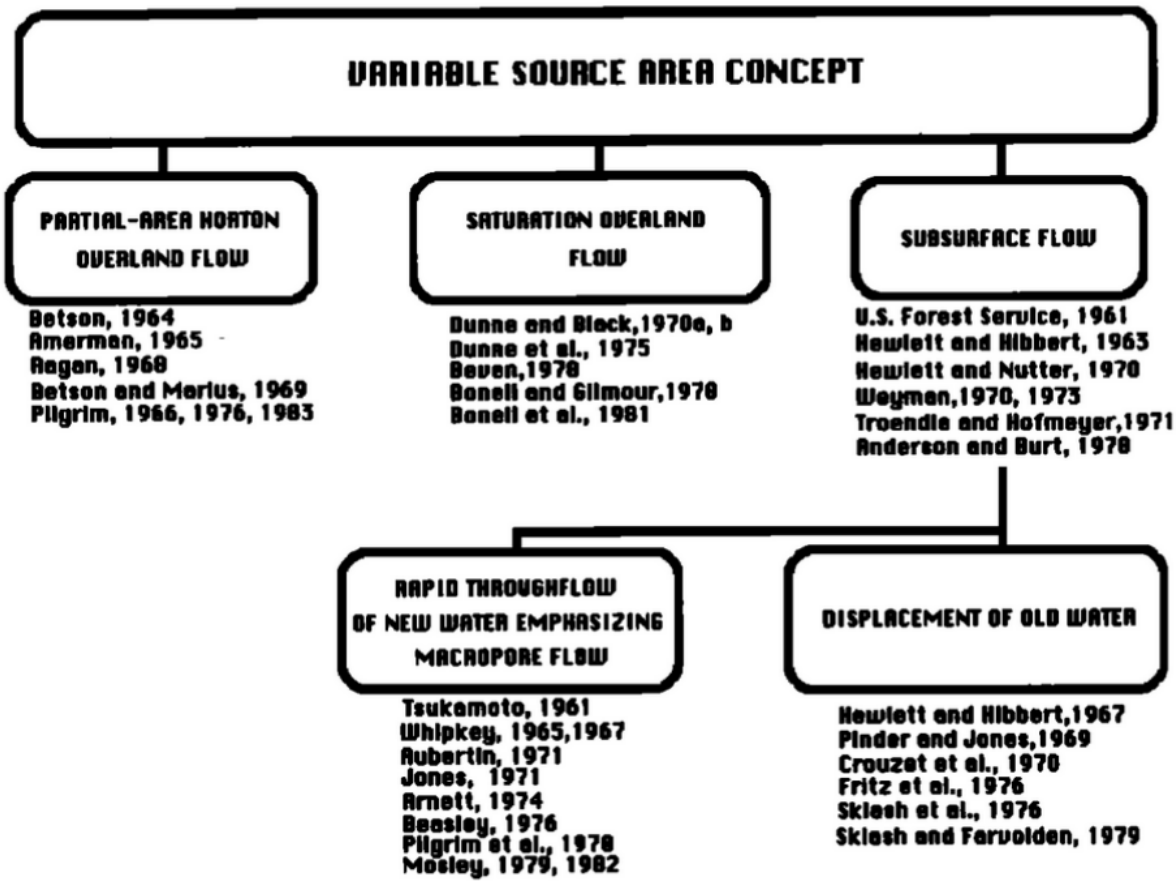

Figure 2 Summary of storm runoff mechanisms applicable to the variable source area concept and studies providing field evidence for mechanisms (Pearce et al., 1986).

Stormflow is mainly generated by combined input of channel precipitation, overland flow, displaced soil water, shallow subsurface flow and groundwater flow (Ladouche et al., 2001). Overland flow may be of two types (Pearce et al., 1986): it may be saturation overland flow (Dunne and Black, 1970) or infiltration excess overland flow (Horton, 1933). Saturation overland flow is generally generated in riparian areas and near-channel zones. These areas become quickly saturated during the events from the bottom upward because the rise of shallow riparian groundwater and the fast infiltration of the rain into the soil (Sklash and Farvolden, 1979). Once the soil is saturated, rainfall stops infiltrating into the soil and flows over the surface generating overland flow. Infiltration excess overland flow is generated when the soil becomes saturated from the top downward. This mechanism occurs when rainfall intensity exceed infiltration capacity during the event, favoring overland flow and the quickly transport of event water to the stream (Pearce et al., 1986). The implications of overland flow generation to runoff response were largely investigated by a considerable amount of researches (Muñoz-Villers and McDonnell, 2012; Penna et al., 2015; Blume et at., 2007; Elsenbeer and Vertessy, 1995; Bonell and Gilmour 1978; Schellekens et al.,

2004). Saturation overland flow and infiltration excess overland flow are responsible of the fast response of streamflow to precipitation input and are generally associated to high event water contributions in runoff response during the events (Pearce et al., 1986). Another pathway that provide a fast flow of event water to the stream during the events is represented by macropores. This type of flow, called subsurface flow or interflow, moves laterally in the soil through macropores without inflowing the groundwater zone (Weiler et al., 2005). Macropores consist in void of the porosity of the soil generated by soil fauna, root decomposition of dead plants, cracks and fissures or natural soil pipes (Beven and Germann, 1982). The size and geometry of macropores regulates the flow rate of water; thus, big macropores, such as the natural soil pipes, are responsible of a faster flow of water to the stream than fine macropores (Beven and Germann, 1982). The importance of macropores in subsurface flow generation was reported in many studies (Sidle et al., 1995; Mosley, 1982; McDonnell, 1990; Mohanty et al., 1998; Buttle and McDonald, 2002; Schellekens et al., 2004; Jones, 2010; van der Velde et al., 2010). Mosley (1982) investigated subsurface flow velocity through the soil in Tawhai, Big Bush and Craigieburn State Forests, and he demonstrated that subsurface flow rate is strictly correlated with antecedent soil moisture conditions as well as soil characteristics and macropore network. Jones (2010) demonstrated that subsurface flow generated from soil pipes can significantly contribute to stormflow and it can represent more than 50% of the total runoff in some areas. Groundwater flow is characterized by longer residence time than overland flow and subsurface flow. Together with vadose water, groundwater is composed by water stored in the catchment prior to a specific event and it is classified as pre-event water or old water (Buttle, 1994). The process behind groundwater generation is the ‘piston-flow’ mechanism by which all precipitation infiltrated into the soil pushing down event water of previously events stored in the soil layers until the deeper saturated layers (Sukhija et al., 2003). Groundwater is subject to fluctuations and the runoff is generated when the water table rises until the ground surface. During periods without precipitation (rainfall or snowmelt), streamflow is generally sustained by riparian groundwater that acts as a reservoir. During the events, groundwater can contribute in high percentage to storm runoff due to the rise in water table (Burns et al. 2003).

1.2 State of art and objectives

Due to the growing importance of water resources management, the hydrologic research community has increasingly recognized the importance to better understand hydrological dynamics and catchment responses to rainfall events. In particular mountainous headwaters are extremely important for water resources but the understanding of their dominant runoff generation mechanisms is still limited.

This interest comes from the observation that the understanding of the impact of vegetation dynamics and land use change on hydrological processes still contains many uncertainties. Whilst plant transpiration and hydrological processes are not necessarily correlated, canopy cover and tree architecture, depending on the nature of the rainfall event, determine the amount of “throughfall” (Iovino, 2009). Vegetation influences the soil moisture spatial distribution and, indirectly, the mechanisms of runoff generation. Soil moisture, besides depending on topographic characteristics of the basin, is a function of the distribution of precipitation between throughfall, precipitation that flows along branches and stems of the plants (stemflow), evaporation of water intercepted by the canopy cover, water absorption by plants at the surface. Such control over soil moisture by vegetation is decisive on the hydrological dynamics of the basin as soil moisture, in particular the antecedent soil moisture conditions, determines the dynamics of the outflows (threshold behavior) and the magnitude of the runoff. Moreover, some authors (Liang et al., 2011; Chang and Matzner, 2000) observed that precipitation that is intercepted by the tree canopy and is transmitted to the base of the tree as stemflow, infiltrates via macropores around roots. Macropores around tree roots allow stemflow water to infiltrate deeper and faster into the soil (Johnson and Lehmann, 2006). Stemflow as a point source of water to the forest floor has important implications for groundwater recharge (Taniguchi et al., 1996) and soil moisture dynamics (Li et al., 2008; Liang et al., 2011). This can cause a localized saturated zone that is not present further away from the tree where throughfall water infiltrates at the soil surface (Liang et al., 2011).

Use of isotopic and geochemical tracers to investigate water movement and flow pathways

The integrated use of isotopic and geochemical tracers, combined with hydrological data, has proved to be an ideal approach to investigate hydrological processes at different spatial and temporal scales and has increasingly be used to study the hydrological cycle (Chen et al., 2011; Cervi et al., 2012; Garvelmann et al., 2012; Yang et al., 2012; Hamed and Dhahri, 2013; Kamdee et al., 2013). Among others, these techniques have been widely used to obtain groundwater information such as its sources, recharge and the interaction between groundwater and surface water (De Vries and Simmers, 2002; Yuko et al., 2002; Yang et al., 2012).

The guiding principle for the use of isotopes as tracers is that evaporation and condensation, which are the basis of the hydrologic cycle, influence the abundance of the isotopes species of water during the natural movement of water through a basin. Consequently, in different parts of hydrologic cycle, water is naturally characterized by isotopic fingerprints and its route through the hydrologic cycle can be traced (Hsueh-Yu Lu, 2014). Concentrations of geochemical tracers change due to adsorption, reduction, dissolution and cation exchange. Pathways and residence times of water in the soil influence the water chemistry: longer residence times imply a longer contact time of water with the soil and result in higher concentrations (Buttle, 1994). The analysis of the chemical composition of precipitation and hydrological components of a basin, allows investigation of the movement of water through the basin, the age and the origin of water (Burns et al., 2003) and was successfully applied in numerous studies (Rusjan et al., 2008; Zhang et al., 2011; Frisbee et al., 2011; Inamdar et al. 2013; Fischer et al., 2015). In particular at the event scale, the geochemistry of stream water changes during the events and is strongly influenced by the origin of water and its pathways (Creed et al., 1996). Event water that reaches the stream through overland flow or subsurface flow via macropores has different concentrations than pre-event water (mainly soil water and groundwater). The latter is generally characterized by high solute concentrations (Burns et al., 2003) because it has been in contact with the soil and the bedrock for a longer time. One important application of ions as tracers is the monitoring of nutrient losses during rainfall events to obtain information on preferential flow pathways as overland flow and lateral subsurface flow. For example nitrate can be used to better understand hydrological processes and pathways at the catchment scale. Nitrate is present in soils due to nitrogen fixation or can come from different sources, both natural and anthropological origin. Agricultural activities, in particular the use of fertilizer, can strongly

affect the availability of nitrate in the ecosystem, introducing a huge amount of these nutrients compared to the amount produced by forests (Hallberg and Keeney, 1993). The direct effects of nitrate excess due to agricultural activities is the contamination of groundwater, as demonstrated in different studies (Ator and Ferrari, 1997, Harter et al., 2002). In particular, the study conducted by Almasri and Kaluarachchi (2014) demonstrated how shallow groundwater is more affected by nutrient contamination than deep groundwater. Another source of nitrates comes from the alteration in physical soil structure due to shrubs and plants. In fact, shrubs and plants might influence the concentrations of solutes that are mobilized by rain water and that reached directly the stream through preferential flow pathways such as macropores. In particular, plants that support symbiotic relationship with nitrogen fixing bacteria have a strong influence on stream water geochemistry because they release fixed nitrogen in the soil and create direct flow pathways for nitrate into the stream. Moreover, soils with low permeability encourage the input of nutrients into the stream because the low infiltration of water in depth and the surface or near surface runoff of these nutrients (Arreghini et al., 2005). Mueller et al. (2016) investigated the influence of shrubs on the alteration of soil properties and the effects of alder species, in particular green alder (Alnus viridis), on the geochemistry of stream water during rainfall events in four small headwater catchments in the Swiss Alps. Alder species are known for their symbiotic relationship with the nitrogen-fixing bacterium Frankia alni. The study of Mueller et al. (2016) highlighted the strong influence of green alder to stream water chemistry and nitrate enrichment during high flow conditions for catchments with a high density of these species. On the other hand, studies carried out by Inamdar et al. (2004) and Creed et al. (1996) correlated the increase in nitrate concentrations in the stream with the increase in water table and the subsequent mobilization of nutrients due to the water table rise into a previously unsaturated area that was enriched in nitrate after long periods without rain. All these studies confirm the high applicability of geochemical tracers to study hydrological dynamics at the catchment scale. In general, the combination of the isotopic and geochemical tracers is a useful tool to clarify how storm runoff is generated and from which part of the catchment water comes from.

Application of hydrograph separation and hydrologic mixing models

In hydrology, the general problem to individuate the stormflow components to runoff has involved numerous studies, from the identification of the temporal origin of streamflow components by the use of mass balance technique (Pinder & Jones, 1969), to the investigation of the spatial origin of water that contributes to runoff by means of isotopic and geochemical analysis (Buttle, 1994; Harris et al., 1995; Turner et al., 1987; among others). Environmental tracers have been successfully used to investigate the stream response to precipitation events. Several applications of mixing models, focused on the role of "pre-event" and "event" water that contribute to stream flow, aim to clarify these mechanisms. These models assume that storm runoff is composed by a defined number of water sources (end-members) that contribute to runoff (Hooper, 2003). The application of the multivariate statistical analysis proposed by Christopherson and Hooper (1992) and Hooper et al. (1990) allows identification of the main end-members by means of a set of tracers (e.g. stable isotopes, EC, major ions) for the mixing models. This technique is called end-member mixing analysis (EMMA) and has been used in a large number of studies to investigate runoff sources (Rice and Hornberger, 1998; Wenninger et al., 2004; Penna et al., 2015; Inamdar and Mitchell, 2007; Inamdar et al., 2013). Mixing models combined with two-component and three-component hydrograph separation have been widely applied to quantify the water sources to stormflow by separating the hydrograph into different water components. The results of the study conducted by Machavaram et al. (2006), using isotopic (^{2}H,^{18}O) and chemical (Cl, SO_4) tracers, reveal the complexity of hydrograph separation and the changing contributions from groundwater and soil moisture, as well as surface water component, before and after rainfall. Ladouche et al. (2001) investigated the spatial and temporal variability of water sources and the origin of water pathways in a small catchment in Eastern France by means of isotopic and geochemical tracers. They identified three distinct areas (riparian area, middle hillslope and upper hillslope) and observed that in the first part of the event the saturated area in the downslope contributed most to stormflow, together with direct channel and near-channel precipitation; in the middle of the event the contribution of the deeper layers in the middle hillslope to stormflow increased; in the final part of the event the contribution of deeper layers to streamflow remained dominant and came from the middle hillslope and the upper hillslope in same proportion. Burns et al. (2001) used end-members mixing analysis and tracer-based hydrograph separation to compute the fraction of water to runoff of three water sources in a 10 ha catchment at the Panola Mountain Research

Watershed (USA). The results in this study indicate that riparian groundwater was the dominant component for runoff, both on the rising limb and on the falling limb of the hydrograph, and that the hillslope soil water contribution was small but significant during the winter season.

Factors controlling runoff generation dynamics

Despite the large numbers of studies that used tracer-based hydrograph separation and end-member mixing analysis to investigate runoff generation processes at the catchment scale, the literature on the changes in runoff sources as a function of seasonal variation and increasing wetness conditions is still restricted to a limited numbers of studies. Muñoz-Villers and McDonnell (2012) monitored the variation in the contribution of the runoff components during a period of 6 weeks with increasing wetness conditions in the central eastern Mexico. They demonstrated that the dominant process involved in runoff generation was the vertical percolation of rainfall to deeper layers and groundwater recharge, rather than shallow riparian pathways. They also show that the new water contribution to runoff rapidly decreased as the antecedent wetness condition increased, with a subsequent increase in the groundwater contribution, especially in the final part of the event. Other studies focused on the importance of antecedent wetness conditions in runoff generation. Among them, Burns and McDonnell (1998) observed a variation in runoff components between dry and wet periods based on isotopic data and H_4SiO_4 concentrations in two tributary catchments of Woods Lake in the west-central Adirondack Mountains of New York. The outcomes of this research showed higher pre-event water contributions at peak flow during wet antecedent conditions than dry conditions. Suarez et al. (2015) analyzed the contribution of event water, represented by direct channel precipitation and overland flow, for different wetness conditions during four rainfall events in the Kaap catchment (South Africa) and found that direct runoff was higher during wetter conditions because of the generation of saturation overland flow. Marc et al. (2001) quantified the pre-event water contribution for three rainfall events in autumn in a mountainous Mediterranean catchment and observed that pre-event water was the dominant component to runoff but an expansion of the contributing areas and an increase of the direct rainwater contribution to streamflow was due to soil saturation with increasing wetness conditions.

Together with the antecedent conditions of the catchment, storm characteristics can exert a strong influence on runoff generation dynamics as well. Hill and Waddington (1993) carried out a study in a permanent groundwater discharge zone near Toronto (Canada) and observed a correlation between the fraction of event water to runoff and event characteristics, with higher event water contributions for events characterized by a higher rainfall intensity and a longer duration. Segura et al. (2012) used a lumped conceptual model combining the rainfall-runoff response of 8 forested catchments with the variation in stable isotopes during four rainfall events between summer and fall. They showed that the fraction of pre-event water increased with increasing rainfall amount, suggesting development of catchment connectivity during larger rain storms. These results underline the large influence of antecedent condition and event characteristics on runoff generation processes. Nevertheless, more studies are needed to better understand the effect of the initial state of the catchment and the event characteristics on the stream response through empirical methods that integrate hydrometric data with isotopic and geochemical tracers and field observations.

Advantages of using isotopic and geochemical tracers in hydrograph separation studies

Although geochemical tracers (EC and major ions) have been used for end-members mixing analysis and hydrograph separation in a large numbers of studies (Pinder and Jones, 1969; Burns et al., 2001; Pellerin et al., 2008; Blume et al., 2008; Maurya et al., 2011), it should be taken into account that EC and ions are not conservative tracers because of their interaction with the soil and rocks during the movement of water through the catchment. On the contrary, stable isotopes of water have proven to be an ideal, conservative tracer for hydrograph separation because they are part of the water molecule itself and change only when waters with different isotopic composition mix together (Kendall and McDonnell, 1998). As a consequence, previous studies have found different results for pre-event water fractions using isotopic and geochemical tracers. Some studies, such as Laudon and Slaymaker (1997), observed an underestimation of the pre-event water fraction using EC and major ions compared to those derived based on stable isotopes of water. On the contrary, other authors (Penna et al., 2015; Meriano et al., 2011) found higher pre-event water fractions using EC and major ions than using the stable isotopes of water. Other studies (Cey et al., 1998; Richey et al., 1998; Pellerin et al., 2008) reported no significant differences in event and pre-event water fractions based on the stable isotopes and EC or

major ions. Despite geochemical tracers having some limitations as indicators of water sources, they are useful as flowpath tracers. Laudon and Slaymaker (1997) demonstrated many advantages of using isotopic and geochemical tracers in hydrograph separation studies. The combination of isotopic and geochemical tracers, for example, allows to perform a multiple-component hydrograph separation in order to discern the pre-event water fraction into more distinctive components such as groundwater and soil water (Hooper et al., 1990). Moreover, the two-component hydrograph separation based on EC is realizable for most of the events because of the large differences in the geochemical signature (especially for EC) between event and pre-event water. In many cases, the isotopic composition of event and pre-event water is similar, so that hydrograph separation is not possible (Sklash and Farvolden, 1979). In some cases, some discrepancies can be verified between the new water fraction computed using $\delta^{18}O$ versus $\delta^{2}H$ data indicating that also isotopes can led to high uncertain in hydrograph separation results. For example, Bansah and Ali (2017) found significant differences in old water fraction computed using $\delta^{18}O$ and $\delta^{2}H$, with larger differences in summer when there were higher fractionation losses due to the high temperature. Furthermore, EC measurements are cheap, simple and can be taken continuously (Pellerin et al. 2008). Since the use of geochemical and isotopic tracers in hydrograph separation techniques has proven to be useful (though with some uncertainties), we need to better clarify the limits and the advantages in their application. In particular, additional studies that apply geochemical and isotopic tracers in hydrograph separation can improve our understanding of the variables that control the event water fraction computed using different types of tracers.

Research objectives

This study is part of a long term research project, in a small forested pre-Alpine catchment (Ressi). Since summer 2011, hydrometric and hydrochemical data have been collected along the Ressi catchment in order to obtain information on the principal mechanisms underlying runoff generation. This particular case of study arises for the need to better understand the rainfall-runoff response of the catchment and especially how it is affected by rainstorm characteristics and antecedent wetness conditions.
The following research questions therefore are addressed in this study:

1. How the catchment responds to precipitation input under different hydrological conditions and which are the main water sources of streamflow?
2. Which control is exerted by rainfall characteristics (amount and intensity) and antecedent wetness conditions on the hydrological response of the catchment?
3. What is the effect of tracer choice (isotopes versus EC versus major ions) on the computed event water contribution to streamflow?

In order to answer these research questions, a relative large number of rainfall events collected during different periods with different antecedent wetness conditions were analyzed. This allows to observe the variation in runoff components between dry and wet periods and the influence of storm characteristics on streamflow generation. The analysis of the spatio-temporal variability of soil moisture, groundwater and streamflow leads to a better understanding of runoff dynamics during baseflow and high flow conditions. Furthermore, the integration of hydrometric data with the monitoring of the runoff components by means of environmental tracers is crucial to have a complete picture of the hydrological functioning and movement of water in the catchment. Therefore, the knowledge of the main factors that regulate the catchment dynamics in response to rainfall input is important to build conceptual models, to calibrate and test them.

In light of the mentioned iusses, the general objective of this study was to analyze runoff generation in a forested mountain catchment in the Italian pre-Alps, how it changes with the magnitude of the rainfall-runoff events and different antecedent wetness conditions.
The main objective is developed into the following specific objectives:

I. compare the response of the water table and soil moisture to the streamflow during rainfall-runoff events;
II. analyze the spatial and temporal variability in tracer signature (stable isotopes of water, EC and major ions) of different end members contributing to stream runoff;
III. assess the control exerted by the main event characteristics on the event water contribution to stream runoff;
IV. investigate how the use of different tracers affects the results of the two-component hydrograph separation.

In the first part of this thesis (chapter 3.1) the hydrological response of the Ressi catchment at event scale and the main hydrometric characteristics for 15 rainfall-runoff events from September 2015 to October 2016 are assessed. The second part of the thesis (chapter 3.2) was dedicated to the study of the streamflow, groundwater and soil water response to precipitation. The time lags between different components that contribute to stormflow were analyzed as a function of the wetness conditions of the catchment and the runoff coefficients of the events. Then the spatio-temporal variability of the isotopic composition and geochemical concentrations in rainfall, stream water, groundwater and soil water and how these concentrations varied during the events and with different hydrological conditions was analysed. Finally, end member mixing analysis (EMMA) was applied to the dataset to identify the potential end members that contribute to stream runoff. In the third part of the thesis (chapter 3.3) the event and pre-event water fractions were computed using δ^2H, EC and major ions for the events sampled in Ressi catchment. It was also analyzed how these fractions varied during the events, with the wetness conditions of the catchment and the event characteristics. The last section of chapter 3.3 was dedicated to the comparison of the new water contributions to streamflow computed using different tracers in order to verify the proper implementation of no conventional tracers for hydrograph separation.

2 MATERIALS AND METHODS

2.1 Study area

The experimental basin for the research project is the Ressi catchment, located in the Southern part of the Posina river basin (116 km^2) in the Italian pre-Alps (45° 47′ 11.79″ N; 11° 15′ 54.12″ E; (Figure 3). The Posina river originates in Borcola Pass and represents the main tributary of the Astico river that flows into the Adriatic Sea. Elevations in Posina basin range from 387 m a.s.l., the basin' outlet at Stancari location, to 2232 m a.s.l. at Cima Palon in Pasubio massif. The climate is humid temperate with rainfall concentrates in spring and fall. The site is characterized by significant mean annual precipitations (1695 mm) and high evapotranspiration fluxes. The average monthly temperatures range between 1.2°C in January and 18.7°C in July and the average annual temperature is 9.7°C.

Due to the land-use abandonment of the last five decades, the Posina basin has increased its forest cover that represents about 74% of the basin (Norbiato et al., 2009).

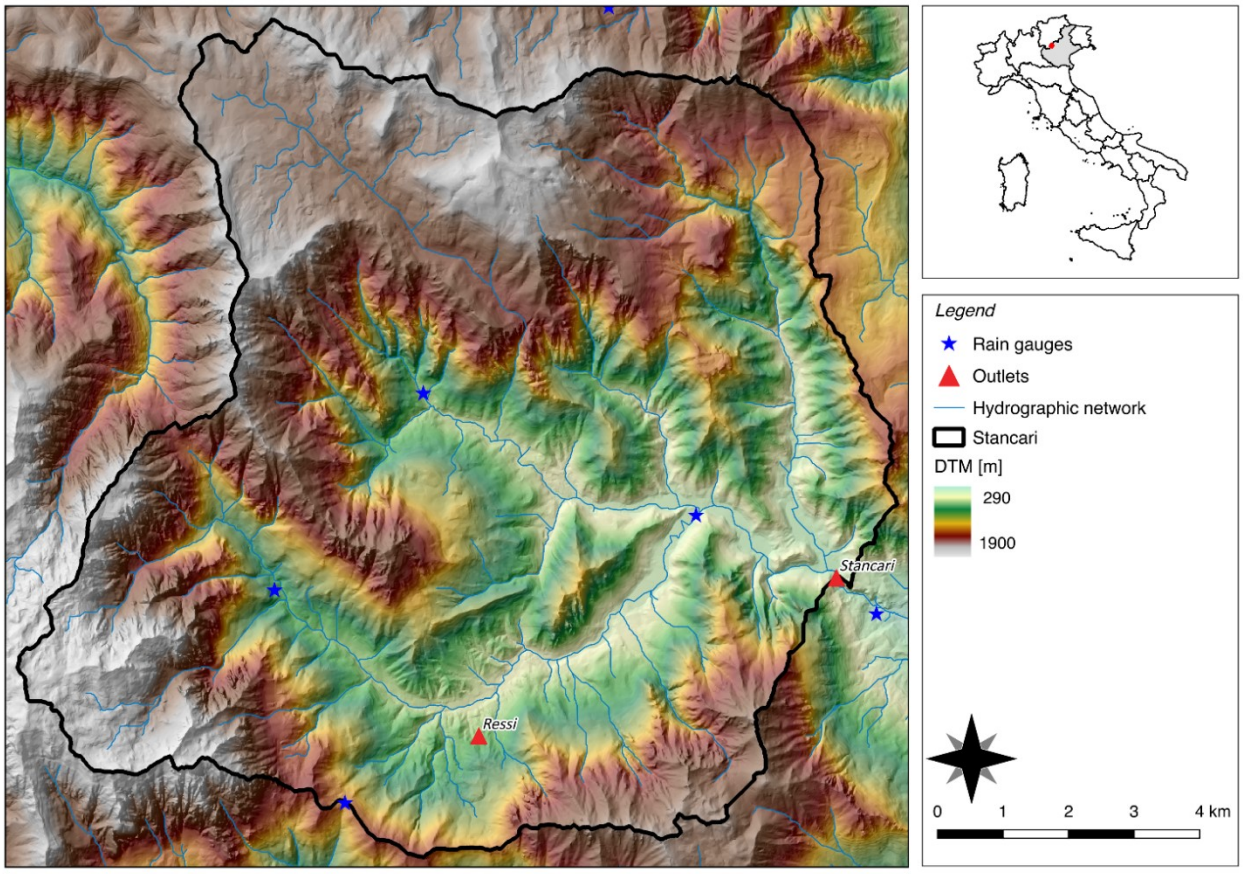

Figure 3: Geographical framework of Posina basin and Ressi catchment.

The Ressi catchment has an extension of 1.96 ha, whereas the elevations range from 609 m a.s.l. at the outlet to 725 m a.s.l. The mean slope is 26° and the aspect is predominantly North-West. The channel is approximately 150 m long and occupies roughly 0.4% of the catchment area.

The area is densely forested and the main tree species are beech (*Fagus sylvatica*), chestnut (*Castanea sativa*), maple (*Acer pseudoplatanus*), alder (*Alnus glutinosa*) and hazel (*Corylus avellana*); hornbeam (*Carpinus betulus*) and ash (*Fraxinus excelsior*) are less common.

The Ressi catchment has a geology that consists of a sequence of rhyolites and dacites from Triassic volcanic extrusions (Sedea et al., 1986). The soil type is cambisol (ARPAV, 2005) and it has low stratification. The first 10 cm of the soil are characterized by a sandy clay loam texture, as deeper soil layers has a sandy clay texture.

2.2 Environmental tracers

2.2.1 Stable isotopes of water

Isotopes are atoms of an element having the same number of electrons, and then of protons, but a different number of neutrons in the nucleus. Therefore, isotopes of a given element have the same atomic number and occupy the same position on the periodic table. Conversely, they have a different mass number, given by the sum of the number of protons (particles with a positive electric charge) and neutrons (particles with the same mass of a proton, but uncharged). It follows that isotopes of an element have similar chemical properties, due to the same number of protons, but different physical properties, because of a different mass number.

An isotope is specified by the chemical symbol of the particular element and the mass number with a superscript at the upper left of the chemical symbol. For example, hydrogen has only one proton and it is represented by ^{1}H. Deuterium, that is an hydrogen isotope with two neutron instead of one, is indicated by ^{2}H (in some cases simply D).

There are two types of isotopes: stable and unstable. Unstable isotopes, or radioactive, are those subject to radioactive decay through which they are disintegrate spontaneously with the release of energy to assume a stable configuration. Every chemical element has one or more than one radioactive isotopes. For example, the unstable isotope of hydrogen is tritium (^{3}H). Stable isotopes are isotopes that have not the tendency to change spontaneously.

Then, their nuclear composition unchanged over the time, remaining constant the relationship between the number of neutrons N and the atomic number Z. For elements characterized by a mass number less than 20, the highest stability is observed when the number of neutrons is equal to the number of protons. For elements with a mass number higher than 20, the isotopic stability is reached when the ratio N/Z is approximately equal to 1.5.

Almost 1700 isotopes are known in nature of which about 300 are stable isotopes while about 1200 are unstable isotopes. Normally each element has a single prevalent isotope. For example, the most common isotope for oxygen is ^{16}O while for carbon is ^{12}C.
Stable isotopes have important applications in various fields ranging from archeology to art, forensic science, pharmaceutical field, geochemistry and environmental studies. They prove to be valid environmental tracers thanks to do not emit radiation, to be abundant in nature according to specific proportions and to change their concentration in the chemical compounds as a function of physical-chemical processes in which they are involved (isotope fractionation).
Thanks to be part of the water molecules itself, stable isotopes of hydrogen and oxygen are mainly used in hydrology and in studies concerning the circulation of water. Considering that stable isotope rations are mainly controlled by the processes of evaporation and condensation, water is characterized by isotopic fingerprints and it is possible to used isotopes of water to identify different water masses and to trace the movement of water in hydrologic cycle (Gat, 1970). Unlike many chemical tracers, stable isotopes of water are ideal conservative tracers. Indeed, the organic and inorganic processes, which the water undergoes during infiltration and its surface and subsurface movement, do not influence the stable isotope ration in water.
Water molecule consists of two atoms of hydrogen and one atom of oxygen bonded together. In nature, oxygen isotopes are about fifteen of which only three are stable: ^{16}O, ^{17}O and ^{18}O, respectively having mass numbers of 16, 17 and 18 and average relative abundance equal to 99,763%, 0.0375% and 0.1995%. Hydrogen has three isotopes, of which only tritium (^{3}H) is an unstable isotopes as the other two (^{1}H and ^{2}H) being stable. The three hydrogen isotopes has respectively mass number of 1, 2 and 3 and average relative abundance equal to 99.9844%, 0.0156% and <0.000%.
The isotopes of oxygen are called with the corresponding mass number, whereas the name given to the isotopes of hydrogen is hydrogen (^{1}H), deuterium (^{2}H or simply D) and tritium

(^{3}H or simply T). All these isotopes are naturally present in water and their abundance ratios vary because of physical-chemical processes involving the chemical elements in question (AA.VV., 1981). Looking at the relative abundances of oxygen and hydrogen isotopes, the most common water molecule in nature is $^{1}H_2\ ^{16}O$. The molecules with more than one rare isotope are very few in nature.

Mass spectrometry is a tool for chemical analysis and it is used, among others, to determine the isotopic concentration in water samples. This technique is based on detection and quantification of ions according to their mass-to-charge ratio. The procedure consists on ionization of a sample bombarding it with electron beam. Then the ionized molecules are separated as a function of their mass-to-charge ration subjecting them to a magnetic field. The relative abundance of detected ions are showed as a spectra according to the mass-to-charge ratio. The identification of the molecules in the sample is obtained by correlating known masses to the identified masses or following specific fragmentation patterns.
The isotopic concentration is often difficult to measure in term of absolute abundance, especially regarding rare isotopes such as ^{18}O. For this reason, absolute abundances of isotopes are commonly reported in terms of relative measure comparing the isotopic ratio of the sample under examination (R_x) and the isotopic ratio of a standard sample (R_{stand}). It has become conventional to express the results of the relative abundances of isotopes using the so-called delta δ notation that expresses the abundance of a specific isotope of a element X in a specific sample relative to the abundance of the same isotope in an arbitrarily designated reference material, or isotopic standard (McKinney et al., 1950) [Equation 1].

$$\delta_x = \frac{(R_x - R_{stand})}{R_{stand}}$$

[Equation 1]

In hydrology, the isotopic concentration of hydrogen and oxygen in generally expressed in terms of part per thousand ‰ instead of part per percent %, according to [Equation 2]:

$$\delta_{‰x} = \left[\frac{(R_x - R_{stand})}{R_{stand}}\right] * 1000$$

[Equation 2]

where $\delta‰_x$ expresses how many parts per thousand the isotopic ratio of the sample under examination (R_x) deviates from the isotope ratio of a standard sample (R_{stand}).

The isotopic ratio R is the ratio of the heavy isotope, generally less abundant in nature, to the light isotope. For example, the isotopic ratio of hydrogen and oxygen are respectively [Equation 3] and [Equation 4]:

$$R_x = \left(\frac{^2H}{^1H}\right)_{sample}$$

[Equation 3]

$$R_x = \left(\frac{^{18}O}{^{16}O}\right)_{sample}$$

[Equation 4]

It follows that the isotopic concentration of hydrogen in terms of part per thousand is [Equation 5]:

$$\delta_{^1H} = \left[\frac{(^2H/^1H)_{sample} - (^2H/^1H)_{standard}}{(^2H/^1H)_{standard}}\right] * 1000$$

[Equation 5]

and the isotopic concentration of oxygen in terms of part per thousand is [Equation 6]:

$$\delta_{^{16}O} = \left[\frac{(^{18}O/^{16}O)_{sample} - (^{18}O/^{16}O)_{standard}}{(^{18}O/^{16}O)_{standard}}\right] * 1000$$

[Equation 6]

The isotopic concentration value in terms of part per thousand is positive when $R_x > R_{stand}$. In this case the sample under examination is enriched in heavy isotopes compared to the standard sample. When δ_x is negative ($R_x < R_{stand}$), the sample is poor in heavy isotopes compared with the standard sample.

Standards are chosen between natural materials as reference for isotopic measurements in laboratory. There are different standards for each element to be analyzed (for example C,

O, H, …) and they are distributed by the International Atomic Energy Authority's laboratories in Vienna. For hydrogen and oxygen, the reference material was initially Standard Mean Ocean Water (SMOW), that is the mean value of the isotopic composition of the ocean water with known $^{18}O/^{16}O$ ratio, conventionally equal to zero (both for hydrogen and oxygen). Accordingly, modern reports often present values of δVSMOW. These are equal to values of δSMOW.

Isotope fractionation

As previously stated, stable isotopes distribution in nature occur in specific proportions and stable isotopes concentration in chemical compounds is subject to variations. These variations could be attributed to fractionation occurring during chemical (for example, chemical reactions), physical (for example, the phase changes as evaporation and condensation) or biological (for example, photosynthesis) processes in which the different isotopic species are separated. This effect, called isotope effect or isotope fractionation, change the isotope ratio of a product (R_{prod}) compared to that of a reagent (R_{rea}). It defines isotope discrimination Δ the deviation of isotope fractionation from the unit [Equation 7].

$$\Delta = \alpha - 1$$

[Equation 7]

where α is the isotope fractionation equal to R_{prod}/R_{rea}.

The isotopic fractionation is because the isotopes of the same element have different masses. Consequently, there are lighter isotopes such as ^{1}H and ^{16}O and heavier isotopes such as D and ^{18}O. This affects the thermodynamic properties of the compounds because the heavier isotope reacts more slowly than the lighter.

The main processes in the generation of isotope fractionation in the terrestrial environment are phase transitions of water between vapor, liquid and ice through evaporation and condensation. During evaporation processes, the water molecules with ^{16}O evaporate before those that contain ^{18}O because they are lighter. Therefore, the greater the difference in relative mass between the two isotopes, the greater the isotopic fractionation.

In water, hydrogen isotopes are fractionated in a similar fashion to those of oxygen isotopes, but with a different magnitude: the difference in relative masses for hydrogen isotopes is less marked than for the oxygen isotopes. The fact that the water changes in the isotopic

content when subjected to physical and chemical processes has important implications for environment and hydrology. For example, using isotopic analysis it is possible to discriminate different water masses, investigate on runoff generation processes, understand if waters have suffered alterations than meteoric waters, etc.

There are two types of isotope fractionation: kinetic fractionation and equilibrium (or thermodynamic) fractionation.

Kinetic fractionation results from irreversible physical or chemical processes and it is determined by the binding energies of the original compounds. In physical processes, kinetic fractionation is because the speed of the lighter isotopes is greater than the speed of the heavier isotopes, as in chemical processes is because the light molecules react more rapidly than the heavier. This type of fractionation occurs during surface water evaporation and in most of the biogeochemical reactions in which lighter isotopes react and move faster than heavier isotopes. In third way, it is produced a difference in water pressure and lighter isotopes tend to concentrate in the final product (for example in the gas phase during the evaporation). The kinetic isotope fractionations are typically more pronounced, for a given temperature, compared to those that occur under equilibrium conditions. They do not depend only on the temperature but by many factors.

Equilibrium fractionation depends on the different thermodynamic properties of the molecules containing different isotopes. In the equilibrium fractionation, the heavier isotopes of an element are separated from the lighter isotopes and are then distributed among the various compounds or, in the same compound, between the various phases. The equilibrium is reached when the different isotopes in each compound (or phase) are constant for a particular temperature. When there is a new phase change, the ratio between heavy and light isotopes change again. For example, in the processes of condensation the heavier isotopes are concentrated in the liquid phase while the lighter isotopes tend to remain in the gaseous phase. This due to the different mass number that leads the water molecules containing ^{16}O to evaporate before those that contain ^{18}O.

The equilibrium fractionation depends largely on the temperature: as the temperature increase, also increase the ability to break bonds and the isotopic differences between two different phases become higher. The equilibrium fractionation between two phases, for example liquid and vapor, is expressed by the fractionation factor (α) which describes the isotope distribution [Equation 8]:

$$\alpha = \frac{R_{liquid}}{R_{vapor}}$$

[Equation 8]

where R is the isotope ratio between the heavier and the lighter isotope.

Isotope fractionation in water cycle

As already described, the water moves from oceans to atmosphere, land surface and soil. During this movement, phase changes continuously occur leading to a variation of the isotopic composition of water. These variations allow to use stable isotopes as natural tracers in the study of the hydrological dynamics.

During the hydrologic cycle, the main process that occur for equilibrium fractionation is condensation (rain) in which the liquid phase is enriched in heavy isotopes with respect to the gaseous phase. This process takes place in saturation conditions (relative humidity of 100%) and mainly depends on temperature. With temperature decreasing, the vapor condenses into cloud masses which increase in size and develop into clouds and precipitation. Therefore, the temperature affects the isotopic composition of meteoric precipitation, where at lower temperatures corresponds lower content of heavy isotopes, and vice versa (Dansgaard, 1964). Consequently, temperature variations during the year generate seasonal variations of isotopic composition of rain (Dansgaard, 1964). In addition, precipitation falling as rain is enriched in deuterium (and also ^{18}O) with respect to snow, due to the difference in vapor pressure between heavier and lighter water (Ehleringer and Dawson, 1992).

Evaporation is the main process in non-equilibrium conditions (kinetic fractionation). During evaporation, the liquid phase, that is the water of oceans, seas and inland waters, evolves toward lighter isotopic compositions (^{18}O and ^{2}H) and tend to produce more positive delta values. On the contrary, the gaseous phase becomes depleted in heavy isotopes producing more negative delta value. This phenomenon in rainfall events where the heavier components are separated by the lighter component is known as "rainout effect". Assuming that the relative humidity of the system remains constant, the enrichment in heavy isotopes develops following the Rayleigh's distillation law described by [Equation 9]:

$$R = R_0 * f^{(\alpha-1)}$$

[Equation 9]

where:

R_0 is the isotopic ratio at the beginning of the evaporation process;

R is the isotopic ratio when a fraction f remains in the basin;

f is the fraction of the liquid phase that remains in the basin compared to the quantity present at the beginning of the evaporation process;

α is the fractionation factor in equilibrium conditions.

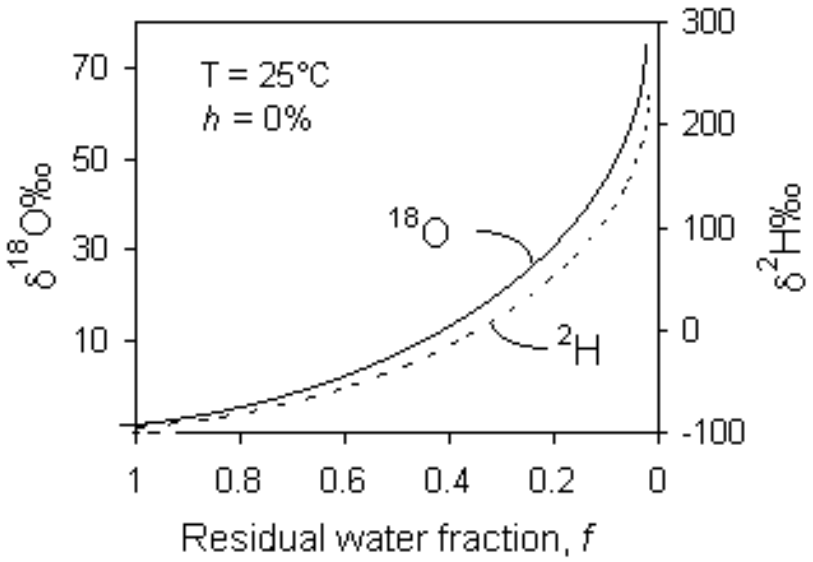

Figure 4: Enrichment of ^{18}O and ^{2}H in distilled water during evaporation of water under controlled conditions (Humidity is 0% and temperature is 25°C).

As the fundamental control on condensation process is temperature, humidity conditions mainly control the depletion in heavy isotopes in water vapor during evaporation (Gat, 1970). Gonfiantini (1986) represents the isotopic variation of δ^2H and $\delta^{18}O$ in evaporating water as a function of humidity conditions (Figure 5). In the different slopes of $\delta^{18}O$-δ^2H lines depend on different humidity conditions present during evaporation.

It follows that the surface water, constantly subjected to evaporative enrichment in δ^2H and $\delta^{18}O$, has different isotopic composition with respect to subsurface water and groundwater. In general, the surface layers are more enrich in heavy isotope because they are exposed to atmospheric agents. For this reason, it is possible to use stable isotope as tracers to investigate the mixing degree of water from different origins (Gofiantini, 1986).

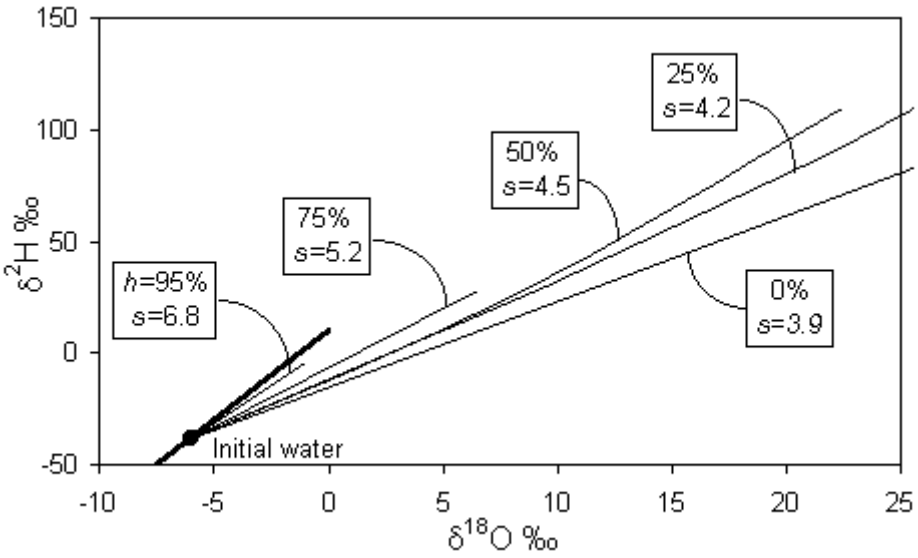

Figure 5: Isotopic enrichment in evaporating water and the effect of humidity (modified from Gonfiantini, 1986).

2.2.2 Ions

An ion is an atom of an element that is electrically charged after the lost (positive charge) or acquisition (negative charge) of an electron. When the number of electrons is less than the number of protons, the ion has a positive charge and it is known as a cation. When the number of electrons is greater than the number of protons, the ion has a negative charge and it is known as an anion.

Because of their electric charges, cations and anions attract each other and form chemical bonds. There is a ionic bond when one or more valence electrons are transferred between atoms of two different elements. In other words, the ionic bond has electrostatic nature, it is established between ions of opposite charge and require at least one electron donor (often a metal) and one electron acceptor (often a non-metal). In contrast, when two atoms share one or more pairs of electrons, it takes a covalent bond. The covalent bond requires less energy than ionic bond to be formed. It occurs between two atoms of the same element or of elements close to each other in the periodic table (similar electronegativity) in order to achieve octet configuration and became more stable.

The type of chemical bond being formed is mainly influenced by electronegativity, that is the tendency of an atom to attract electrons. There are different scales of electronegativity. The most commonly used scale is that one originally proposed by Linus Pauling. The Pauling scale was obtained by relating experimental data derived from ionization energy (amount of energy required to remove an electron from an atom to form a cation) and affinity for

electrons (amount of energy released when an electron is added to an atom to form an anion) (Figure 6).

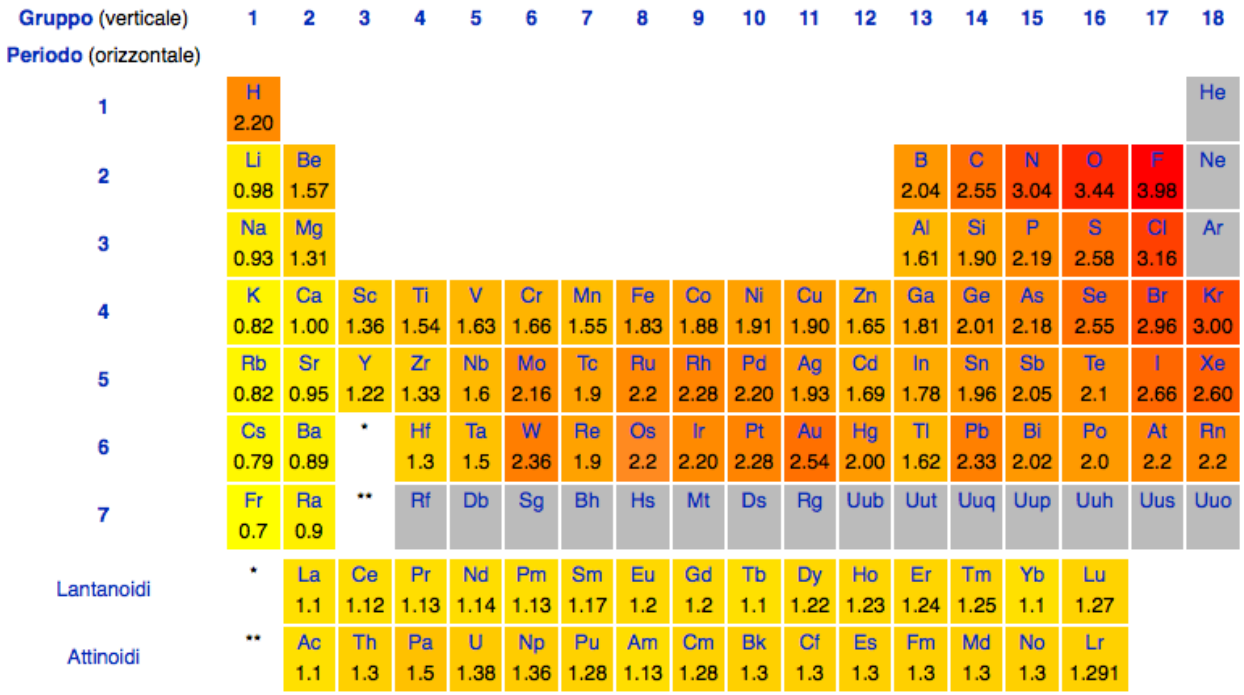

Gruppo (verticale)	1	2	3	4	5	6	7	8	9	10	11	12	13	14	15	16	17	18
Periodo (orizzontale)																		
1	H 2.20																	He
2	Li 0.98	Be 1.57											B 2.04	C 2.55	N 3.04	O 3.44	F 3.98	Ne
3	Na 0.93	Mg 1.31											Al 1.61	Si 1.90	P 2.19	S 2.58	Cl 3.16	Ar
4	K 0.82	Ca 1.00	Sc 1.36	Ti 1.54	V 1.63	Cr 1.66	Mn 1.55	Fe 1.83	Co 1.88	Ni 1.91	Cu 1.90	Zn 1.65	Ga 1.81	Ge 2.01	As 2.18	Se 2.55	Br 2.96	Kr 3.00
5	Rb 0.82	Sr 0.95	Y 1.22	Zr 1.33	Nb 1.6	Mo 2.16	Tc 1.9	Ru 2.2	Rh 2.28	Pd 2.20	Ag 1.93	Cd 1.69	In 1.78	Sn 1.96	Sb 2.05	Te 2.1	I 2.66	Xe 2.60
6	Cs 0.79	Ba 0.89	*	Hf 1.3	Ta 1.5	W 2.36	Re 1.9	Os 2.2	Ir 2.20	Pt 2.28	Au 2.54	Hg 2.00	Tl 1.62	Pb 2.33	Bi 2.02	Po 2.0	At 2.2	Rn 2.2
7	Fr 0.7	Ra 0.9	**	Rf	Db	Sg	Bh	Hs	Mt	Ds	Rg	Uub	Uut	Uuq	Uup	Uuh	Uus	Uuo
Lantanoidi	*	La 1.1	Ce 1.12	Pr 1.13	Nd 1.14	Pm 1.13	Sm 1.17	Eu 1.2	Gd 1.2	Tb 1.1	Dy 1.22	Ho 1.23	Er 1.24	Tm 1.25	Yb 1.1	Lu 1.27		
Attinoidi	**	Ac 1.1	Th 1.3	Pa 1.5	U 1.38	Np 1.36	Pu 1.28	Am 1.13	Cm 1.28	Bk 1.3	Cf 1.3	Es 1.3	Fm 1.3	Md 1.3	No 1.3	Lr 1.291		

Figure 6: Periodic table of electronegativity by Linus Pauling scale (yellow: elements with lower electronegativity; red: elements with higher electronegativity).

Compared to the Pauling scale, when the difference in electronegativity between two atoms is greater than 1.9 the elements tend to form ionic bonds, when the difference in electronegativity is lower than 1.9 the elements tend to form covalent bonds.

Looking at the periodic table, ionization energy, electron affinity and electronegativity increase on passing from left to right along a period and decrease on descending a group (Figure 7).

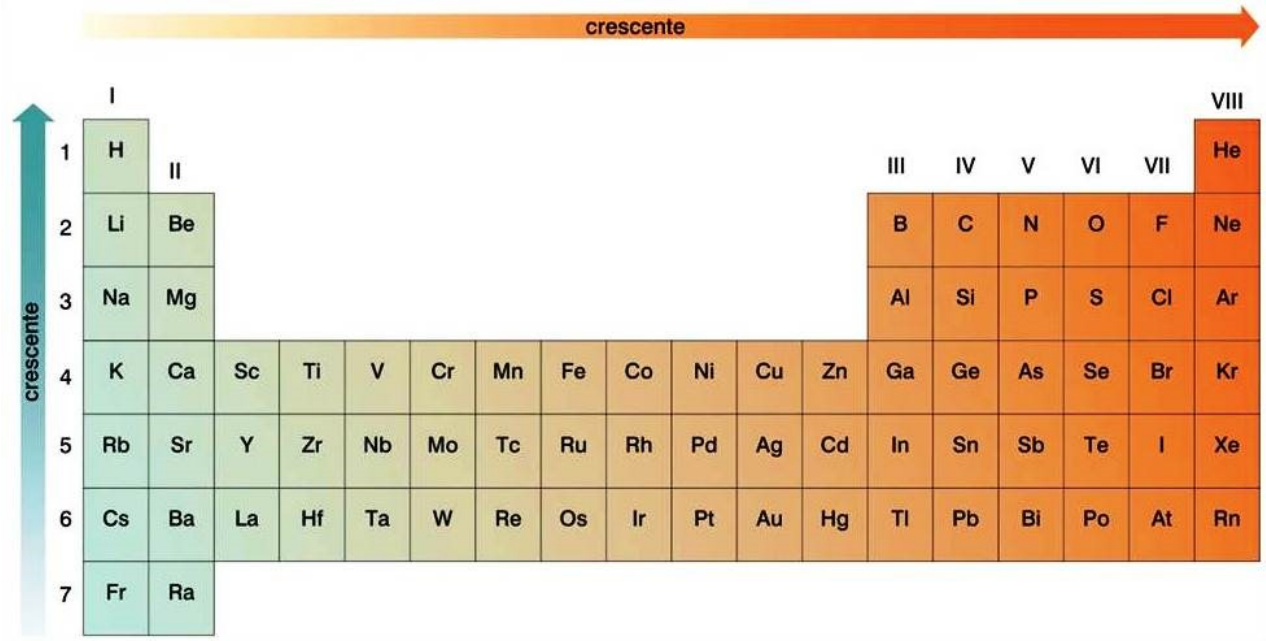

Figure 7: Ionization energy, electron affinity and electronegativity trend.

In nature, ions are ubiquitous and are generated in high abundance wherever energy is transferred into organic and inorganic material including air, soil and water. Ions are extremely important for ecosystems, in particular the interaction of ions with water. They are involved indifferent phenomena from the existence of ionosphere to the synthesis of specific organic compounds.

Water is the prevalent solvent present in nature and it plays a central role in the transport of ions as well as in the formation and breakage of chemical bonds. Since many substances have a certain solubility in water, the water in nature is never pure but it contains many dissolved substances and suspended particles, most of which are microscopic. The chemical characterization of water takes place in the so-called hydrological cycle when the water moves between hydrosphere, atmosphere, soil, surface water, subsurface water and living beings.

The chemical composition of water is widely used as natural tracers to identify different water masses and their movements through hydrological systems. Along with isotopes, certain ions can be used successfully as tracers because they are conservative and do not participate in ion association reactions. This is particularly the case for anions such as chloride and bromide (Cl^- and Br^-) which have high stability in their chemistry. Thanks to be abundant in natural water masses and reliable tracers for tracking water movement, ions are applied in many studies. Ions as tracers has been widely used to better understand

groundwater dynamics and the relation between groundwater and runoff (De Vries and Simmers, 2002; Yuko et al., 2002; Yang et al., 2012). In additions, the investigation of the spatial and temporal variability of ions concentration in groundwater can increase the knowledge on the evolution of pathways of groundwater and the geochemical reaction within the aquifer (Cook and Herczeg, 1999).

Chromatography is an analytical method to determine ions concentration in different substances among which water. This technique follows the principles of liquid chromatography and it is applicable in the complete concentration range of ppt - %. Chromatography is based on different separation and detection techniques and it is characterized by suppression reactions to reduce the background conductivity.

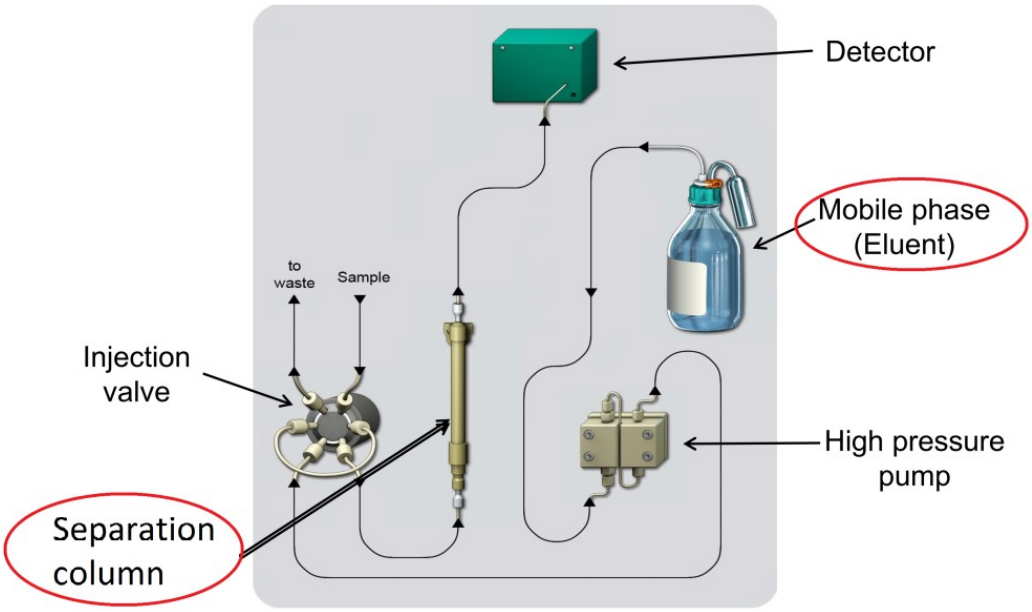

Figure 8: General setup of an Chromatograph.

In chromatography, the sample (and then the analytes) is dissolved and transported by a mobile phase (eluent); then it pass through a stationary phase (inside the column) where the separation of the sample takes place (Figure 8). Every component of the sample needs a specific and unique time to pass the column. This time is called “retention time” and it is relative to the flow ratio and the type of the eluent. The retention time is used for the identification of the analyte. When the analyte has a strong interaction with the column, it has slow movement and long retention time. On the contrary, when the analyte has a weak interaction with the column, it moves faster and it has short retention time.

There are three different types of chromatography: the ion exchange chromatography, the absorption chromatography, and the distribution chromatography. The three methods are different in the specific separation mechanism, where the stationary phase respectively reacts with, absorbs and dissolves the analytes of the mobile phase.

As regards the ion exchange chromatography, the analytes compete for places on the stationary phase with the eluent according to their charge and size ration. Consequently, the analytes will be eluted earlier or later depending on the strength of binding (ion exchange equilibrium constant). Different ion exchange equilibrium constants lead to different retention times of the respective cations or anions. This implies that the substances that are «chemically quite similar» are separated. In ion exchange chromatography the stationary phase is composed by a substrate, a spacer group (alkyl chain) and a functionality group. The substrate may consist of polystyrene/divinylbenzene, polymethacrylate, polyalcohol Hydoxyethylmethacrylate (HEMA) or silica gel. For anions, the functionality group may consist of quaternary ammonium groups, alkyl amines, hydroxy-alkylamines or alkyl amines with acrylate type crosslinking. For cations, the functionality group may consist of sulfonates or carboxylates. The mobile phase may have different compositions according to stationary phase and it has similar chemical properties as the analytes. Some examples of mobile phase composition are benzoic acid, borate, carbonate/bicarbonate for anions and nitric acid, oxalic acid, citric acid for cations.

After the separation of the components in the column, the sample is pass through the detector to measure the concentration. There are several types of detector including conductivity detector that measure the electrical conductivity of ions in a solution. Conductivity is linked to the concentration of the individual ions as follows [Equation 10]:

$$k = \sum(\Lambda_i * z_i * c_i)$$

[Equation 10]

where:

Λ_i= equivalent conductivity [S*cm2/mol];

z_i = charge;

c_i = concentration [mol/L];

k = specific conductivity [1/Ω or S];

∑= sum of all ions minus anions and cations.

Because in ion chromatography the mobile phase is frequently composed by aqueous solutions of electrolytes, the detector must be able to respond to relatively small variations of the total conductivity of the eluent caused by the ions of the analyte. Using the so-called suppression techniques, the background conductivity of certain eluents can be reduced until become nearly zero.

The output data of each analysis are represented by an ion chromatogram as in Figure 9. Each peak represents a separate ion from the sample solution. Each ion specie is collocated in the diagram depending on its retention time. For example in , Floride take less time than other ions to move through the column (shorter retention time). Consequently, they correspond to the first peak of the chromatogram. The ion concentration is computed for each species in the sample solution using the height and the breadth of the peaks. Firstly, it is calculated the area under the peak which is then converted in ppm or other quantity using calibration standard solutions.

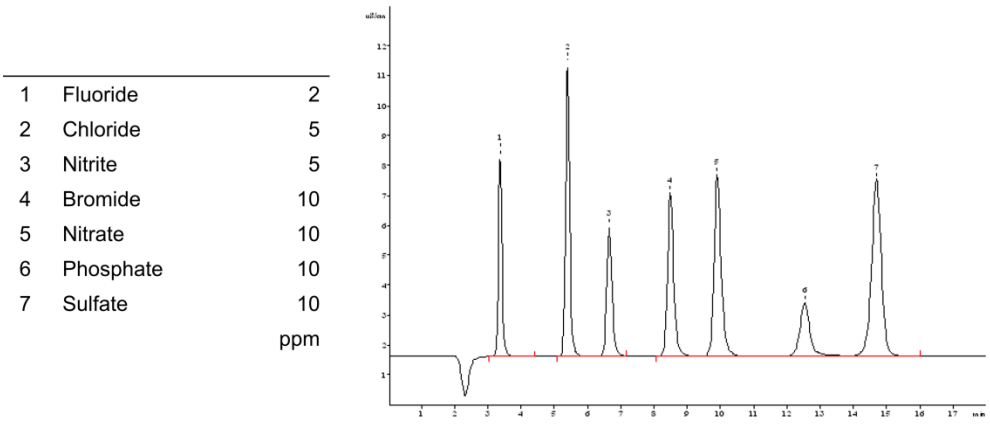

1	Fluoride	2
2	Chloride	5
3	Nitrite	5
4	Bromide	10
5	Nitrate	10
6	Phosphate	10
7	Sulfate	10
		ppm

Figure 9: Chromatogram.

2.2.3 Electrical conductivity

The electrical conductivity is a measure of the material's ability to conduct an electric current. The SI unit is microsiemens per centimeter (μ S / cm) and the US unit is micromhos per centimeter (μ mhos / cm). Distilled water has a low conductivity value which varies between 0.5 and 3 μ S / cm, while stream water range from 100 to 1500 μ S/cm (Figure 10).

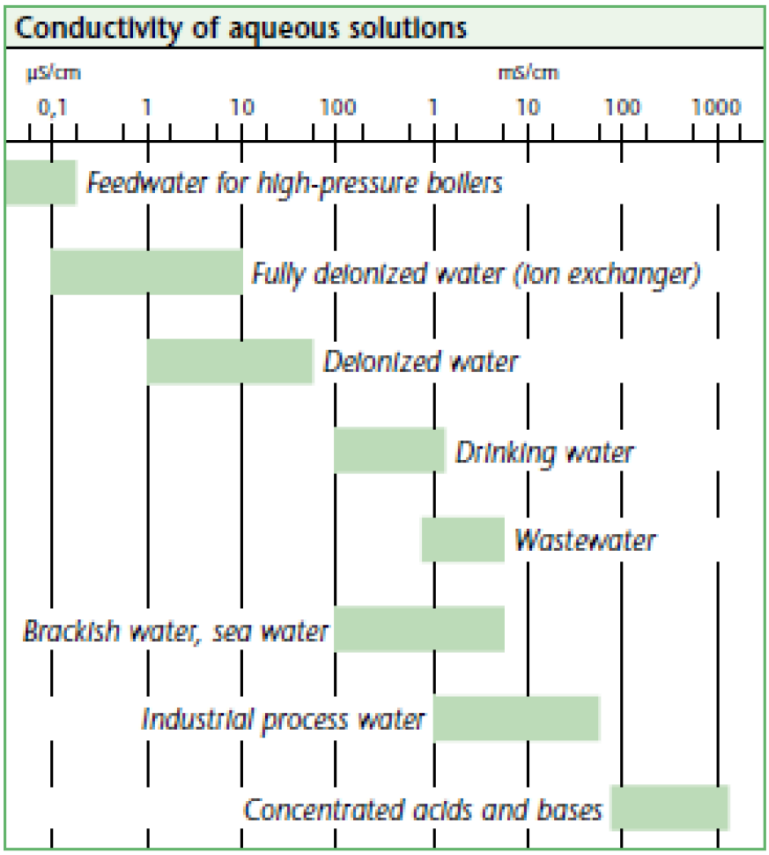

Figure 10: Range of conductivity value for different waters.

Since the electric current is transported by ions in solution, as the water conductivity increases, the concentration of the dissolved solid inorganic substance, such as chloride, nitrate, sulfate and phosphate (ions with a negative charge) or sodium, magnesium, calcium, iron and aluminum (ions with a positive charge) become higher. Temperature also affects conductivity: the higher temperatures, the higher kinetic energy of the particles and the higher the conductivity. Consequently, measurements of conductivity must be conducted at constant temperature, or alternatively it would be necessary to proceed to temperature compensation.

The electrical conductivity in streams is mainly influenced by the geology of the crossed area. Torrents with granite riverbed present low conductivity values because granite is mainly composed by inert material which is not able to ionize. On the contrary, streams with clay beds have higher conductivity value due to the ability of clay to ionize when it get in touch with water. Each tributary influence the conductivity of the water course in which it enters, depending on its water chemistry.

Therefore, electrical conductivity can be used as a natural tracer to investigate the spatial origin of water and the mechanism generating runoff. Indeed, since the ionic content

depends on the interaction of water with the lithological substrate, it is possible the analysis of preferential pathways (Kendall et al., 2001). Conductivity analyses combined with hydrometric data allow to investigate in more detail the temporal variation and spatial movement of water and to evaluate the hydrological response of the system (Lee et al., 2007; Tetzlaff and Soulsby, 2008).

2.3 Field activities

2.3.1 Instruments installation

Since summer 2011, data about precipitation, temperature, stream water level, groundwater level and soil moisture have been collected along the Ressi catchment (Figure 11).

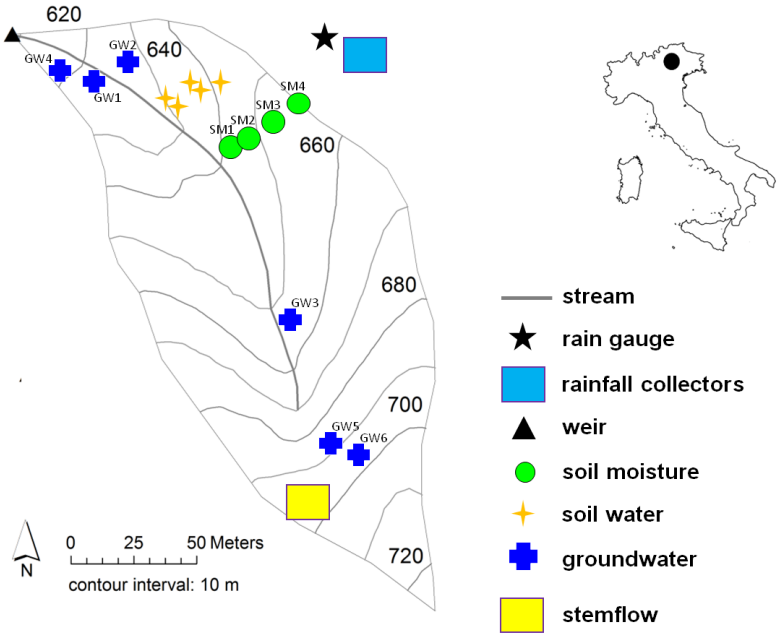

Figure 11: The Ressi catchment with available instrumentations.

An hydrometric station equipped with a V-notch weir to gauge the stream water stage (Figure 12) was installed in Ressi stream, few meters upstream of the point where the Ressi

catchment enter into a tributary of the Posina River. The stream stage level was measured at 5 minutes of interval by a pressure transducer (Keller AG für Druckmesstechnik, Switzerland). Streamflow was measured during different flow conditions using the volumetric method to check the weir equation. Electrical conductivity of the stream was measured at 5 minutes of interval by a conductivity sensor (Solinst Ltd., Canada, from July 2012 to March 2016; In Situ Inc. Aquatroll, U.S.A., from July 2016).

Figure 12: Hydrometric station in Ressi stream equipped with a V-notch weir.

Rainfall was measured using a tipping bucket (Spectrum Technologies Inc., U.S.A.; Decagon Devices Inc., U.S.A.) that was collocated in an open area just outside the Ressi catchment (Figure 13). Due to rainfall data loss for some periods (

Table 1), caused by a malfunctioning of the data-logger, it was also taken into account rainfall data measured at three weather stations operated by the Regional Agency for Environmental Protection and Prevention of Veneto (ARPAV): Passo Xomo (1056 m a.s.l., 2.3 km from the Ressi catchment), Contrà Doppio (725 m a.s.l., 3.9 km from the Ressi catchment) and Castana (430 m a.s.l., 4.8 km from the Ressi catchment). Comparison of measured rainfall at Ressi catchment and the inverse distance weighted (IDW) mean

precipitation from the three weather stations showed that there was a very good correlation between the two data series for event-based total rainfall (R^2=0.91; n=25) and average rainfall intensity (R^2= 0.44; n=25), respectively. The correlation between the two data series were good in all seasons and the data plotted almost on a 1:1 line (Penna et al, 2015).

Start date	End date	Number of missing events
12/7/12	6/8/12	3
12/9/12	21/9/12	3
18/10/12	29/3/13	8
4/5/13	12/7/13	12
16/9/13	22/9/13	0
23/9/13	27/1/14	14
26/4/15	31/5/15	8

Table 1: The table indicates the periods that were subject to rainfall data loss by the tipping bucket installed in Ressi catchment and the number of events that were missed for each period.

Figure 13: Rain gauge in Ressi catchment.

Groundwater was measured at 5 minutes interval in six wells equipped with a pressure transducer by “Solinst Ltd., Canada” (GW1 and GW2 in the riparian zone (Figure 14), GW3

at the bottom of the hillslope, GW5 and GW6 in the upper part of the catchment) or by “Keller AG für Druckmesstechnik, Switzerland” (GW4 in the riparian zone). The depth of the wells was 2.04 m for GW1, 1.04 m for GW2, 0.68 m for GW3, 1.80 m for GW4, 0.8 m for GW5 and 0.7 m for GW6.

Figure 14: Piezometric well GW1 equipped with a pressure transducer by Solinst Ltd., Canada.

Near-surface (0-30 cm) soil moisture was measured in four point along a transect showed in Figure 15 (SM1, in the riparian zone, approximately 1 m from the stream; SM2, at the transition between the riparian zone and the hillslope (footslope); SM3, in the middle part of the hillslope; SM4, in the upper part of the hillslope). Soil moisture data were taken at 10 minutes interval using a reflectometers (CS625, Campbell Scientific Inc., USA). Because we did not need to know the real soil moisture content for our purpose, but we were interested in monitoring the variation of soil moisture in time, we did not need to calibrate the reflectometers for the specific soil in Ressi catchment. Therefore, we used the manufacturer’s equation for clay soils to compute the soil moisture content.

Figure 15: Four probes along a transect to measure soil moisture in Ressi catchment.

Since July 2014, stemflow was measured along the trunk of two beech trees (*Fagus sylvatica*) located in the upper part of the catchment (Figure 16). Each stemflow collector consisted in a PVC tube longitudinally sectioned and tight fixed to the trunk. To prevent stemflow leaks, the PVC tube was wrapped multiple times around the trunk. The PVC tube was then connected and funneled into a tipping bucket (UP GmbH, Germany) for stemflow measurements. The tipping bucked was equipped with a bottle for the stemflow collection.

Figure 16: Stemflow collector connected to a tipping bucket.

2.3.2 Water sampling collection

Stable isotopes of water (^{2}H and ^{18}O), major ions and electrical conductivity were measured in rain water, stream water, groundwater, soil water, stemflow and throughfall during different wetness conditions and at rainfall-runoff event scale.

Bulk precipitation was sampled using a 5-L high-density plastic bottle, that was collocated just outside the Ressi catchment, for the assessment of the seasonal isotopic composition of precipitation. The bottle was filled with about 2 cm of mineral oil to prevent the isotopic fractionation of the sample and it was replaced about monthly. Stream water was sampled near the outlet manually directly from the stream or using an automatic water sampler (Teledyne ISCO, USA) situated near the weir (Figure 17). Groundwater was sampled at six different locations (GW1-6) using a syringe connected to a plastic tube. Samples of soil water were extracted using a lysimeters (Eijkelkamp A.E., the Netherlands) in the riparian zone at two different depth (SOWR at 20 cm depth and SOWR3 at 10 cm depth), in the lower hillslope at two different depth (SOW-LH30 at 30 cm depth and SOW-LH10 at 10 cm depth) and in the upper hillslope at 30 cm depth (SOW-UH30).

Water samples of stream water, groundwater, rain water, stemflow and soil water were taken with at least two weeks from June 2011 to September 2016. Moreover, the same water sources were sampled at rainfall-runoff event scale during two sampling campaigns carried out in Ressi catchment at different wetness conditions. The first campaign was two months long and it was carried out by mid-September 2015 to mid-November 2015. The second campaign lasted four months and it was carried out by mid-June 2016 to the end of October 2016. In total were sampled 15 rainfall-runoff events, of which 4 in the first campaign and 11 in the second campaign. At rainfall-runoff event scale, groundwater, stream water and soil water were sampled before and after the rainfall events. During the rainfall events, stream water was sampled regularly every 1 cm increase in the hydrometric level and decrease in stream water level. At the same time, precipitation was sampled each 10 mm from a rainfall collector collocated near the rain gauge. The interval of 1 cm increase in hydrometric level and 10 mm increase in rainfall was identify as the best interval that allows to monitor the variation of the isotopic composition, EC and major ions concentration in stream water and rainwater with the minimum number of samples during the events in Ressi catchment. Throughfall and stemflow samples were taken at the end of the events.

Figure 17: Box near the stream gauge containing the automatic water sampler ISCO.

Each sample was collocated in two 50 ml high-density plastic bottles with a double cap to prevent the evaporation and it was stored in the dark at 4 °C. The water of one bottle was acidified within 48 hours of sampling with acid nitric to prevent the precipitation of calcium and it was used for cations analysis. The water of the second bottle was used for isotopic and anions analysis.

2.4 Laboratory activities

Groundwater, soil water, stemflow, throughfall and rainfall electrical conductivity was measured in the field by portable conductivity (WTW-Cond 330i) whereas stream water electrical conductivity was measured continuously every 5 minutes using a conductivity sensor (Solinst Ltd., Canada).

All samples were analyzed within a few days after collection in the laboratory in Legnaro (Dip. TESAF, University of Study of Padova) for isotopic composition of ^{2}H and ^{18}O and ion concentration. The isotopic composition of ^{2}H and ^{18}O was analyzed by laser absorption spectroscopy in Figure 18 (model DLT-100 908-0008, Los Gatos Research Inc., USA, Baer et al., 2002). The ion concentration was measured by ion chromatograph in Figure 19 (model 930 Compact IC Flex, Metrohm Italiana srl). The main anions and cations that were analyzed are indicated in Table 2.

ANIONS	
fluoride	F
chloride	Cl
nitrite	NO_2
nitrate	NO_3
bromide	Br
phosphates	PO_4^3
sulfates	SO_4
CATIONS	
sodium	Na
lithium	Li
ammonium	NH_4
potassium	K
calcium	Ca
magnesium	Mg

Table 2: The table indicate the anions and cations that were analyzed from the samplers collected from September 2015 to October 2016 in Ressi catchment. The column on the right of the table indicate the term used in this thesis relative to each ion.

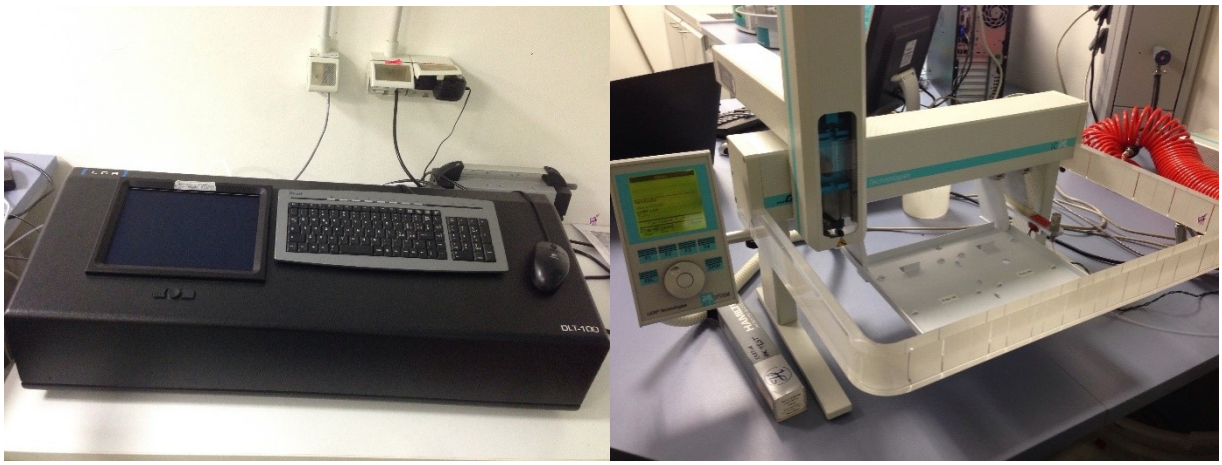

Figure 18: Laser absorption spectroscopy (model DLT-100 908-0008 , Los Gatos Research Inc. United States of America).

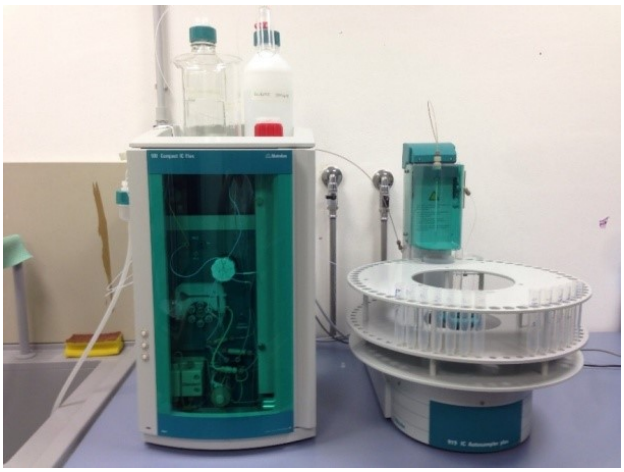

Figure 19: Ion chromatograph (model 930 Compact IC Flex, Metrohm Italiana srl).

The IC anion-separation columns used for analyses was the model Metrosep A Supp 4 - 250/4.0 with chemical suppression (Figure 20). The separation phase was comprised of polyvinyl alcohol particles with quaternary ammonium groups and a diameter of 9 µm. This structure guarantees great stability and a greater tolerance to very small particles which could pass through the integrated filter plate. The carbonate eluent was composed by 1.7 mmol/L of sodium hydrogen carbonate and 1.8 mmol/L of sodium carbonate. The chromatogram for the column model Metrosep A Supp 4 - 250/4.0 is showed in Figure 21.

a)

Technical information	
Substrate	Polyvinyl alcohol with quaternary ammonium groups
Column dimensions	250 x 4.0 mm
Column body	PEEK
Standard flow	1.0 mL/min
Maximum flow	2.0 mL/min
Maximum pressure	12 MPa
Particle size	9 µm
Organic modifier	0...100%
pH range	3...12
Temperature range	20...60 °C
Capacity	71 µmol (Cl^-)

b)

Figure 20: IC Anion-separation Column Model Metrosep A Supp 4 - 250/4.0 (a) and relative technical information (b).

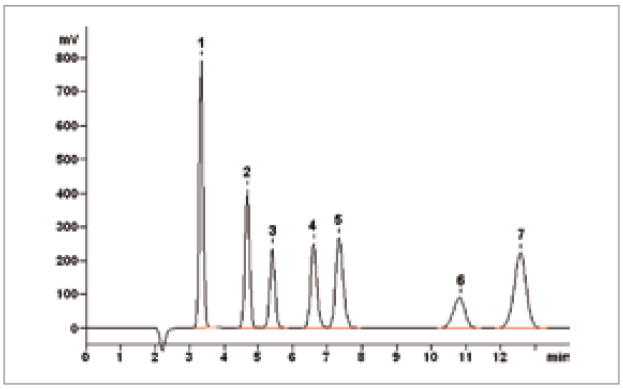

Carbonate eluent, standard					Conc. (mg/L)
1	Fluoride	5.00	5	Nitrate	10.00
2	Chloride	5.00	6	Phosphate	10.00
3	Nitrite	5.00	7	Sulfate	10.00
4	Bromide	10.00			

Figure 21: Chromatogram of standards with carbonate eluent.

The IC cation-separation columns used for analyses was the model Metrosep C 6 - 150/4.0 without chemical suppression (Figure 22). The separation phase was comprised of silica gel with carboxyl groups and a diameter of 5 µm. This structure guarantees the optimum solution for the separation of standard cations with high differences in concentration in conjunction with reasonable. The eluent was composed by 1.7 mmol/L of nitric acid. The chromatogram for the column model Metrosep C 6 - 150/4.0 is showed in Figure 23.

Technical information

Substrate	Silica gel with carboxyl groups
Column dimensions	150 x 4.0 mm
Column body	PEEK
Standard flow	0.9 mL/min
Maximum flow	2.5 mL/min
Maximum pressure	20 MPa
Particle size	5 µm
Organic modifier	0...100% (no methanol)
pH range	2...7
Temperature range	20...60 °C
Capacity	30 µmol (K^+)

b)

Figure 22: IC Cation-separation Column Model Metrosep C6 - 150/4.0(a) and relative technical information (b).

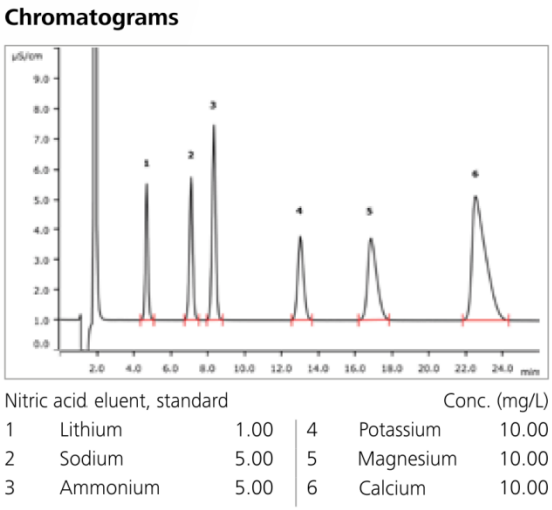

Figure 23: Chromatogram of standards with nitric acid eluent.

2.5 Data analysis

2.5.1 Definition of rainfall-runoff events

A single rainfall event was identified when there was more than 5 mm of precipitation separated by at least 3 hours of no precipitation. For each rainfall-runoff event was computed the runoff coefficient by dividing the hydrograph into baseflow and stormflow according with the constant-k method proposed by Blume et al. (2007). The constant-k method is based on the assumption that baseflow storage is linear. Therefore, the separation technique proposed by Blume et al. (2007) is to subtract baseflow from total flow until a point in time t_e that identifies the end of event runoff. The time t_e is the point after which the recession coefficient, k, is approximately constant where k is defined as [Equation 11]:

$$k = -\frac{dQ}{dt} * \frac{1}{Q(t)}$$

[Equation 11]

where Q(t) is discharge at time t.

In this study, the only difference with the constant-k method proposed by Blume et al. (2007) is that we fixed the break in slope in the falling limb to sign the end of event runoff (time t_e) visually and not analytically (Penna et al., 2011).

2.5.2 Classification of events based on event total precipitation and antecedent soil moisture

The distinction between dry and wet conditions was made based on threshold behavior in the total amount of direct runoff as a function of the combination of antecedent soil moisture index (ASI) and precipitation (P)

ASI is the Antecedent Soil-moisture Index determined as (Haga et al., 2005) [Equation 12]:

$$ASI = \Theta * D$$

[Equation 12]

where:

Θ is the average volumetric soil moisture content of the four soil moisture probe installed in Ressi catchment (SM1-4; m^3/m^3);

D is the installation depth of the probes (0.3m).

The threshold was chosen on the basis of the runoff coefficients. Events with runoff coefficients above the 4% threshold had ASI+P values higher than 84.8 mm and were classified as events in wet periods; events with runoff coefficients below the 4% threshold had ASI+P values lower than 84.8 mm and were classified as events in dry periods (Figure 24). During the sampling period from September 2015 to October 2016, 6 rainfall-runoff events were sampled with wet conditions and 9 rainfall-runoff events were sampled with dry conditions.

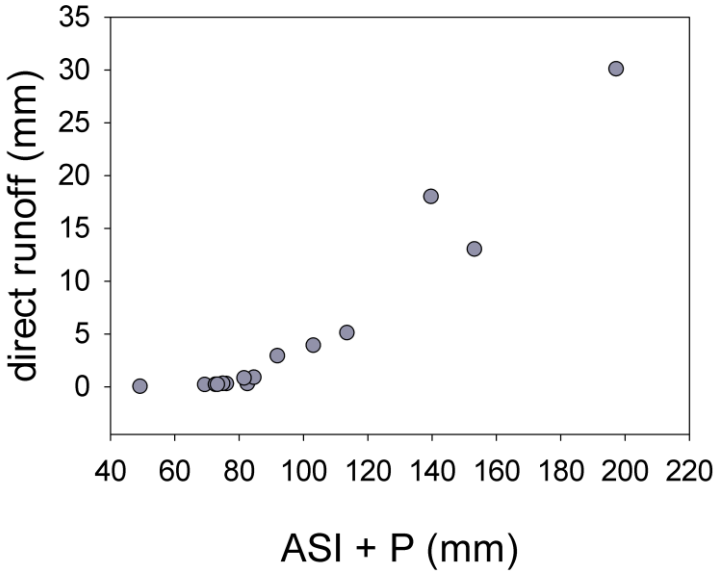

Figure 24: Threshold relation between antecedent soil moisture index (ASI) plus precipitation (P) and direct runoff (a) for events sampled between September 2015 and October 2016.

2.5.3 Definition of time lag index

Lag times analysis was performed to investigate the stream, groundwater and soil moisture response to rainfall input for the 15 rainfall-runoff events sampled from September 2015 to October 2016 in Ressi catchment.

Two different Normalized Time to Peak index (NTP) were used:

- NTP_{Tstart}: this index was calculated as the time differences between the time when the 90% of the peak groundwater (T_{GWpeak}) or peak soil moisture (T_{SMpeak}) was reached and the time of the beginning of the rainfall (T_{start}), normalized for event duration [Equation 13] and [Equation 14].

$$\mathrm{NTP}_{\mathrm{T_{start}}} = \frac{\mathrm{T_{GWpeak}} - \mathrm{T_{start}}}{\mathrm{event\ duration}}$$

[Equation 13]

$$NTP_{T_{start}} = \frac{T_{SMpeak} - T_{start}}{event\ duration}$$

[Equation 14]

- $NTPQ_{peak}$: this index was calculated as the time differences between the time when the 90% of peak groundwater (T_{GWpeak}) or peak soil moisture (T_{SMpeak}) was reached

and the time when the 90% of peak streamflow (TQpeak) was reached, normalized for event duration [Equation 15] and [Equation 16].

$$\mathrm{NTP}_{\mathrm{Q_{peak}}} = \frac{\mathrm{T_{GWpeak}} - \mathrm{T_{Qpeak}}}{\text{event duration}}$$

[Equation 15]

$$\mathrm{NTP}_{\mathrm{Q_{peak}}} = \frac{\mathrm{T_{SMpeak}} - \mathrm{T_{Qpeak}}}{\text{event duration}}$$

[Equation 16]

Time to peak was defined as the time when the 90% of the peak was reached. We used 90 % of the maximum rise in streamflow, groundwater and soil moisture to avoid the inclusion of late long peaks (Rinderer et al., 2016). Event duration was defined as the time from the beginning to the end of the rainfall input.

2.5.4 Hydrologic mixing model

The study on water origin and flow pathways, as well as the analysis of mixing processes and runoff generation processes, can be implemented with the use of environmental tracers such as stable isotopes of water (^{2}H and ^{18}O), electrical conductivity (EC) and major ions (Ca, Mg, K, Na…). Tracer-based techniques such as end-member mixing analysis (EMMA), developed by Christophersen et al. (1992) and Hooper et al. (1990), and mixing models allow to identify and quantify the mixture of water contributors (end-members) to stream water. These techniques are based on the assumption that stream water is composed by a defined and limited set of end-members each of which originates from a specific source area and it is clearly distinguish from the other contributors. Specifically, the assumption for a mixing model are the following:

- Tracers are conservative (no chemical reactions);
- All components have significantly different concentrations for at least one tracer;
- Tracer concentrations in all components are temporally constant or their variations are known;
- Tracer concentrations in all components are spatially constant or treated as different components;
- Unmeasured components have same tracer concentrations or do not contribute significantly.

The starting point for the identification of the mixing patterns is the “mixing diagrams” which is exemplified in Figure 25. The mixing diagrams are defined by two tracers and they are linear x-y plots of all stream water samples (indicated by open squares in Figure 25) and of the median and quartiles values of all the end-members (indicated by black squares in Figure 25). It is used to present only the medians of the end-member because it is assumed that the concentration of each solutes within an end-members has low temporal variability, unlike stream water composition which is generally more variable. Consequently, all stream water samples need to be plotted in the mixing space to check if they are bounded by the triangle delineated by the end-members in the vertices. In case the stream water are not well bounded, it could be that one or more end-members are missing, or the tracers are not conservative, or there is an error in sampling and analyzing the samples.

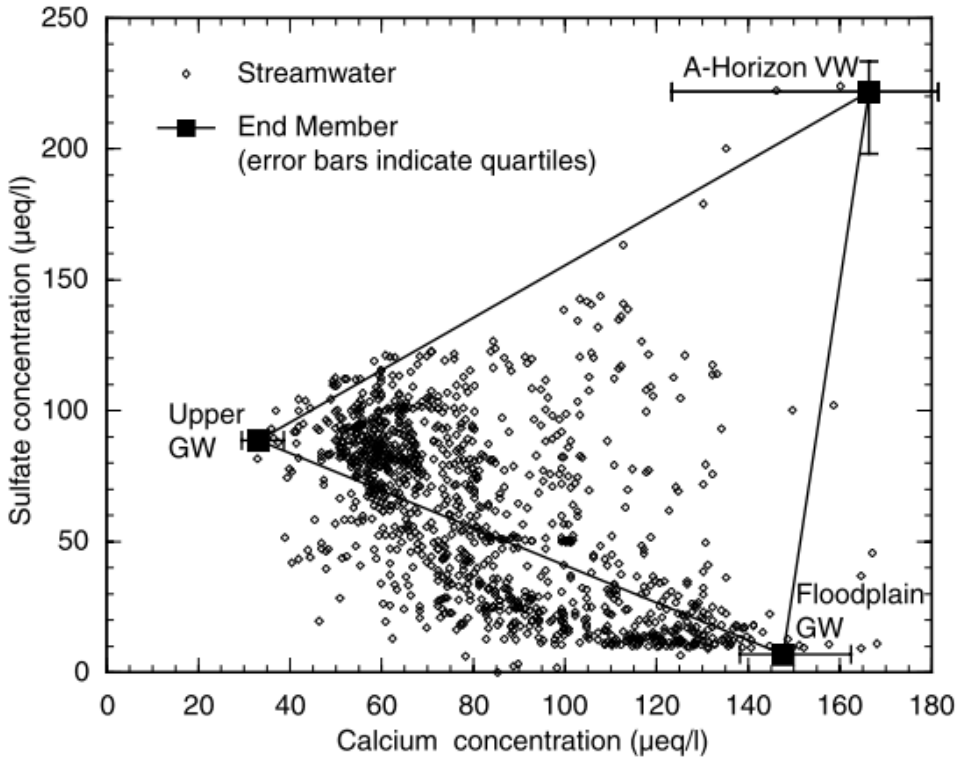

Figure 25: Example of mixing diagram (Hooper, 2001) with three end-members: groundwater from the floodplain (floodplain GW), groundwater from the upper part of the catchment (upper GW), and vadose zone water collected at the bottom of the A-horizon of the soil (‘A-horizon VW’).

2.5.5 Hydrograph separation

Hydrograph separation aims to quantify the source contributors to stormflow separating the hydrograph into different water components. Following the general principles of the mixing law, the stormflow hydrograph at any time can be divided into two, three or more different

components based on the traditional steady-state mass-balance equations of water and on the fluxes of chemical solutes along the catchment.

The mass-balance equation is defined for *n* components and *n-1* observed tracers t_1, t_2, .. t_{n-1} as follow [Equation 17] and [Equation 18]:

$$\boldsymbol{Q_T = Q_1 + Q_2 + \cdots + Q_n}$$

[Equation 17]

$$\boldsymbol{c_T^{ti} Q_T = c_1^{ti} Q_1 + c_2^{ti} Q_2 + \cdots + c_n^{ti} Q_n}$$

[Equation 18]

where:

Q_T is the total runoff;

Q_1, Q_2, .. Q_n are the runoff components;

c1ti, c2ti, … cnti are the respective concentrations of one observed tracer ti.

Two-component hydrograph separation

Isotopic and chemical tracers are used to discern two water components in the stream during runoff events: the pre-event water component, that is also called “old water” and it is the water stored in the catchment before the beginning of the event, and the event water component, that is also called “new water” and it is the precipitation (or snow-melt) contribution during the event (Figure 26).

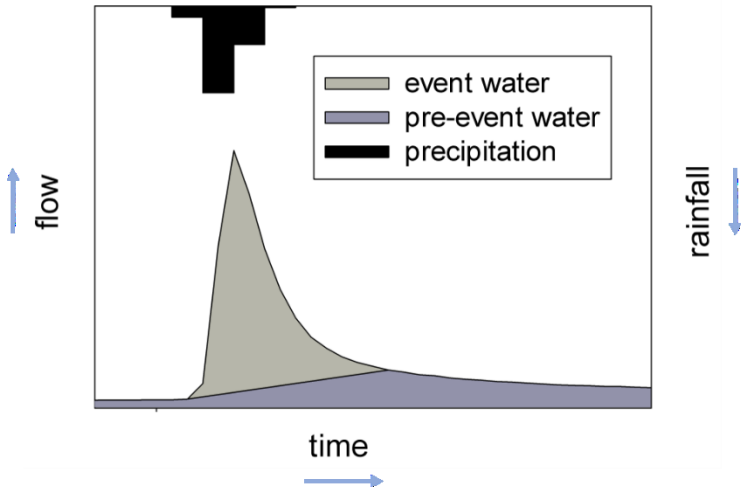

Figure 26: A hydrograph of pre-event water and event water.

The rainfall (or snow-melt)-runoff hydrograph can be separated into pre-event and event water by the application of the following mass balance equations [Equation 19] and [Equation 20] describing the water fluxes and the tracer signature in the stream (Sklash and Farvolden, 1979):

$$\boldsymbol{Q_t = Q_p + Q_e}$$

[Equation 19]

$$\boldsymbol{C_t Q_t = C_p Q_p + C_e Q_e}$$

[Equation 20]

where:

Q is the discharge;

C is the tracer concentration;

subscript t, p and e refer to the total discharge measured at the outlet, the pre-event component and the event component respectively.

The assumption for the two-component hydrograph separation are the following (Sklash and Farvolden, 1979):

- The isotopic, ionic or EC signature of the event component is significantly different from that one of the pre-event component;
- The isotopic, ionic or EC concentrations in event an pre-event water are spatially and temporally constant or any variations can be accounted;
- The groundwater and soil water isotopic, ionic or EC signature are equivalent or the contributions of soil water to runoff are negligible;
- Surface storage contributes minimally to runoff events.

According to this method, the one-tracer, two-component hydrograph separation technique was applied to the 15 monitored events in Ressi catchment in order to determine the contribution of event and pre-event water to runoff. The event water component was estimated by the isotopic, ionic and EC concentration in rainwater. The pre-event water composition was estimated by the isotopic, ionic and EC concentration in stream water during baseflow conditions.

Due to the small size of the study area (< 2 ha), it was assumed that there was no spatial variability of isotopic, ionic and EC composition of event water. For events where more than one rainwater sample was collected, the incremental weighted mean (McDonnell et al., 1990) was used to account the variation in isotopic, ionic and EC composition of event water over the event duration as follow [Equation 21]:

$$\boldsymbol{C_t} = \frac{\sum_{i=1}^{n} P_i C_i}{\sum_{i=1}^{n} P_i}$$

[Equation 21]

where:

C_t is the isotopic composition of the event water at a certain sampling time "t";

P_i and C_i denote fractionally collected precipitation depth and isotopic, ionic or EC value, respectively;

"i" denote all the sampling time of event water up to the time "t".

In this way, rainfall that had not yet fallen with respect to time "t", did not affect the hydrograph separation. It is assumed that geochemical composition of pre-event water did not change rapidly so it was not considered the temporal variability of water sources before the event. The spatial variability in pre-event water was accounted for by taking the last sample before the event.

3 RESULTS

3.1 Hydrological response during the selected rainfall-runoff events

The Ressi catchment was characterized by high variability in monthly and seasonal rainfall amounts and wetness conditions in the period September 2015-October 2016 (Figure 27 and Table 3). A wetting-up period in late summer-early fall 2015 was preceded by a long dry period. November and December 2015 had the lowest values of rainfall amount (only 11 mm in these two months) and the longest time of the entire observation period without rainfall with an average soil moisture of 22%. Conversely, in the period between February and mid March 2016, there was 451 mm of rainfall. Another wet period occurred between mid May and mid June 2016, with about 380 mm of rainfall and a significant increase in soil moisture average value of 23%, resulting in the second wettest period of the entire observation period. A second dry period occurred in summer 2016, which was characterized by rainfall events with short durations, high rainfall intensities and low antecedent soil moisture conditions. This dry period lasted until the early fall 2016 and was followed a wet period starting in September.

Start date	End date	Mean air temperature (°C)	Cumulative precipitation (mm)	Average soil moisture (%)	Number of days without rainfall
01/09/2015	13/10/2015	13.2	234	21	40
13/10/2015	29/10/2015	8.4	209	24	14
29/10/2015	03/01/2016	5.6	11	22	65
03/01/2016	03/02/2016	1.7	79	22	30
03/02/2016	16/03/2016	3.1	451	23	35
16/03/2016	11/05/2016	9.7	76	21	54
11/05/2016	19/06/2016	13.1	380	23	36
19/06/2016	20/08/2016	18.7	296	20	60
20/08/2016	12/10/2016	14.9	94	18	52
12/10/2016	31/10/2016	9.6	147	21	17

Table 3: Mean air temperature, cumulative precipitation, average soil moisture and days without rainfall for different period from 1 September 2015 to 31 October 2016.

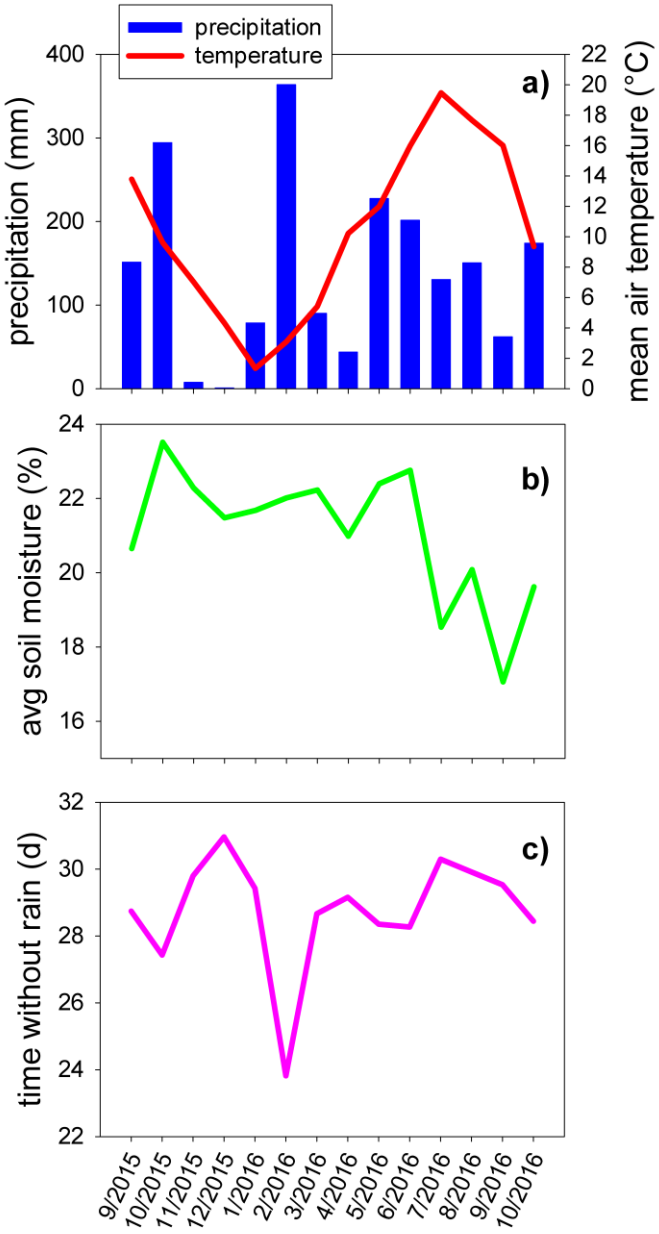

Figure 27: Monthly mean air temperature (a), total precipitation (b), average soil moisture (b) and days without rainfall (c) for each month from September 2015 to October 2016.

Streamflow, groundwater and soil moisture trends reflected the alternation of wet and dry periods. The Ressi catchment generally responded quickly to precipitation input. Streamflow usually increased very fast during rainfall events and the recession limbs were shorts for events in summer and early fall that were characterized by high rainfall intensity. Consequently, the time to peak was generally extremely short. The same trends were observed in groundwater level (Figure 28b and Figure 29b) and soil moisture (Figure 28c and Figure 29c).

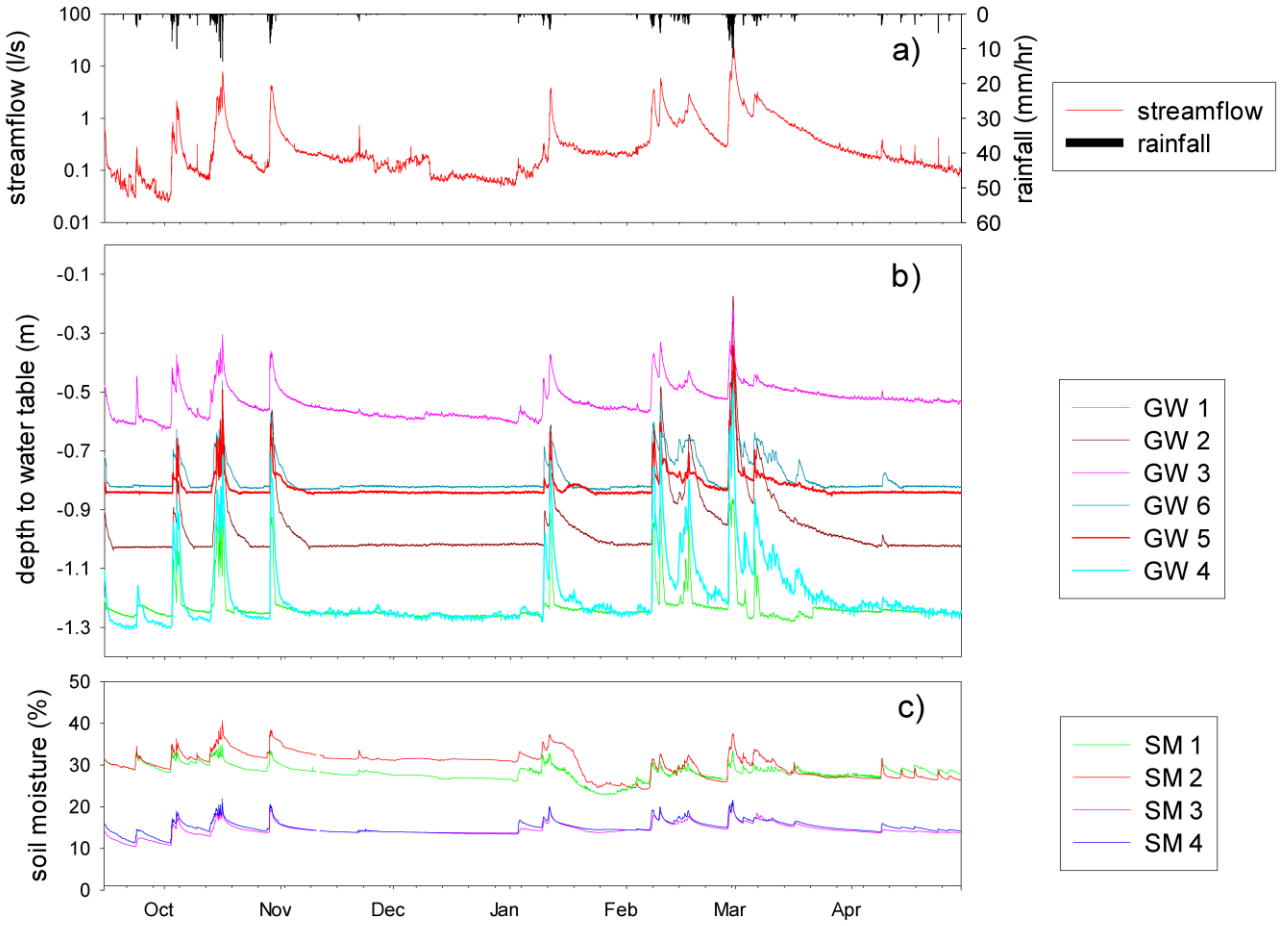

Figure 28: Time series from 15/9/2015 to 30/04/2016 of (a) precipitation and streamflow; (b-c) groundwater at six locations in the riparian zone (GW1 and GW4), at the bottom of the hillslope (GW2 and GW3) and the hillslope (GW5 and GW6); (d) soil moisture at six locations along a transect in the hillslope (SM 1-4).

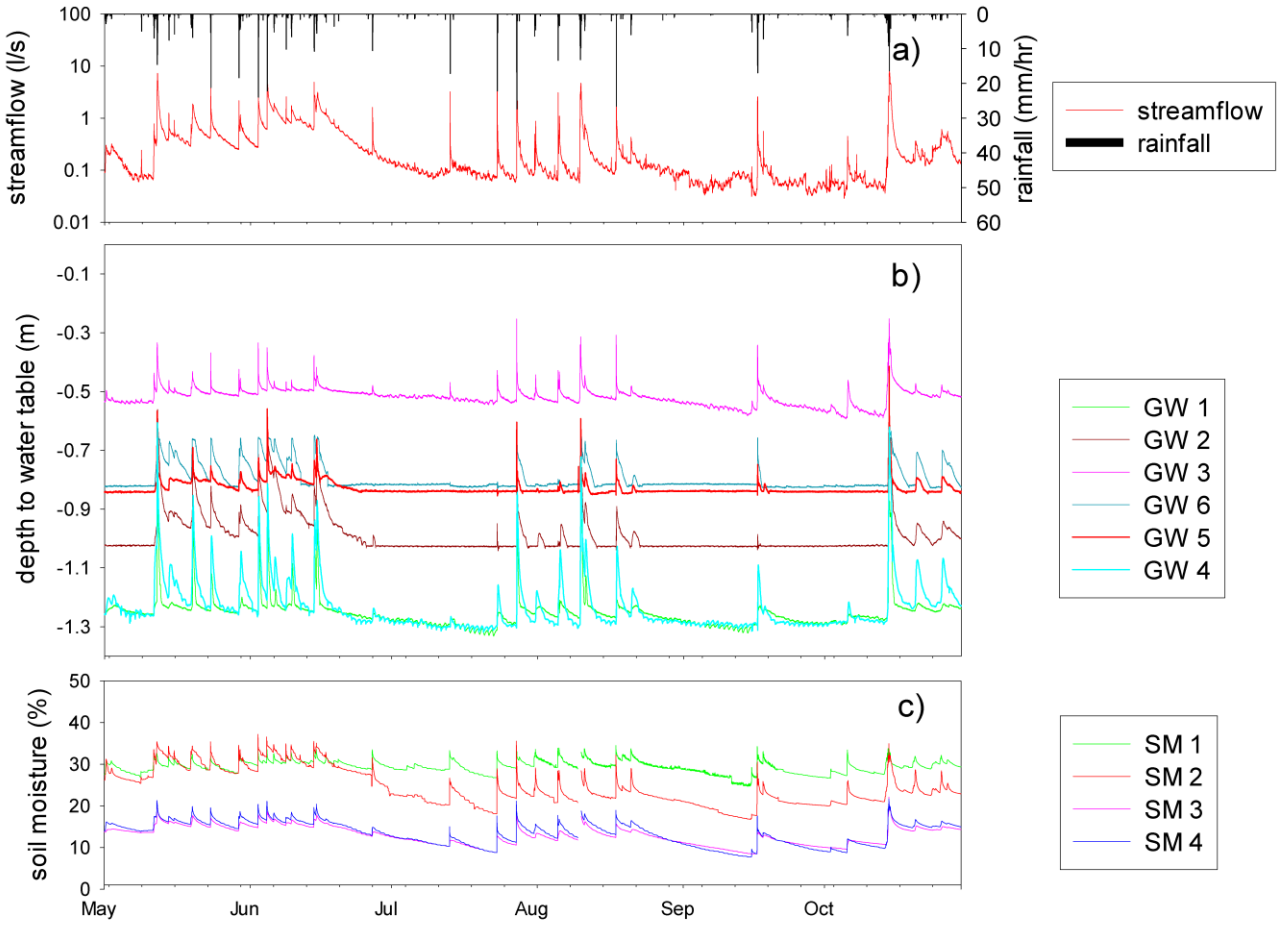

Figure 29: Time series from 1/05/2015 to 30/10/2016 of (a) precipitation and streamflow; (b-c) groundwater at six locations in the riparian zone (GW1 and GW4), at the bottom of the hillslope (GW2 and GW3) and the hillslope (GW5 and GW6); (d) soil moisture at six locations along a transect in the hillslope (SM 1-4).

Sampling campaigns for selected rainfall-runoff events were carried out from mid September 2015 to mid November 2015 and from mid June 2016 to the end of October 2016. The number of sampled rainfall-runoff events was 4 and 11 for the first and the second period, respectively. During these two periods, 6 rainfall-runoff events were sampled during wet conditions and 9 rainfall-runoff events were sampled during events with dry antecedent conditions. Rainfall amounts during the events ranged from 5 mm (event 13) to 132 mm (event 3). Mean rainfall intensity ranged from 1.6 mm/hour (event 3) to 17.2 mm/hour (event 7). Maximum rainfall intensity ranged from 1 mm/10 min (event 9 and event 10) to 13.6 mm/10 min (event 11). Runoff coefficient ranged from 0.2 % (event 13) to 25.3 % (event 4).

Rainfall amount and the mean and maximum rainfall intensity were not correlated (Figure 30). The maximum rainfall intensity and the runoff coefficient did not show a clear relation due to a random distribution (Figure 32). For wet conditions, rainfall-runoff events clearly

had longer event durations and higher runoff coefficients than small events and events in the dry period (Figure 31). Large event in wet conditions had the highest volume of total runoff (Figure 33). Runoff coefficients were highest for the largest events in fall (Table 4). Conversely, events during dry conditions were typical summer storms and had the lowest runoff coefficients. For these events, the maximum and mean rainfall intensity was the highest values of the entire period. The stream response for events in dry season was rapid and the recession limbs were shorter than for events in the wet season (Figure 34).

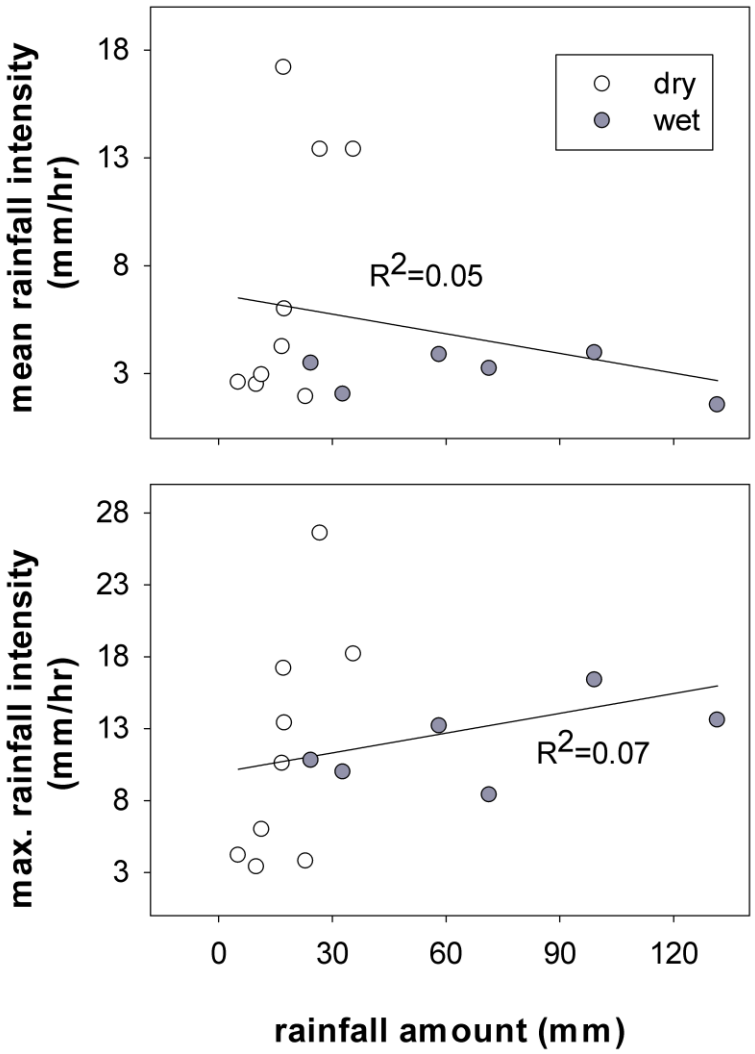

Figure 30: Relation between event rainfall amount and the event mean (upper panel) and maximum (lower panel) rainfall intensity for the sampled events between September 2015 and October 2016. Events during the dry season are indicated with white dots, events during the wet season are indicated with grey dots.

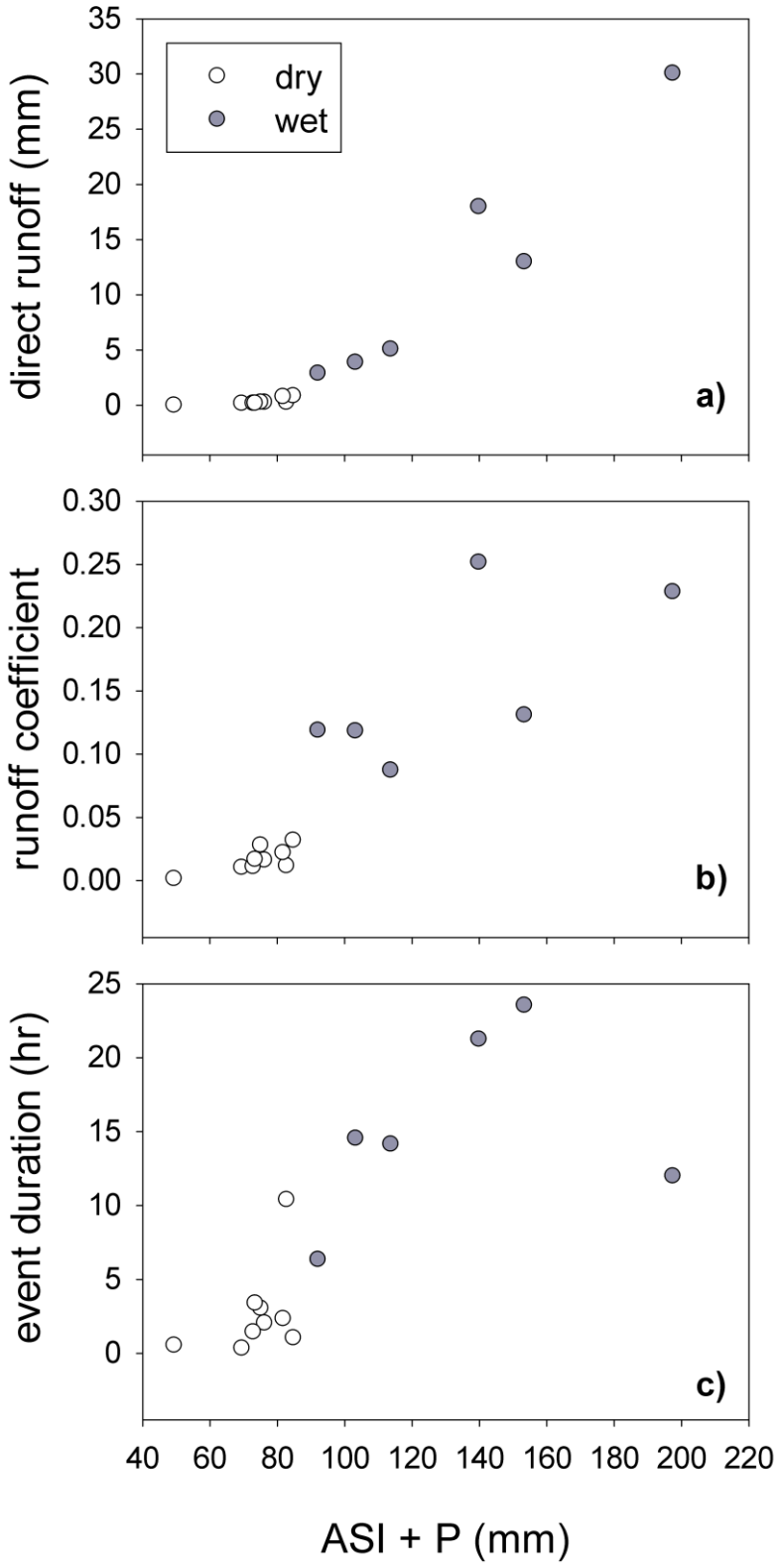

Figure 31: Relation between antecedent soil moisture index (ASI) plus precipitation (P) and direct ruonff (a), runoff coefficient (b) and event duration (c) for the events sampled between September 2015 and October 2016. Events during the dry season are indicated with white dots, events during the wet season are indicated with grey dots.

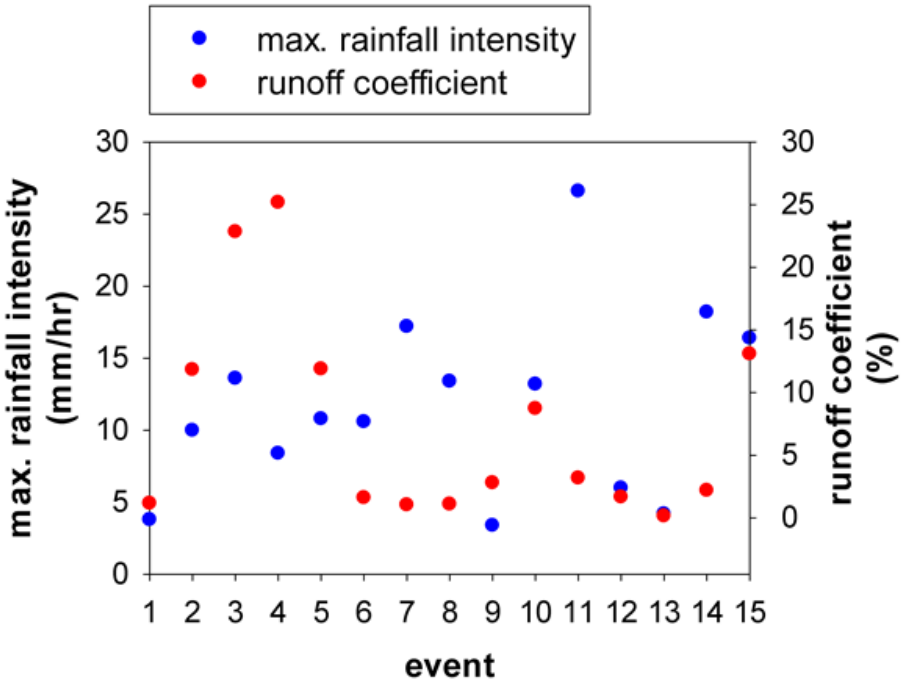

Figure 32: Maximum rainfall intensity and runoff coefficient for the sampled events between September 2015 and October 2016.

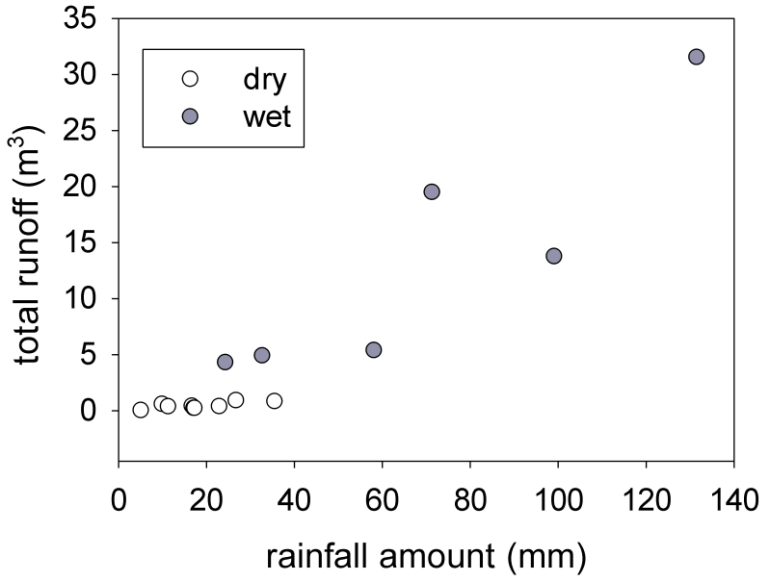

Figure 33: Relation between rainfall amount and total runoff for the events sampled between September 2015 and October 2016. Events during the dry season are indicated with white dots, events during the wet season are indicated with grey dots.

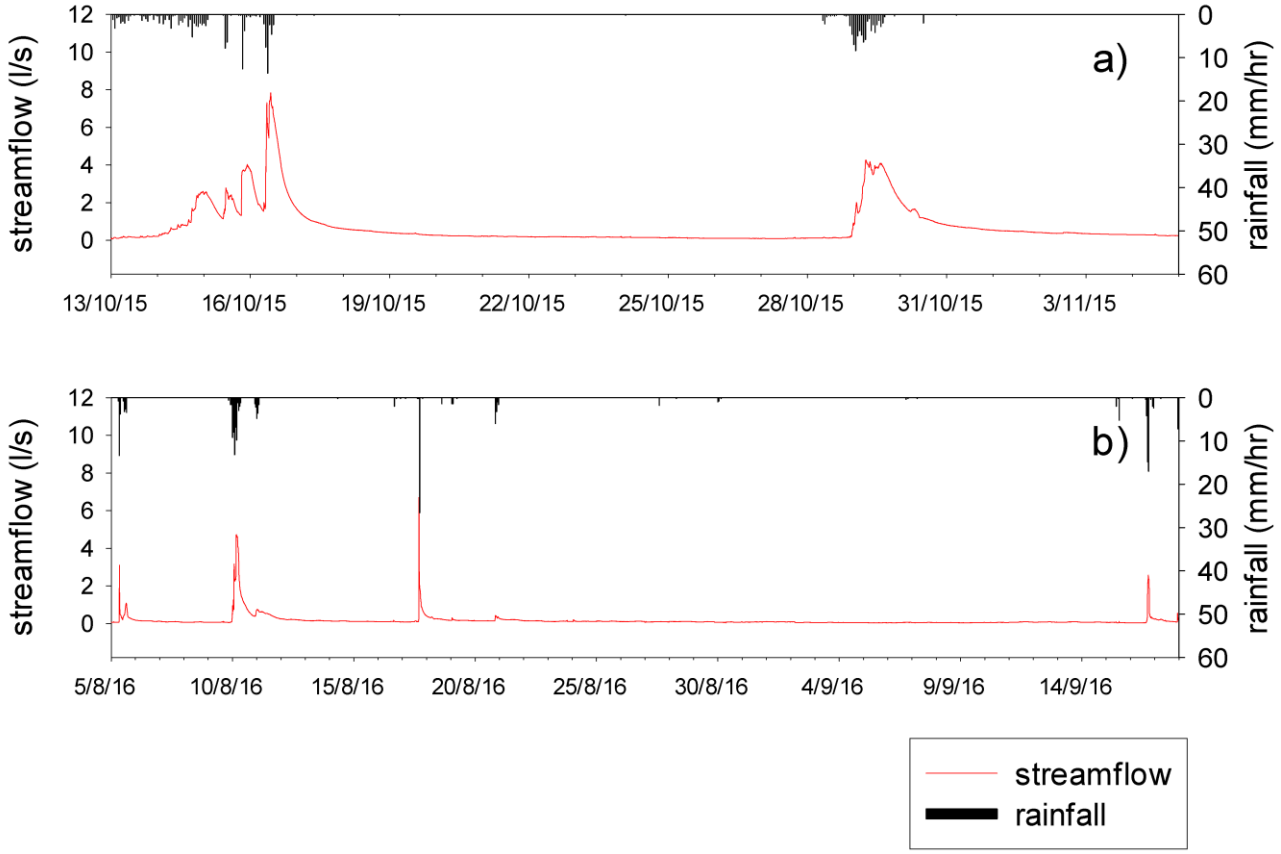

Figure 34: Time series (a) from 13/10/2015 to 5/11/2015 and (b) from 5/8/2016 to 18/9/2016 of precipitation and streamflow

Measured variable	Pre-event time	Event duration	Total rainfall	Mean rainfall intensity	Max. rainfall intensity	Runoff coefficient	Direct runoff	ASI	ASI + P	Wetness status
Units	Date-Solar time	hour	mm	mm/hour	mm/10 min		m^3	mm	mm	
ID										
1	23/09/2015 04:50	10:40:00	23,0	1,9	1,2	0,012	5,4	59,7	82,7	Dry
2	04/10/2015 01:45	14:55:00	32,8	2,1	2,8	0,118	77,7	70,4	103,2	Wet
3	12/10/2015 23:40	12:00:00	131,6	1,6	4,6	0,228	601,4	65,8	197,4	Wet
4	28/10/2015 18:35	21:25:00	71,4	3,2	2,2	0,252	359,6	68,5	139,9	Wet
5	14/06/2016 10:25	06:35:00	24,4	3,5	7,0	0,119	58	67,7	92,1	Wet
6	26/06/2016 21:15	02:05:00	16,8	4,3	5,8	0,016	5,4	59,4	76,2	Dry
7	13/07/2016 09:05	00:35:00	17,2	17,2	10,8	0,010	3,6	52,3	69,5	Dry
8	05/08/2016 06:45	01:45:00	17,4	6,0	9,2	0,011	3,8	55,4	72,8	Dry
9	05/08/2016 11:45	03:05:00	10,0	2,5	1,0	0,028	5,6	65,1	75,1	Dry
10	09/08/2016 17:35	14:15:00	58,2	3,9	5,8	0,087	101,7	55,5	113,7*	Wet
11	17/08/2016 15:55	01:05:00	26,8	13,4	13,6	0,032	17,1	57,9	84,7	Dry
12	20/08/2016 19:10	03:40:00	11,4	3,0	1,6	0,017	3,8	62,0	73,4	Dry
13	15/09/2016 12:05	00:55:00	5,2	2,6	2,8	0,002	0,2	44,1	49,3	Dry
14	16/09/2016 15:25	02:35:00	35,6	13,4	5,0	0,022	15,7	46,1	81,7	Dry
15	14/10/2016 00:10	23:55:00	99,2	4,0	6,2	0,131	260	54,1	153,3	Wet

*Data of soil moisture are not available from 9/8/16 at 14.40 to 10/8/16 at 8.00. We used the last soil moisture record on data 9/8/16 at 14.35 to compute ASI for event n. 10 on 9/8/2016.

Table 4: Main hydrometric characteristics of the rainfall-runoff events sampled between September 2015 and October 2016. Events during the dry season are highlighted in white, events during the wet season are highlighted in grey. Events 1-4 belong to the first sampling period, events 5-15 belong to the second sampling period.

3.2 Variability in streamflow, groundwater and soil water response to precipitation input

3.2.1 Catchment response time to precipitation input

The time lag between the different components that contributed to streamflow were analyzed for the 15 rainfall-runoff events to investigate the stream, groundwater and soil moisture responses to rainfall. The main results of this analysis are shown in Figure 35 to Figure 37 and in Table 8 and Table 9 (Appendix).

Streamflow in Ressi catchment reached the peak very fast and the recession limbs were short, especially for events in summer and early fall characterized by high rainfall intensity. Consequently, the time to peak was generally short.
Groundwater level in the riparian zone had a slower response to rainfall input (higher values of NTP_{Tstart}) than groundwater level at the bottom of the hillslope and in the upper part of the catchment. In particular, groundwater at the bottom of the hillslope (GW3) had the shortest time to rise with low values of NTP_{Tstart} (Figure 35a). Soil moisture was generally more reactive than groundwater; the variability in NTP_{Tstart} was also smaller (Figure 35b). The NTP_{Qpeak} for groundwater and soil moisture measured at different locations followed the same pattern (Figure 35, c and d). These differences in time lag increased during the dry season, as shown in Figure 36. During the wet season, groundwater and soil moisture tended to be more reactive and peaked near or before the peak of streamflow at the catchment outlet (Table 8 and Table 9, Appendix).

The time lag between the groundwater peak and streamflow peak was longer than the time lag between soil moisture peak and streamflow peak. In particular, riparian groundwater at location GW1, GW2 and GW4 had longer time lags than groundwater in the upper part of the catchment and soil moisture (Figure 37). For events with high runoff coefficients, groundwater and soil water peaked before streamflow. On the contrary, for events with little direct runoff, groundwater peaks were consistently delayed and the soil moisture peaked after streamflow (Figure 37). Differences in time lag between groundwater peak and streamflow peak and between soil moisture peak and streamflow peak were longer for events with low runoff coefficients (Figure 37).

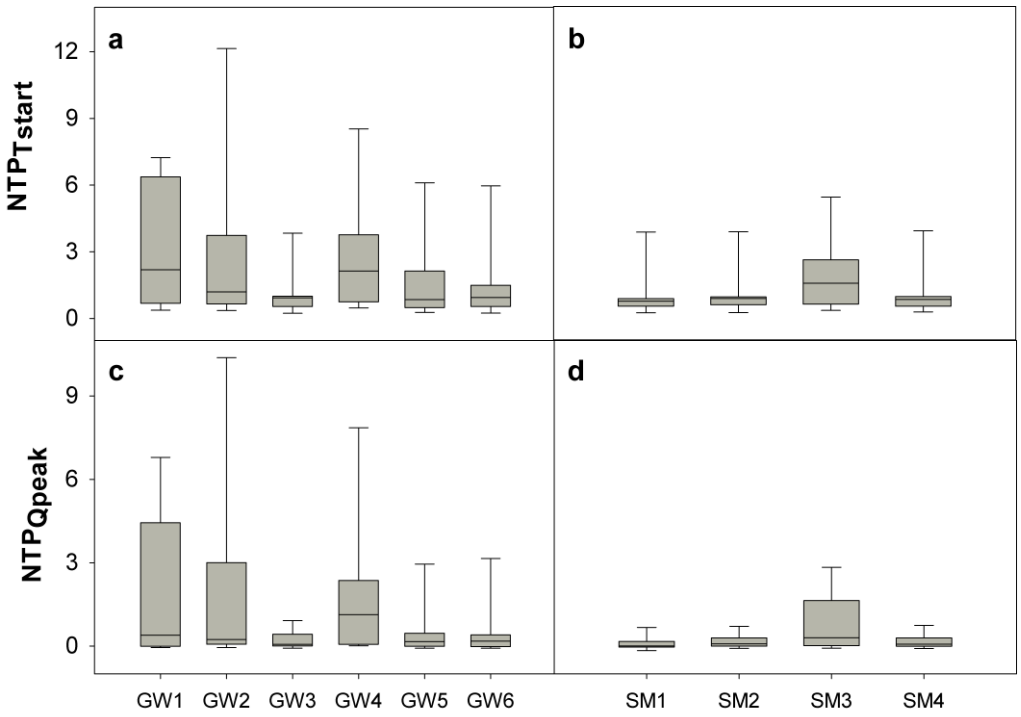

Figure 35: Box-plot of NTPTstart for groundwater at six locations (GW1-GW6; a) and soil moisture at four locations (SM 1-4; b) and box-plot of NTPQpeak for groundwater at six locations (GW1-GW6; c) and soil moisture at four locations (SM 1-4; d). Data includes 15 rainfall events between September 2015 and October 2016.

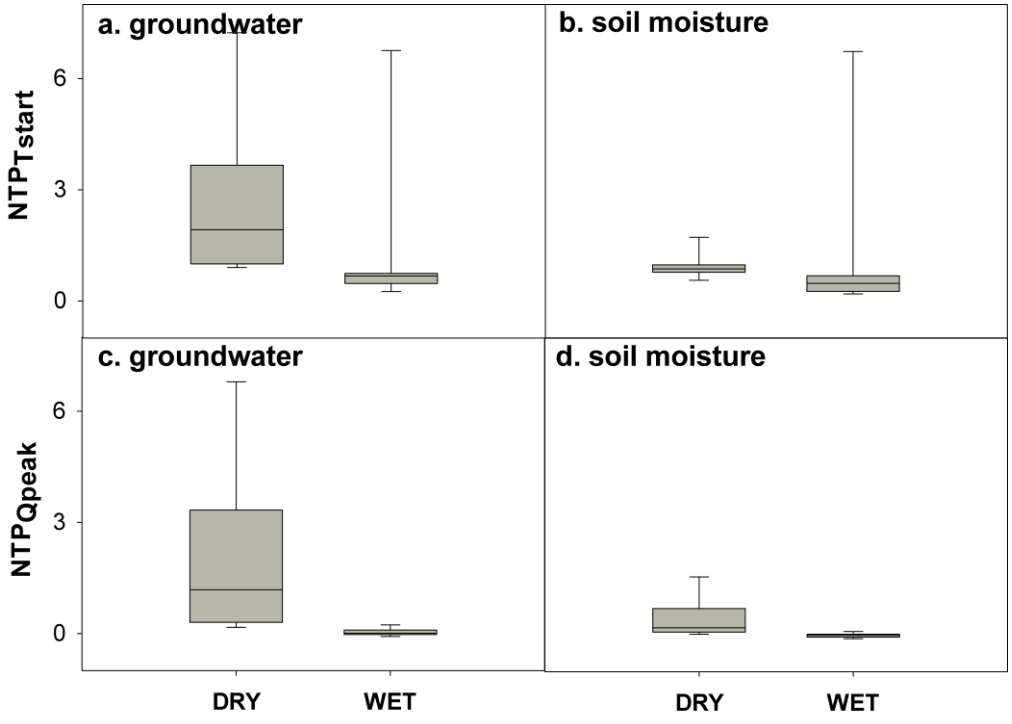

Figure 36: Box-plot of NTPTstart for groundwater at six locations (GW1-GW6; a) and soil moisture at four locations (SM 1-4; b) and box-plot of NTPQpeak for groundwater at six locations (GW1-GW6; c) and soil moisture at four locations (SM 1-4; d) for the dry season and wet season. Data are shown for 15 rainfall events between September 2015 to October 2016.

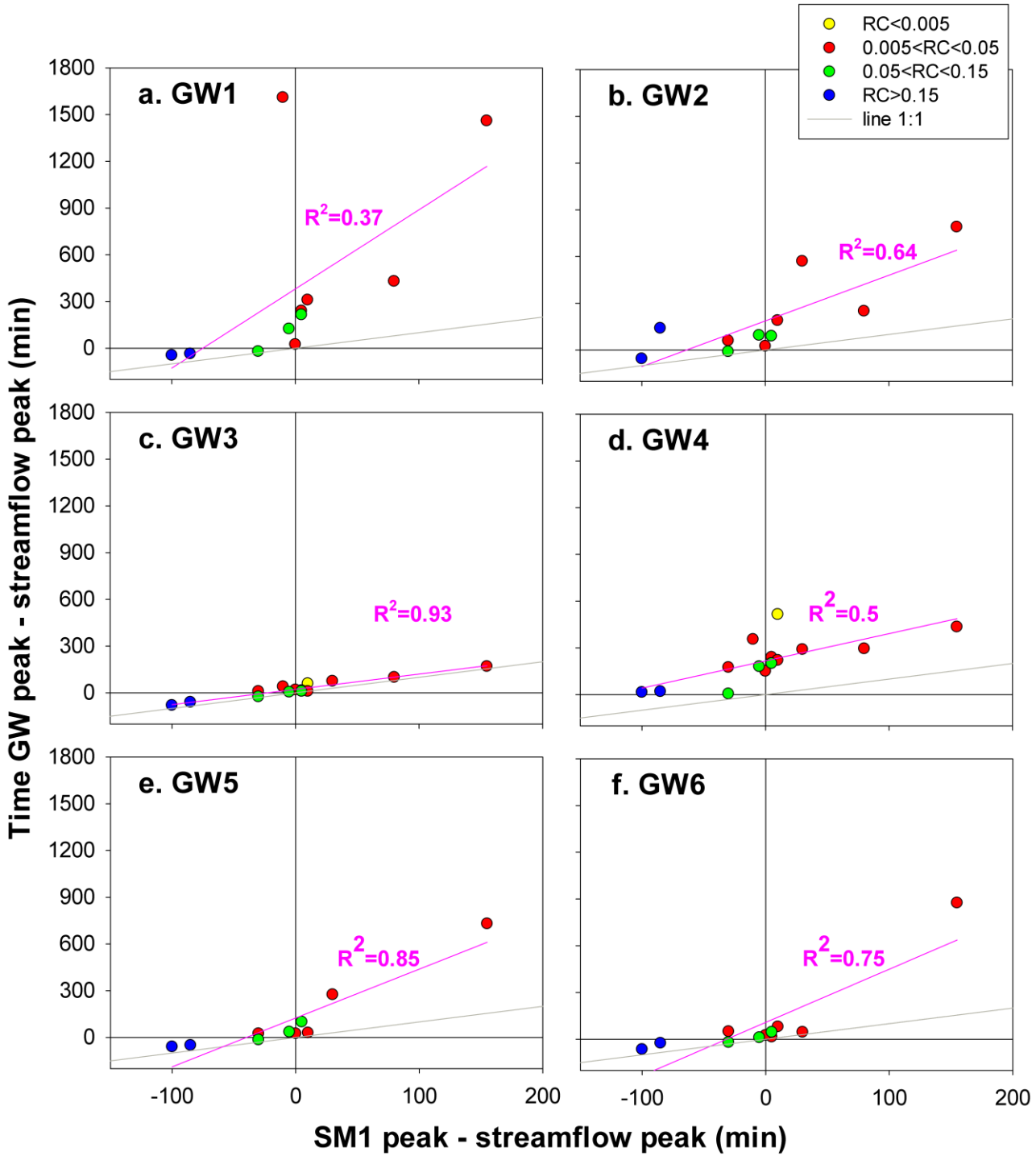

Figure 37: Relation between time lag between streamflow peak measured at the outlet and the soil moisture peak measured at location SM1 and the time lags between streamflow peak measured at the outlet and groundwater peak (GW peak) for different locations (a: GW1, b: GW2, c: GW3, d: GW4, e: GW5, f: GW6). Each dot (representing one event) is colored according to its runoff coefficient (RC). Data are shown for the 15 rainfall events between September 2015 to October 2016. Time to peak is when the 90% of the total rise is reached. Negative values indicate that soil moisture or groundwater peaked before streamflow. Linear regression lines and the 1 to 1 line are shown as well.

3.2.2 Spatio-temporal variability of isotopic and geochemical tracers

Figure 38 and Figure 39 show the seasonal and event-scale variation in δ^2H and Mg concentration in the main water sources.

As expected, Mg content in rain water was always low (Figure 38a). The enrichment in solutes in rain water, even at low concentrations, happens because of the interaction of water vapor with particles, dust and pollutants dissolved in atmosphere. When meteoric water reached the ground and started to move through the catchment following different pathways, a series of chemical reactions started. One of these reactions was when the meteoric water interacted with soils and rocks, releasing ions and increasing the ionic content of water.

There was a remarkable spatial variability in Mg in shallow groundwater throughout the study period. There were generally higher Mg concentrations in riparian groundwater than in groundwater at the bottom of the hillslope and at the hillslope. Mg concentrations in shallow groundwater in the riparian zone (GW1 and GW4) were also more stable ever time. On the contrary, the temporal variability in concentrations in shallow groundwater at the bottom of the hillslope (Figure 38c), as well as in soil water (Figure 38d), was higher.

Mg concentrations in stream water during baseflow conditions were higher during the dry season than in the wet season. These concentrations changed rapidly with precipitation input, reflecting the rainfall signal. The rapid decrease in Mg content during high flow conditions was due to the dilution effect of water from precipitation and hillslope (Figure 38b). For summer events, Mg content in stream water after rainfall events returned immediately to the pre-event value, but for events in the wet season the pre-event value was reached slowly. Similar patterns were recognized in groundwater and riparian soil water (Figure 38, c-d) and were confirmed for other solutes like SO_4, Ca, Na and electrical conductivity.

The spatial and temporal variability in the isotopic composition during the studied period was relatively small for shallow groundwater and larger for stream water and soil water. Stream water, groundwater and soil water had more negative delta values in winter, partly reflecting the signal of infiltrating rainfall (Figure 39). But, this variability was less prominent than the large temporal variability in rainfall.

δ^2H and $\delta^{18}O$ in stream water ranged from -26.7 ‰ to -66.7 ‰ and from -5.5 ‰ to -9.7 ‰, respectively, with a mean value of about -50 ‰ and -8 ‰, respectively. Groundwater, soil water in the riparian zone at 20 cm depth and rainfall had lower mean values of δ^2H and

$\delta^{18}O$ than stream water. Made an exception groundwater at the bottom of the hillslope and in the upper part of the catchment at locations GW2 and GW6, respectively (Table 10, Appendix).

EC in stream water ranged from 89 μS/cm to 309 μS/cm. Ca, Mg and Na were the ions with the highest concentration in all water sources. The average concentration in streamflow were 26 for Ca, 10.9 ppm for Mg and 4.5 ppm for Na (Table 10, Appendix). NO_3 had higher average concentrations than Na only in stream water (5.3 ppm of NO_3) and rainfall (1.2 ppm of NO_3 and 0.2 ppm of Na). For all the other water sources was the opposite (higher average concentration in Na than in NO_3). The average concentration of SO_4 in the stream was 2.7 ppm. Cl and K were the ions with the lowest concentrations in stream water and in all water sources. The sources of Cl and SO_4 might have been the atmosphere, the accumulation on the soil surface due to evaporation of precipitation or the weathering of bedrock in the deeper layers. NO_3 and K are generally considered to be due to biological activity (Ladouche et al., 2001).

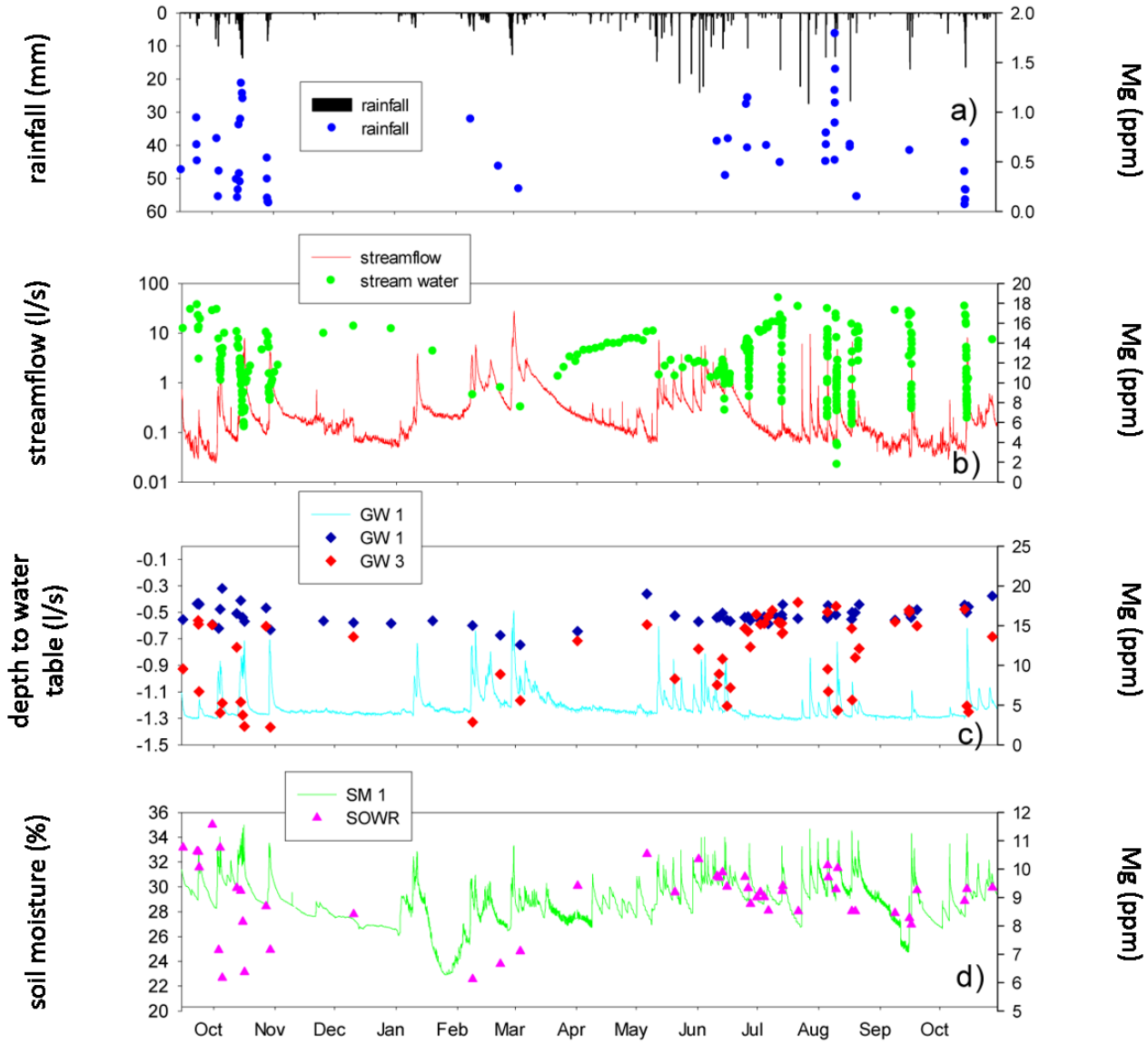

*Figure 38: T*ime series of a) rainfall, b) streamflow measured at the catchment outlet , c) groundwater in the riparian zone (GW1), d) soil moisture measured in the lower part of the hillslope (*SM* 1); and Mg concentrations in a) rainfall, b) stream, c) groundwater in the riparian zone (GW1) and at the bottom of the hillslope (GW3), d) riparian soil water from September 2015 to October 2016. *Lines are time series and dots are tracer concentrations.*

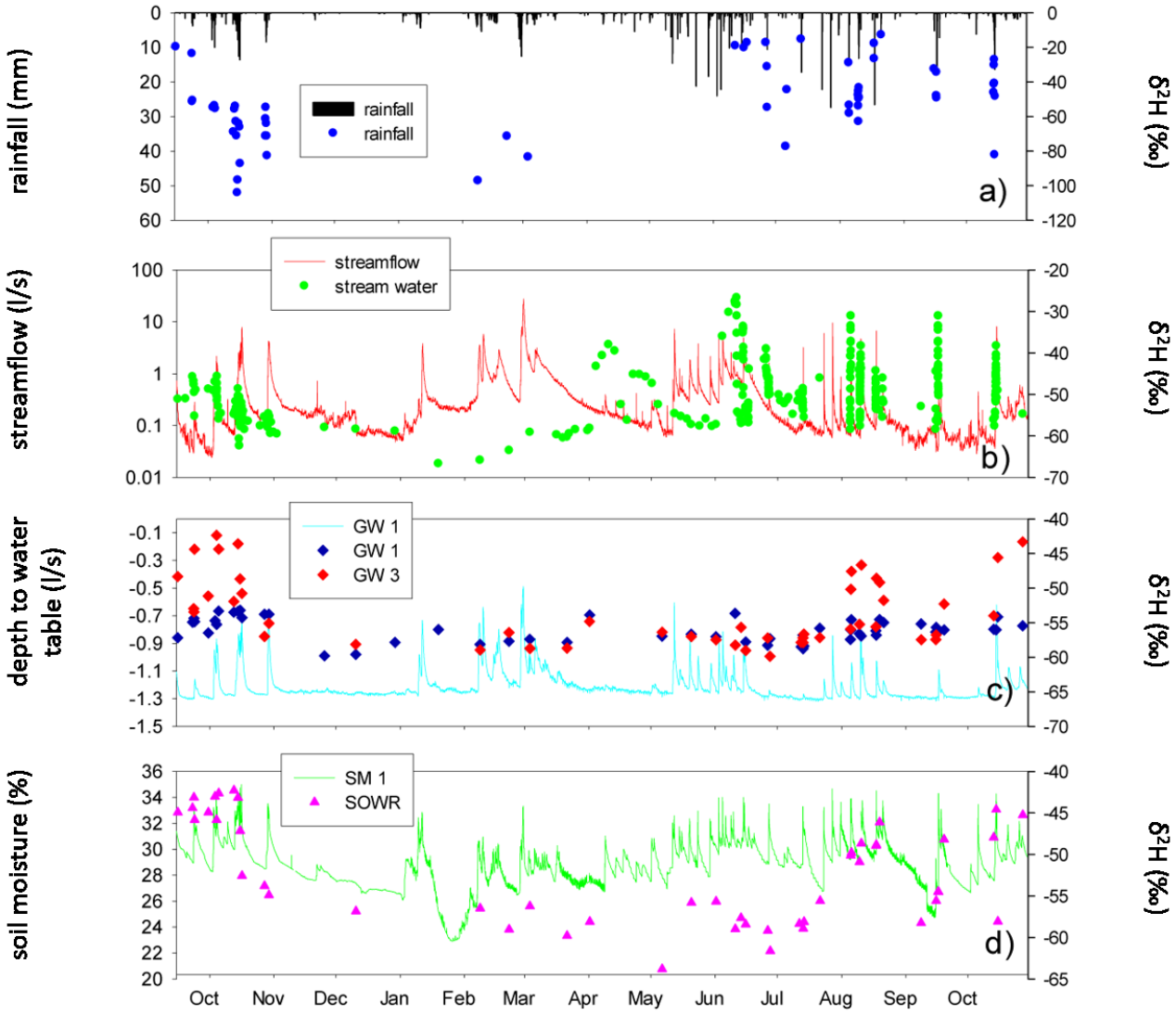

*Figure 39:T*ime series of a) rainfall, b) streamflow measured at the catchment outlet , c) groundwater in the riparian zone (GW1), d) soil moisture measured in the lower part of the hillslope (*SM* 1); and δ^2H in a) rainfall, b) stream, c) groundwater in the riparian zone (GW1) and at the bottom of the hillslope (GW3), d) riparian soil water from September 2015 to October 2016. *Lines are time series and dots are tracer concentrations.*

The chemical and isotopic composition of stream water, groundwater, soil water and rainfall are shown in Figure 40 and Figure 41.

Cl, SO_4, Na, Mg and Ca differed most for the different water sources (Figure 41). Concentrations of F, NO_2 and Li were very low in all water sources. Boxplots for these solutes show that stream water generally differed from groundwater, soil water and precipitation (Whitney rank sum test, $p<0.05$) but was more similar to groundwater than soil water and precipitation (Figure 40). In some cases, stream water did not statistically differ from groundwater or soil water. For example, stream water and groundwater in the riparian zone (GW1) had similar concentrations of Cl (Mann-Whitney rank sum test, $p>0.05$); stream

water and groundwater at the bottom of the hillslope (GW3) were similar in Ca, Mg, EC and δ^2H (Mann-Whitney rank sum test, $p>0.05$); soil water in the riparian zone sampled at 20cm depth (SOWR) was similar to stream water for δ^2H, SO_4, Na and Cl (Mann-Whitney rank sum test, $p>0.05$).

Groundwater in the riparian zone sampled at two locations (GW1 and GW4) were similar for all tracers during wet season. GW1 and GW4 were statistically different in SO_4, Na, Mg and Ca (Mann-Whitney rank sum test; $p<0.05$) for the dry period. This suggested that groundwater recharge during wet periods was quite similar in both locations, but was less similar during dry periods. The chemistry and isotopic composition of the groundwater at GW1 and GW4 remained quite stable during the sampling period. Groundwater at GW2 and GW3 was statistically different in Cl, SO_4 and Na concentrations (Mann-Whitney rank sum test, $p<0.05$), but were similar in Ca, Mg, EC and δ^2H (Mann-Whitney rank sum test, $p>0.05$). Groundwater in the upper part of the catchment (GW5 and GW6) was similar for most of the tracers, except for Cl, Mg and EC.

High variability in chemistry and isotopic composition was measured in groundwater sampled at the bottom of the hillslope (GW3). During baseflow, GW3 chemistry and isotopic composition was similar to riparian groundwater (GW1) during dry periods. With increasing wetness conditions, GW3 and GW1 tended to be different (Figure 42). During the events, GW3 tended to change consistently in ionic and isotopic concentrations. The event on August, 9 2016 was one of the events with more variability in GW3. For this event, there was a decrease of about 32 ppm, 13 ppm, 3.6 ppm and 174 μS/cm and -8.6‰ in Ca, Mg, Na, EC and δ^2H, respectively. The change in ionic concentration at GW3 was not correlated with antecedent soil moisture conditions (ASI) and event duration, but it was correlated with the rainfall amount and the streamflow increase during the events (Table 5). When GW3 changed in ionic content during the event, it became more similar to rainfall for most of the cases. This behavior indicates a mixing of groundwater at GW3 with event water probably due to a fast recharge of the piezometer by the lateral expansion of the stream or a rapid infiltration of event water at the bottom of the hillslope.

Soil water sampled in the riparian zone at 10 cm depth (SOWR3) had the highest concentrations for most of the ions. SOW3 had a different signature than soil water sampled at the same location at 20 cm depth. This difference could be due to the specific portion of the soil where SOWR3 was sampled that it was more enriched in some ions (e.g., Cl, Ca and Mg) and more depleted in other ions (SO_4 and Na).

Higher concentrations of Cl in the near surface layers of the soil can be explained by the enrichment by evaporation. Cl decreased along the soil profile, with low values in groundwater, especially in the lower part of the catchment. The higher concentration of NO_3 at 10 cm depth than at the same locations, but at 20 cm depth in the riparian zone and at 30 cm depth in the lower hillslope (Table 10, Appendix), can be explained by the fact that it originates from biological activity and the atmosphere rather than from rocks and soil weathering. Consequently, the near surface layers of the soil have high concentration of these nutrients (Muraoka and Hirata, 1988). On the contrary, high concentrations of Ca, Mg in groundwater are due to the weathering of calcareous dolomitic bedrock in the area that releases Ca and Mg in abundance when new water infiltrates. High concentrations of Na in groundwater are due to the weathering of argillified rhyolite bedrock that is rich in Na.

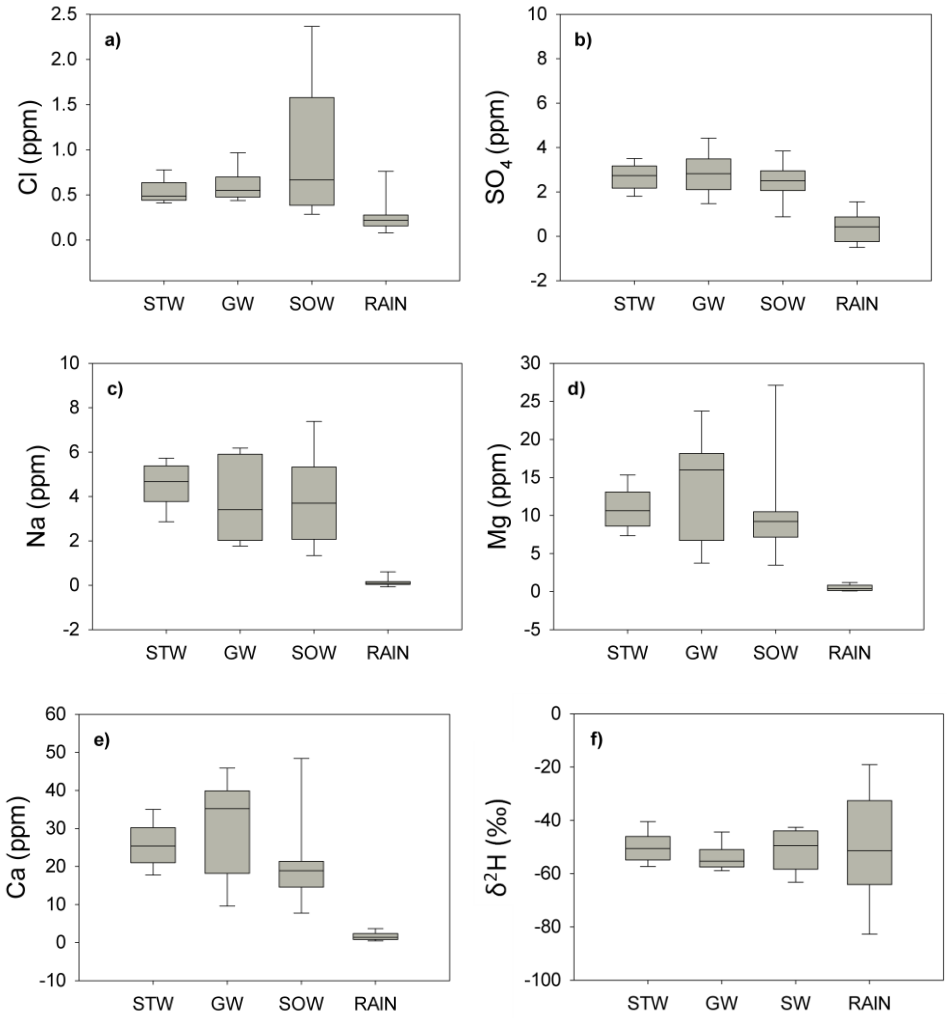

Figure 40: Box-plots of ion concentrations in streamflow (STW), groundwater at different locations (GW) soil water at different locations (SOW) and rainfall (RAIN) for rainfall events sampled between September 2015 and October 2016.

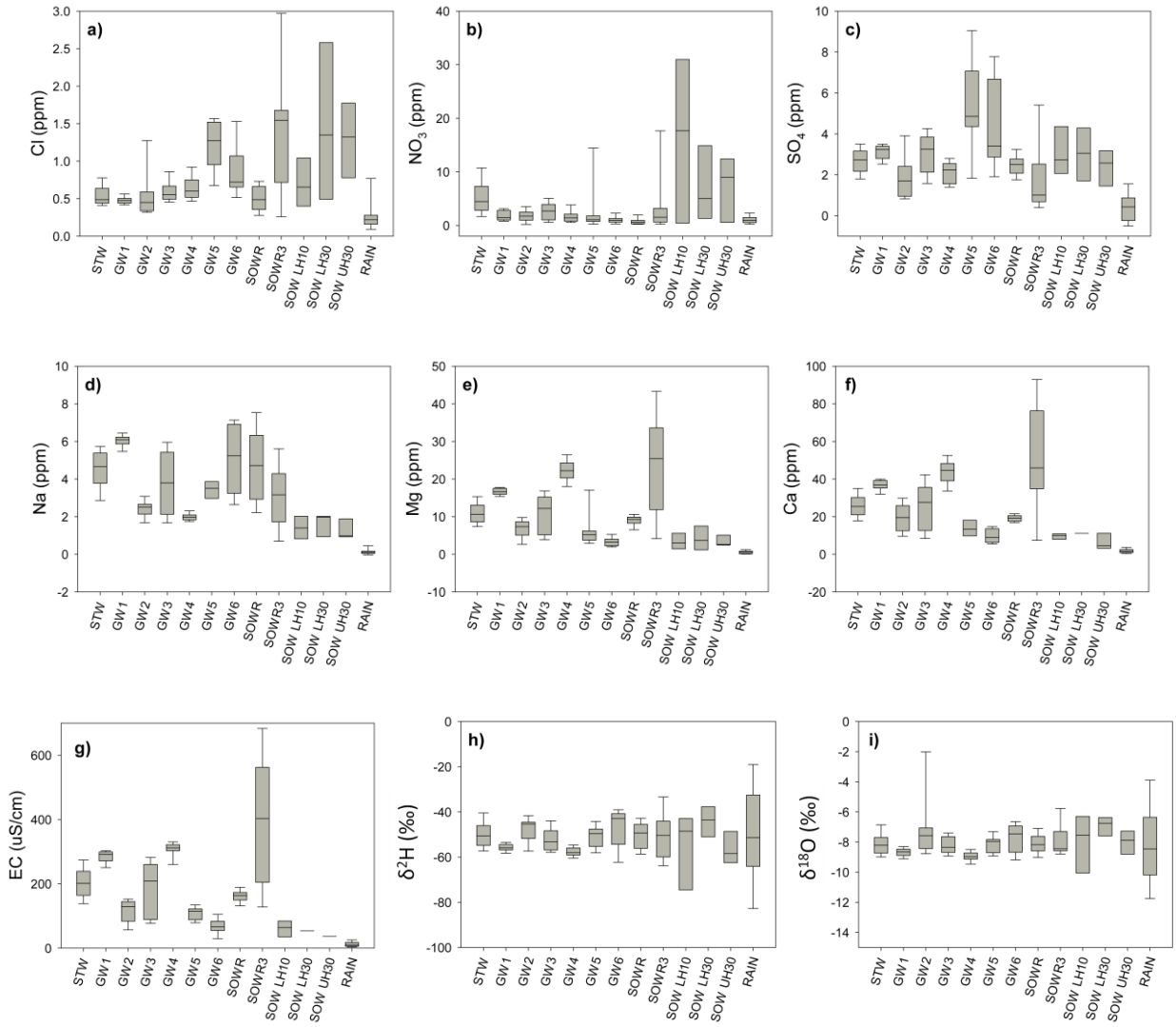

Figure 41: Box-plots of major ions (a-f), EC (g), δ^2H (h) and $\delta^{18}O$ (i) of streamflow (STW), groundwater at different locations (GW1 and GW4: riparian; GW2 and GW3: bottom of the hillslope; GW5 and GW6: upper part of the hillslope), soil water at different locations (SOWR and SOWR3: riparian at 20cm and 10 cm depth respectively; SOW-LH10 and SOW-LH30: lower part of the hillslope at 10cm and 30 cm depth respectively; SOW-UH30: upper part of the hillslope at 30cm depth) and rainfall (RAIN) for rainfall events sampled between September 2015 and October 2016. The boxes and whiskers indicate the 25th-75th and 10th-90th percentiles, respectively; the horizontal line in the box marks the median.

		Total rainfall	Max. rainfall intensity	ASI	Event duration	Streamflow increase
		mm	mm/10min	mm	hours	l/s
δ^2H	ρ	-0,364	-0,175	0,339	-0,164	-0,236
	p-value	0,176	0,523	0,209	0,549	0,388
EC	ρ	0,632	0,264	0,011	0,482	0,618
	p-value	0,011	0,332	0,964	0,066	0,014
SO_4	ρ	0,697	0,363	-0,015	0,468	0,613
	p-value	0,005	0,195	0,952	0,087	0,019
Na	ρ	0,682	0,354	-0,014	0,479	0,739
	p-value	0,005	0,189	0,954	0,069	0,001
Mg	ρ	0,657	0,261	0,046	0,493	0,696
	p-value	0,007	0,339	0,863	0,060	0,004
Ca	ρ	0,596	0,236	0,100	0,389	0,607
	p-values	0,018	0,388	0,714	0,146	0,016

Table 5: Spearman rank correlation coefficients (ρ)(and respective p-values) for the relation between the difference in isotopi composition, EC and ionic concentrations of groundwater at the bottom of the hillslope (GW3) sampled before and after each rainfall event and the event characteristics. The event characteristics are the total rainfall amount (mm), the maximum rainfall intensity of the event (mm10minr), ASI (mm), event duration (hr) and the difference between the streamflow measured at the outlet before the event and at peak flow (streamflow increase; l/s). Positive correlation coefficients indicate that GW3 tends to become more enriched in isotopic composition and diluted in ions during events with larger durations, rainfall amounts, maximum rainfall intensity, antecedent soil moisture conditions and the streamflow increase.

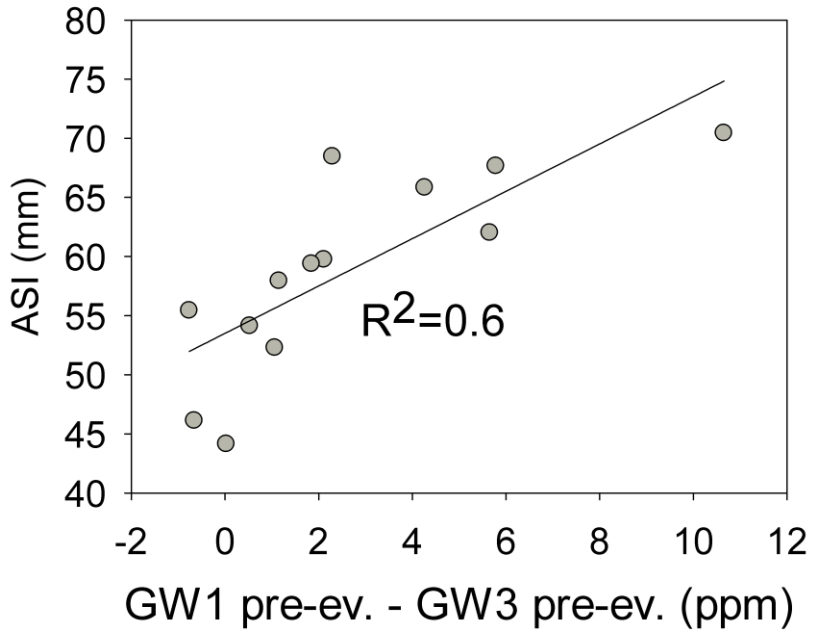

Figure 42: Relation between the antecedent soil moisture conditions (ASI, %) and the difference between the pre-event Mg concentration of riparian groundwater (GW1) and the pre-event Mg concentration of groundwater at the bottom of the hillslope (GW3) for the events sampled between September 2015 and October 2016.

3.2.3 Temporal dynamics of isotopic and geochemical tracers during the events

At the event scale, all tracers responded rapidly to precipitation input. An example of typical event scale variation in isotopic composition, EC and major ions concentrations in stream water is shown in Figure 43, showing the time series of streamflow, rainfall and major ions for the events on August 5, 2016 and October 12, 2015. Stream water EC and major ion concentrations typically decreased during rainfall-runoff events (Figure 43). This is due to the dilution effect by the inflow of new water to the system. At the same time, stream water became richer in heavy isotopes during the summer event on August 5, 2016 and more depleted during the autumn event on October 12, 2015. This was due to the more negative δ2H in winter rainfall. For the summer event on August 5, 2016, the pre-event values of δ2H , EC and Na, SO4 and Ca concentrations were -9.14 ‰, 283 µS/cm, 5.7 ppm, 3.5 ppm, 38 ppm, respectively. The values for stream water sampled at streamflow peak for this same event were -6.54 ‰ for δ2H, 129.9 µS/cm for EC, 3.1 ppm for Na, 2.4 ppm for SO4 and 17.5 ppm for Ca. For the event on October 12, 2016 δ2H, EC, Na, SO4 and Ca changed from -55.94‰, 275 µS/cm, 5.8 ppm, 1.6 ppm, 32.9 ppm before the event to -57.08 ‰, 110.8 µS/cm, 2.7 ppm, 1.1 ppm, 13.3 ppm at the peak streamflow on October 16, 2015 at 8.35 am (solar time), respectively.

For some rainfall-runoff events the changes in NO3 and K concentrations were different from those for the other major ions. Looking the evolution of NO3 concentration in streamflow during the events on October, 28 2015 and on September, 16 2016 (Figure 44), concentrations in NO3 in stream water increased with the increase in streamflow. For most events sampled between September 2015 to October 2016 in Ressi catchment for which NO3 concentrations in stream water increased in response to rainfall input, the NO3 concentration peaked a few hours after the streamflow peak (e.g. two rainfall-runoff events in Figure 44). During baseflow conditions, NO3 content was generally low for all groundwater sources, ranging from 1.1 ppm to 3.1 ppm, and in soil water in the riparian zone, ranging from 1.1 ppm to 3.6 ppm (Table 10, Appendix). Especially groundwater in the riparian zone at location GW1 and GW2 had low variability of NO_3 concentrations. NO_3 concentrations in GW4 and GW3 were more variable with a maximum of 11 ppm and 17 ppm, respectively. Stream water in baseflow also had low NO_3 concentrations and was generally similar to the NO_3 concentration measured in groundwater in the riparian zone (GW1), (Figure 44). Rainfall had a low average NO_3 concentration (1.2 ppm), although for some events it was

more than 5 ppm. Higher concentrations of NO_3 were measured in soil water sampled at the lower and upper part of the hillslope. At these locations, the average NO_3 concentrations ranged from about 7 ppm at 30 cm depth to 16 ppm at 10 cm depth, with peaks above 30 ppm. Soil water sampled at 10 cm depth in the riparian zone was more enriched in NO_3 than soil water at 20 cm depth. These results highlight the decrease in NO_3 concentration from the surface to the deeper layers in the soil to shallow groundwater.
For all events there was a positive correlation between K concentrations and streamflow but, differently to NO_3, the maximum concentrations were reached before or at some time as the streamflow peak (Figure 45).

The response of Cl was different to that of the other solutes in some cases. Cl peaked at the very initial phase for most events (Table 6). This initial peak followed a decrease in Cl in the stream that was inversely correlated with streamflow (Figure 46). The increase in Cl during the initial phase of the events was negatively correlated with stream level before the event (Figure 47). We attribute the quick increase in Cl concentrations at the start of the event to the mobilization of Cl that accumulated in the ephemeral portion of the stream as it dried out. The events without an increase in Cl content (n.9 on August 9, 2016; n.10 on August 9, 2016; n.12 on August 20, 2016) had the shortest time since the last event. Event n.14 on September 16, 2016 was an exception because it showed an increase in Cl concentration even though it occurred closely after event n.13 on September 15, 2016. We attribute this behavior was to the low rainfall for event n.13 that was not enough to wash away all the Cl that accumulated in the ephemeral portion of the stream. The mobilization of ions accumulated in the ephemeral portion of the stream was also observed for Na, Mg, Ca and, in general, for EC during events with high rainfall intensity (event n.7 on July 13, 2016 and event n.11 on August 17, 2016).

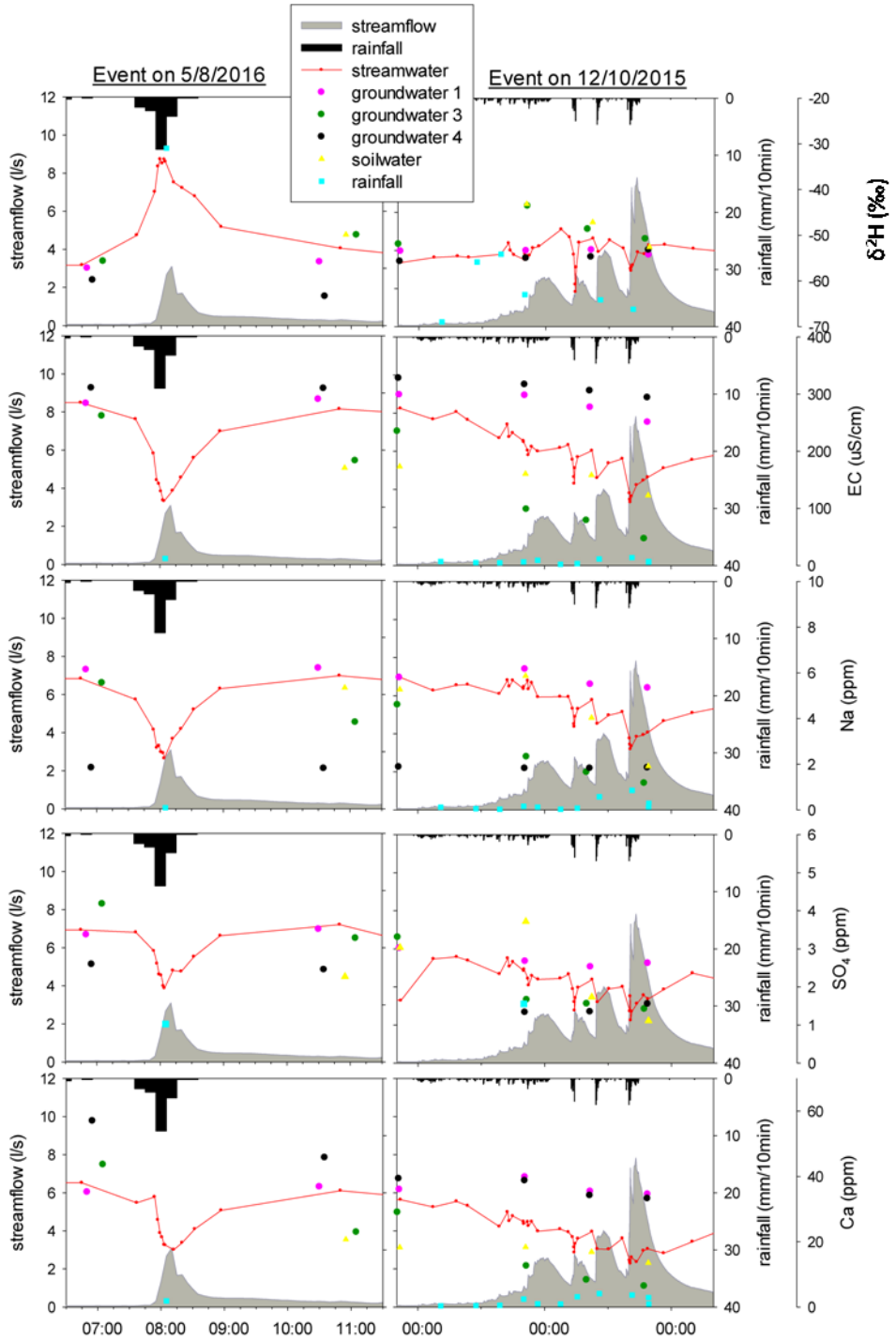

Figure 43: Time series of streamflow at the catchment outlet, rainfall and different tracers (δ^2H, EC, Na, SO_4, Ca) in the stream (red line), groundwater at different locations (GW1 pink dots, GW3 green dots, GW4 black dots), soil water in the riparian zone at 20 cm depth (yellow triangles) and rainfall (light blue squares) during the events on August 5, 2016 (left panel) and October 12, 2015 (right panel).

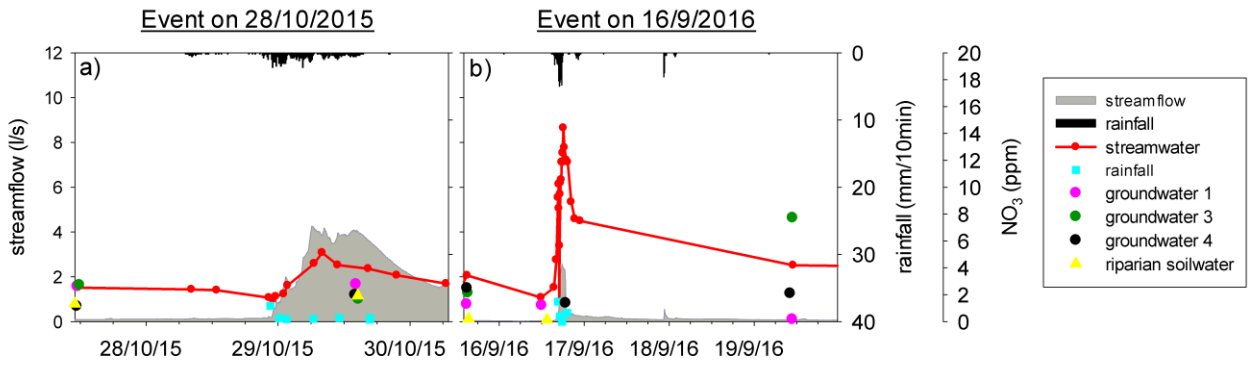

Figure 44: Time series of streamflow at the catchment outlet, rainfall and NO_3 concentrations in the stream (red line), groundwater at different locations (GW1 pink dots, GW3 green dots, GW4 black dots), soil water in the riparian zone at 20 cm depth (yellow triangles) and rainfall (light blue squares) during the event on (a) October, 28 2015 and on (b) September, 16 2016.

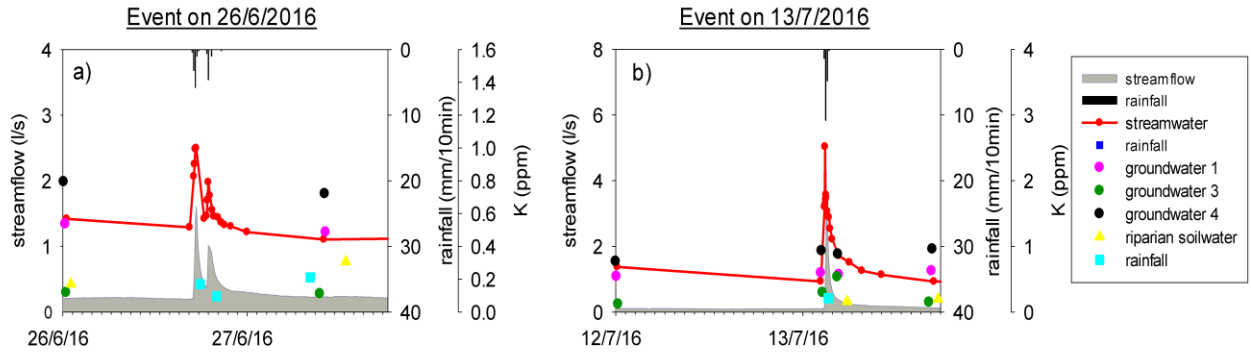

Figure 45: Time series of streamflow at the catchment outlet, rainfall and K concentrations in the stream (red line), groundwater at different locations (GW1 pink dots, GW3 green dots, GW4 black dots), soil water in the riparian zone at 20 cm depth (yellow triangles) and rainfall (light blue squares) during the event event on (a) June, 26 2016 and on (b) July, 13 2016. Note the different y-axis scale compared to figures 37, Figure 44, Figure 46.

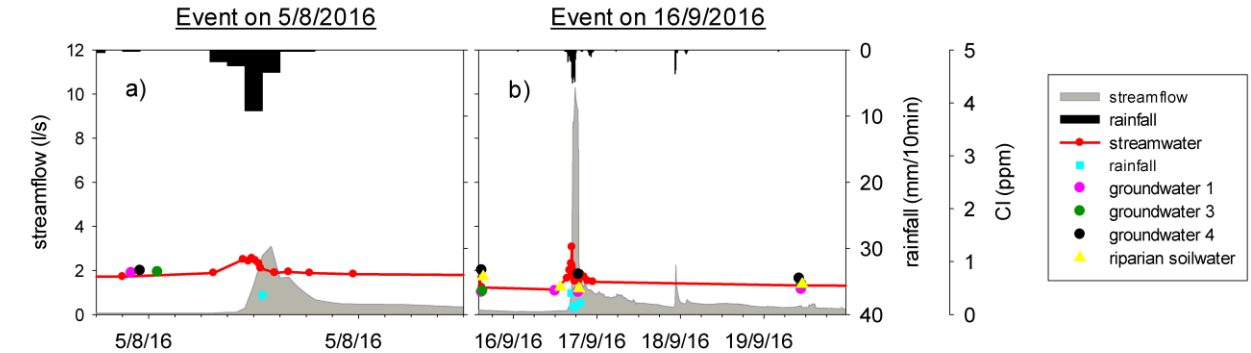

Figure 46: Time series of streamflow at the catchment outlet, rainfall and Cl concentrations in the stream (red line), groundwater at different locations (GW1 pink dots, GW3 green dots, GW4 black dots), soil water in the riparian zone at 20 cm depth (yellow triangles) and rainfall (light blue squares) during the event event on (a) August, 8 2016 and on (b) September, 16 2016.

ID	Date	EC	Cl	SO_4	Na	Mg	Ca	Time since last event (days)	Max rainfall intensity (mm/10 min)
1	23/09/2015	No	Yes	No	No	No	No	9,2	1,2
2	04/10/2015	No data						10,9	2,8
3	12/10/2015	No	Yes	Yes	No	No	No	8,9	4,6
4	28/10/2015	No	Yes	No	No	No	No	15,8	2,2
5	14/06/2016	No	Yes	No	No	No	No	4,8	7,0
6	26/06/2016	No	Yes	No	No	No	No	12,5	5,8
7	13/07/2016	Yes	Yes	No	Yes	No	Yes	16,5	10,8
8	05/08/2016	No	Yes	No	No	No	No	22,9	9,2
9	05/08/2016	No	No	No	No	No	No	0,2	1,0
10	09/08/2016	No	No	No	No	No	No	4,2	5,8
11	17/08/2016	Yes	Yes	Yes	Yes	Yes	Yes	7,9	13,6
12	20/08/2016	No	No	No	No	No	No	3,1	1,6
13	15/09/2016	No	Yes	No	No	No	No	25,7	2,8
14	16/09/2016	No	Yes	Yes	No	No	No	1,1	5,0
15	14/10/2016	No	Yes	Yes	No	No	No	27,4	6,2

Table 6: Overview when there was (cell 'Yes' in green) and there was not (cell 'Not' in white) an increase in concentration of the major ions or EC at the beginning of the event for events sampled between September 2015 and October 2016.

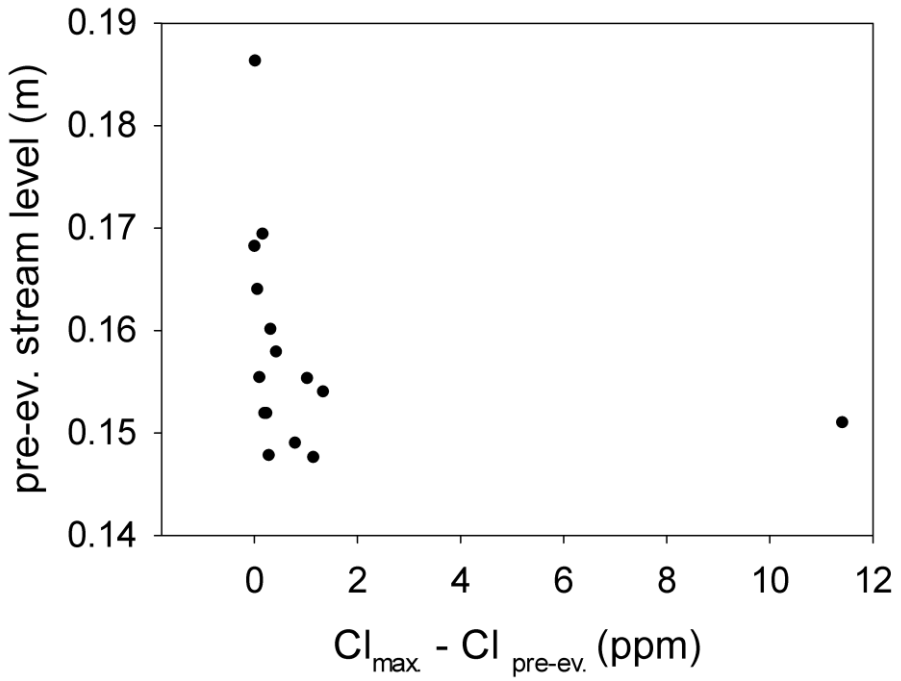

Figure 47: Relation between streamflow level before the event and the increase in Cl content in stream water (CLmax. – Clpre-ev.) for the events sampled between September 2015 and October 2016.

3.2.4 Identification of the end members for runoff

To better identify the potential end members that contribute to stream runoff, end member mixing analysis (EMMA) was applied to the dataset. The mixing plots show that rainfall, shallow groundwater and soil water in the riparian zone were the main end members of stream runoff (Figure 48). These end members define the mixing space (polygon) that encompass the majority of the stream water samples. Some stream water samples lied outside the polygon. Nevertheless, most of them were included in the mixing space that included the error bar of the end members that represented their large temporal variability (e.g., isotopic composition of rainfall). The fact that some samples lied outside the mixing space and the error bar of the end members, is a recurrent result in EMMA analysis as commonly showed in different studies such as Hooper (2001), Katsuyama et al. (2001), Fischer et al. (2015), and Liu et al. (2008). This behavior can be due to 1) the uncertainty in sample collection and laboratory analysis, 2) the temporal variations of the end-members and the characterization of a non-conservative mixing space and 3) the lack in the determination of at least one end member (Christophersen et al., 1990; Barthold et al., 2010).

Figure 48 shows that groundwater at the bottom of the hillslope (GW3) and soil water in the riparian zone at 20 cm depth (SOWR) were located in the middle of the mixing space, close to stream water samples. The similarity between GW3 and SOWR and the stream water (about 50 cm away), may indicate a lateral expansion of the stream during large rainfall-runoff events and mixing of groundwater and stream water and soil water and stream water. Shallow groundwater in the upper part of the catchment (GW5 and GW6) was located far from riparian groundwater in the mixing space and had lower concentration of most of major ions and EC than riparian groundwater. As expected, rainfall had the lowest ion concentrations. Soil water in the hillslope at 10 cm and 30 cm depth was close to rainfall signature.

The results of EMMA analysis at event scale showed that stream water changed in isotopic and geochemical concentrations during the event following specific patterns as indicated in Figure 49. During baseflow conditions, stream water was close to riparian groundwater. At the beginning of the event, stream water changed towards the rainfall signal. Stream water sampled in the second part of the event had an isotopic and geochemical signature more similar to riparian soil water and groundwater in the upper part of the catchment. At the end

of the event, stream water returned to a pre-event composition with isotopic and geochemical concentrations similar to riparian groundwater.

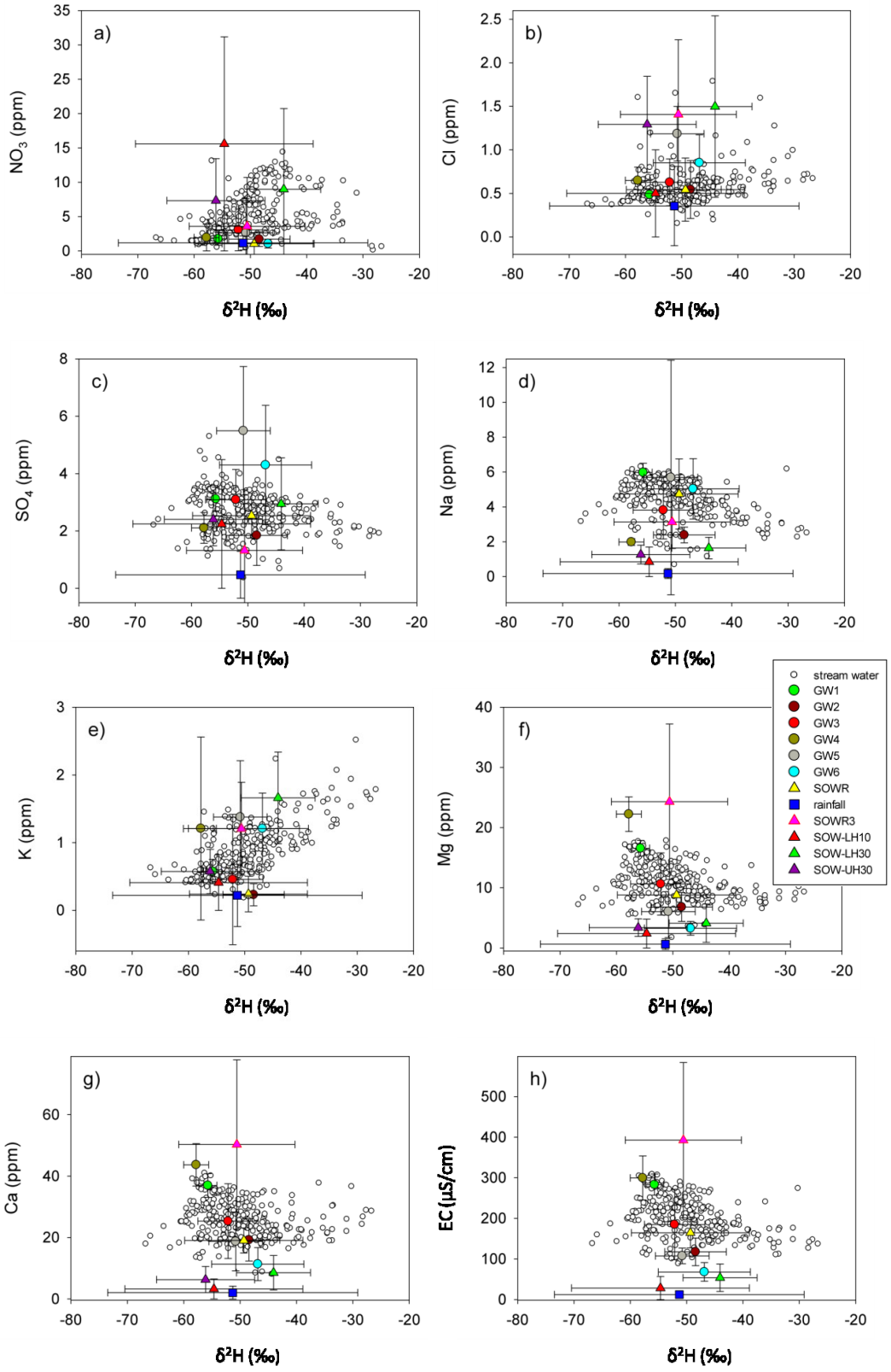

Figure 48: Mixing plots of different water sources in Ressi catchment for events between September 2015 and October 2016. The mixing plots were determined using δ^2H with NO_3 (a), Cl (b), SO_4 (c), Na (d), K (e), Mg (f), Ca (g) and EC (h). Each coloured dot represents the mean value of the samples for that end member collected before the event. Green dots represent stream water. Error bars indicate the standard deviation.

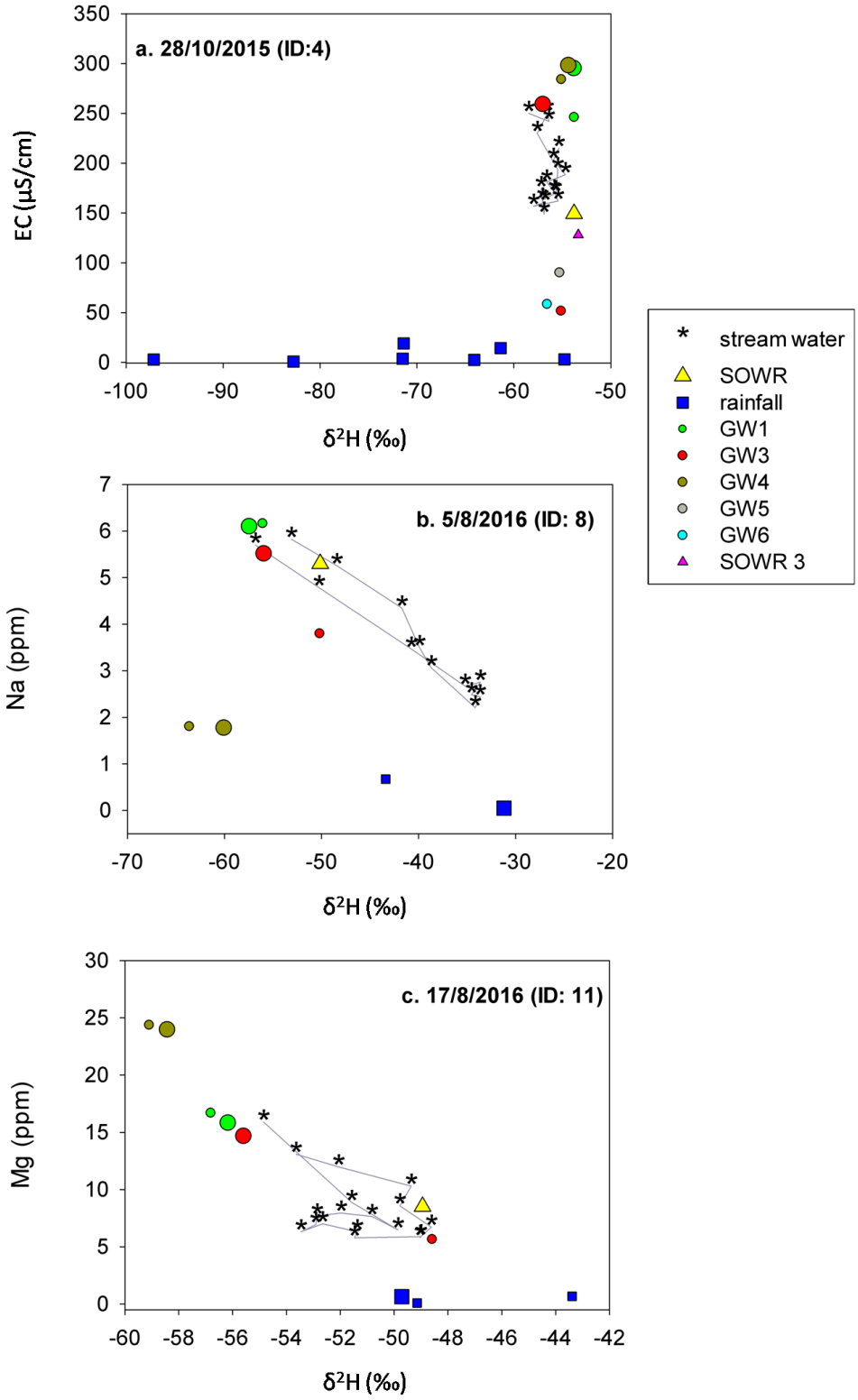

Figure 49: Mixing plots of different water sources sampled in Ressi catchment during the event on a) Octobe 28, 2015, b) August 5, 2016 and c) August 17, 2016 using δ^2H and EC, δ^2H and Na and δ^2H and Mg, respectively. Coloured dots are groundwater samples at different locations , triangles are soil water samples at different locations, squares are rainfall samples, black stars are stream water samples. Big dots, squares and triangles are the pre-event samples for each end member.

3.3 Contribution of end-members to runoff

3.3.1 Two-component hydrograph separation

Two-component hydrograph separation was applied to all events sampled from September 2015 to October 2016 using isotope, EC and major ions as tracers. The computation of the new water fraction was done assuming that the sample of stream water collected immediately before the beginning of the event was representative of old water. The results are shown in Figure 59 and Figure 60 and Table 11 (Appendix). For some events it was not possible to compute the percentage of new water using δ^2H (event n.2, n.3, n.4, n.9, n.11 and n.15), SO_4 (events n.3, n.10 and n.13) and Cl (all events except events n.1 and n.5). This was due to small difference between the isotopic composition or ionic concentrations of the stream water and the rainfall during the events.

The average event water contributions to total streamflow based on δ^2H ranged between 10 % for event n.5 on June 14, 2016 to 77 % for event n.8 on August 5, 2016; based on EC it ranged between 7 % for event n.12 on August 19, 2016 to 62 % for event n.11 on August 17, 2016; based on Ca it ranged between 6 % for event n.12 on August 19, 2016 to 49 % for event n.15 on October 13, 2016 (Table 11, Appendix). The maximum event water contribution was close to the streamflow peak for most of the events (Table 11, Appendix), with values in some cases above the 50 %. The sampling time closest to the streamflow peak had a new water fraction based on δ^2H that ranged between 22 % for event n.12 on August 19, 2016 to 79 % for event n.10 on August 9, 2016; based on EC it ranged between 15 % for event n.2 on October 3, 2015 to 71 % for event n.11 on August 17, 2016; based on Ca it ranged between 8 % for event n.2 on October 3, 2015 to 67 % for event n.3 on October 12, 2015 (Table 11, Appendix). Values of new water contribution at the peak flow higher than 50 % were characterized by high rainfall intensity or high groundwater levels before the event (Figure 50).

The average percentage of new water was higher for large rainfall events (Table 7). Event n.7 on July 13, 2016, event n.8 on August 5, 2016 and event n.11 on August 17, 2016 were an exception (Figure 51). These events had relatively low total rainfall (17 mm, 17 mm and 26 mm, respectively) and high average new water contributions (35 %, 36 % and 53 %, respectively).

The average new water contributions were significantly positive correlated with rainfall intensity and peak streamflow (Table 7). This means that with increasing mean and

maximum rainfall intensity resulting in a higher streamflow peak, the new water contribution to streamflow was larger. Similar patterns were observed for the percentage of new water close to the streamflow peak, the average new water fraction on the rising limb and the average new water fraction on the falling limb (Table 7).

Because the total rainfall amount was not significantly correlated to the average rainfall intensity (Figure 30), it was possible to identify the effects of these two event characteristics on the hydrological response of the catchment separately. The average new water contribution to the stream was a function of the average rainfall intensity during the entire event, with correlation coefficients equal to or higher than 0.79 for the rising limb, near the streamflow peak and in the falling limb (Table 7). The correlation between the average new water contribution and the rainfall amount was stronger in the falling limb ($p<0.05$) and not significant at the beginning of the event and near the streamflow peak ($p>0.05$).

The average new water fraction on the rising limb was significantly and negatively correlated to ASI and riparian groundwater level (at GW1) ($p<0.05$). Figure 52 (a and b) shows that with high values of ASI, the average percentage of new water on the falling limb was higher than or similar to the average percentage of new water on the rising limb. With decreasing ASI, the contributions of new water in the rising limb increased and was always higher than in the falling limb. These patterns were clear when using δ^2H, EC, SO_4 and Na (Sperman rank order correlation $\rho=-0.63$ $n=9$ $p=0.06$ for analyses based on δ^2H data; $\rho=-0.53$ $n=15$ $p=0.04$ for analyses based on EC data; $\rho=-0.53$ $n=13$ $p=0.06$ for analyses based on SO_4 data; $\rho=-0.60$ $n=15$ $p=0.02$ for analyses based on Na data) but were not significant using Mg and Ca (Sperman rank order correlation $\rho=-0.38$ $n=15$ $p=0.15$ for analyses based on Mg data; $\rho=-0.17$ $n=15$ $p=0.051$ for analyses based on Ca data).

At the same time, events with more than 75 mm of rainfall had larger new water contributions during the falling limb and events with moderate rainfall amounts (between 30 mm and 75 mm) had similar contributions of new water in the rising and falling limb. With decreasing rainfall amount, the contribution of new water on the rising limb increased and was always higher than in the falling limb (Figure 52, c and d). These patterns were clear when using EC and the major ions (Sperman rank order correlation $\rho=-0.75$ $n=15$ $p=<0.001$ for analyses based on EC data; $\rho=-0.53$ $n=13$ $p=0.06$ for analyses based on SO_4 data; $\rho=-0.60$ $n=15$ $p=0.02$ for analyses based on Na data; $\rho=-0.65$ $n=15$ $p=0.01$ for analyses based on Mg data; $\rho=-0.58$ $n=15$ $p=0.02$ for analyses based on Ca data), but the correlation was weaker for δ^2H (Sperman rank order correlation $\rho=-0.58$ $n=9$ $p=0.09$)

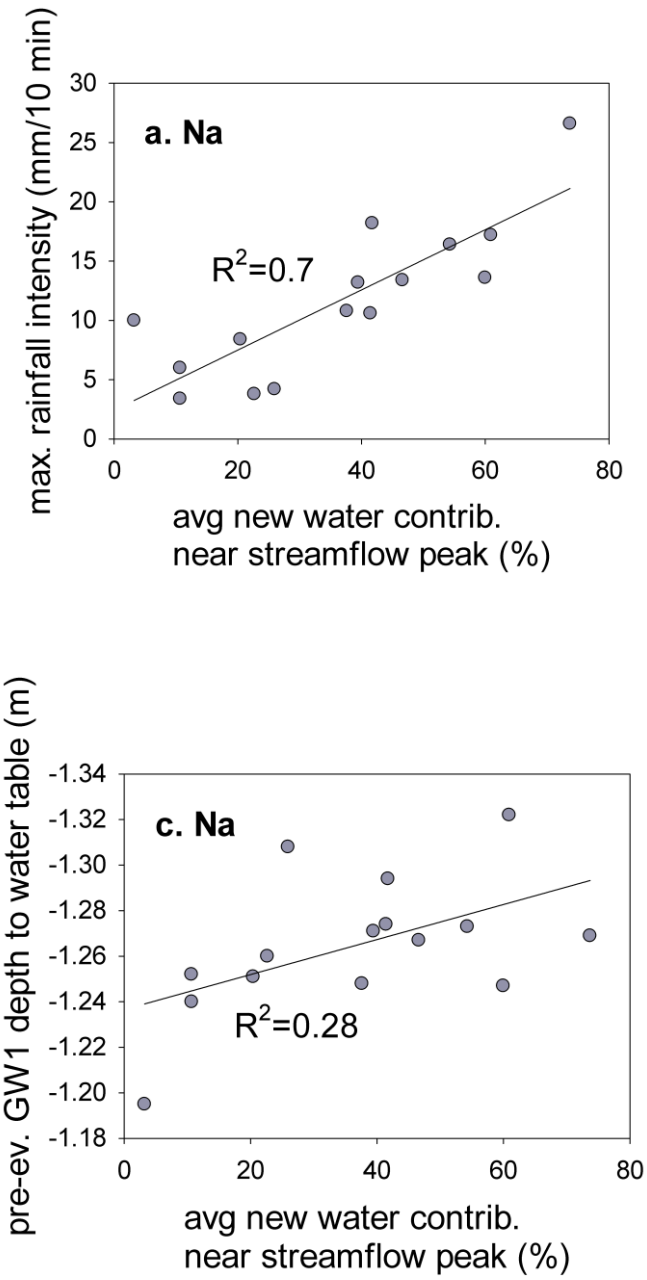

Figure 50: Relation between the average new water contribution near the streamflow peak computed using Na (a and c) and Mg (b) and the maximum rainfall intensity (a), total rainfall amount (b) and groundwater level at location GW1 before the event (c) for events sampled between September 2015 and October 2016.

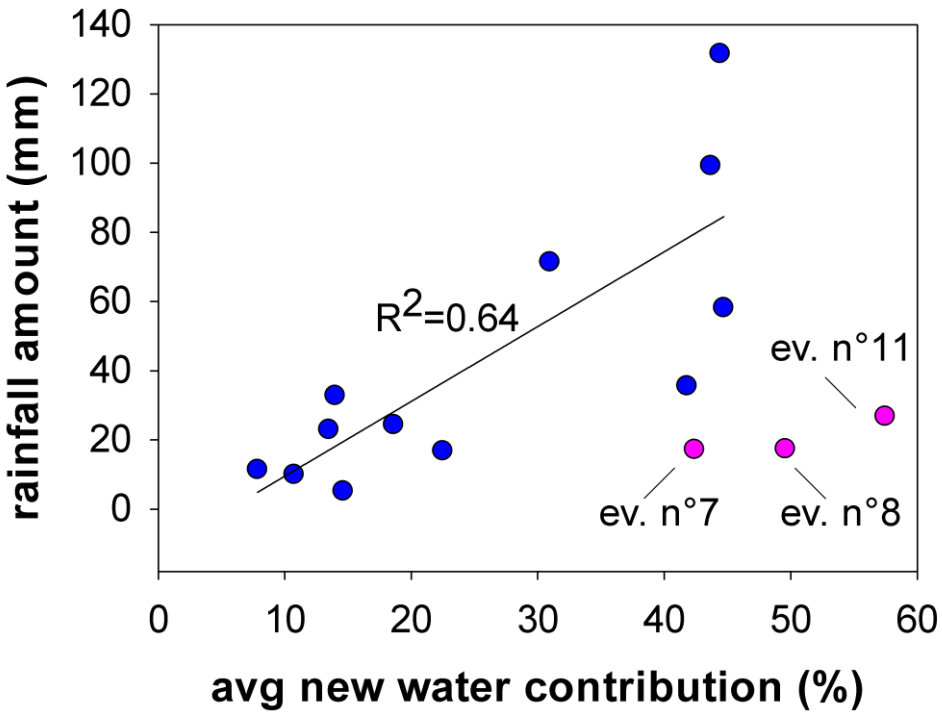

Figure 51: Relation between the average new water contribution and the total rainfall amount for each event sampled between September 2015 and October 2016. The average new water contributions are the mean value of the average new water contributions computed using EC, SO_4, Na, Mg, Ca. The regression line is relative to blue dots and exclude the pink dots for event n. 7 on July 13, 2016, event n. 8 in August 5, 2016 and event n.11 on August 17, 2016 during dry conditions.

		Rainfall amount (mm)	ASI (mm)	Mean rainfall intensity (mm/hr)	Max rainfall intensity (mm/hr)	Streamflow peak (l/s)	Groundwater level at GW1 (m)
Total event	ρ	0.543	-0.361	0.614.	0.836	0.764	-0.336
Avg new water contrib.	p-value	0.035	0.180	0.014	0.000	0.000	0.214
Near streamflow peak	ρ	0.400	-0.425	0.607	0.857	0.679	-0.436
Avg new water contrib.	p-value	0.134	0.110	0.016	0.000	0.005	0.101
Rising limb only	ρ	0.350	-0.550	0.836	0.857	0.546	-0.586
Avg new water contrib.	p-value	0.194	0.033	0.000	0.000	0.034	0.021
Falling limb only	ρ	0.600	-0.400	0.511	0.789	0.775	-0.396
Avg new water contrib.	p-values	0.018	0.134	0.050	0.000	0.000	0.138

Table 7: Spearman rank correlation coefficients (ρ) and p-values computed for the relation between new water fractions (event average, close to the streamflow peak, average for the rising limb and average for the falling limb) and the rainfall amount (mm), the antecedent soil moisture conditions (ASI; mm), the mean rainfall intensity (mm/hr), the maximum rainfall intensity of the event (max rainfall intensity; mm/hr), the streamflow peak (l/s) and riparian groundwater level measured at GW1 (m). The new water fractions are the average new water fractions computed using EC, SO_4, Na, Mg, Ca.

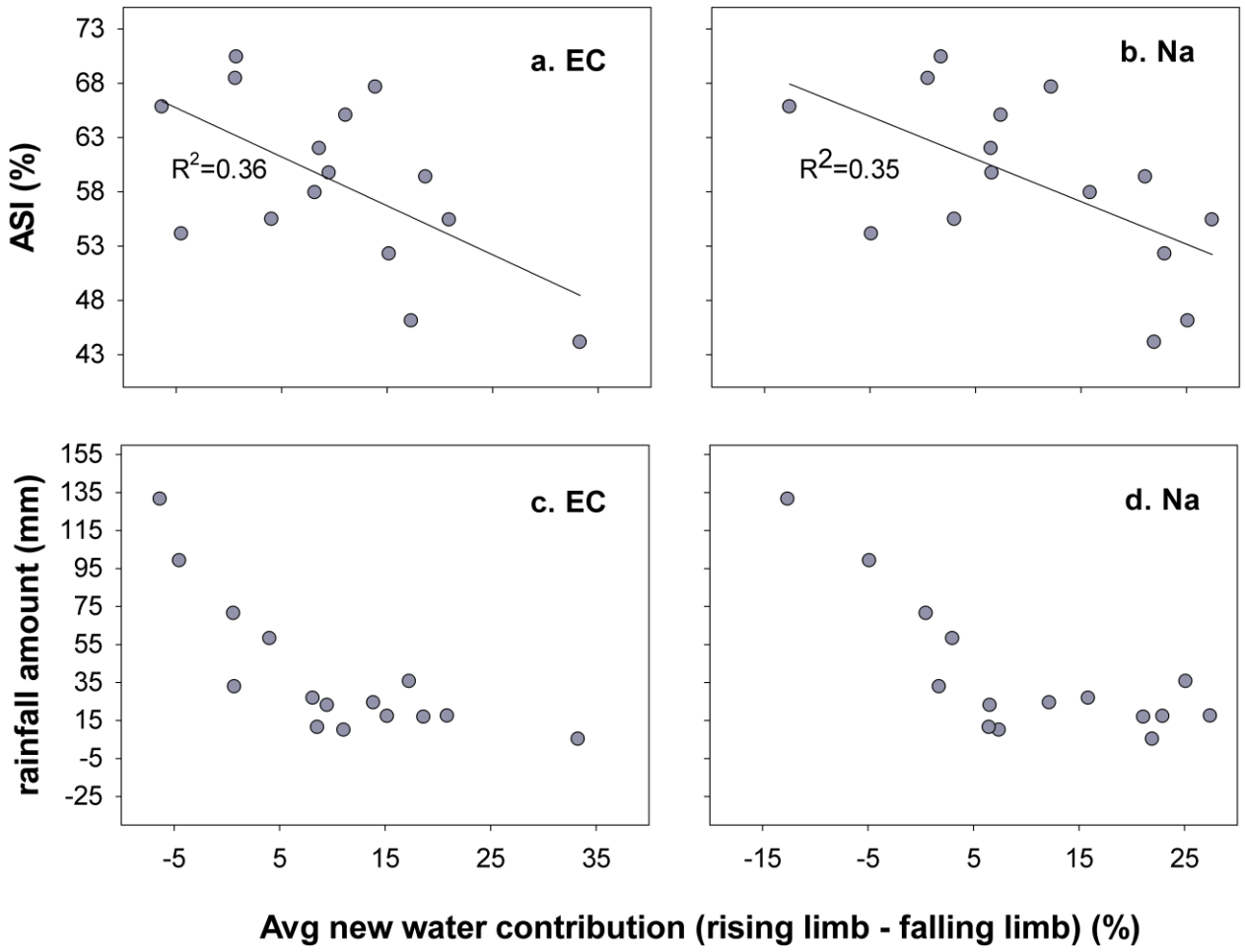

Figure 52: Relations between ASI (a and b) or the total rainfall amount (c and d) and the difference between the average new water contribution in the rising limb and the average new water contribution in the falling limb computed using EC (a and d) and Na (b and d) for all events sampled between September 2015 and October 2016.

3.3.2 Comparison of isotope-based, EC-based and major ions-based two-component hydrograph separation

The average new water contributions of the two-component hydrograph separation differed based on different tracers (Figure 53). Major ions-based and EC-based two-component hydrograph separation gave similar results, but these results differed from those obtained using δ^2H. For most of the events, δ^2H-based hydrograph resulted in higher average new water contribution than major ions-based and EC-based hydrograph separation. For some events, results based on δ^2H were much higher than those based on EC and major ions. For example, the average new water contributions based on δ^2H and Ca for event n.7 on July 13, 2016 and event n.8 on August 5, 2016 differed by 35 % and 30 %, respectively. Generally, these differences were larger for events with dry antecedent soil moisture conditions and high mean and maximum rainfall intensity but a few events showed the opposite. For example, event n.5 on June 14, 2016 had a lower average new water contribution based on δ^2H hydrograph separation than on EC and major ions. Event number 10 on August 09, 2016 had a lower maximum new water contribution based on δ^2H hydrograph separation than on EC and major ions. Event n.1 on September 22, 2015 and event n.12 on August 19, 2016 also had lower average new water fractions on the rising limb and near the streamflow peak of δ^2H than Mg and SO_4, respectively. All of these events were characterized by high antecedent soil moisture conditions and a short time since the last event (less than 10 days) (Table 12, Appendix). Event n.14 on September 16, 2016 had a higher average new water contribution computed using δ^2H than EC and major ions, even though it was characterized by short time since the last event (about 1 day). This results can partially be explained by the low rainfall amount of the previous event (n.13) on September 15, 2016 (5.2mm) and the consequently small difference between the two events (event n.13 and event n.14) in antecedent soil moisture conditions, the lowest of the entire sampling period.

A higher average new water fraction computed using δ^2H-based hydrograph separation than using major ions-based and EC-based hydrograph separation was more marked on the rising limb than on the falling limb (Figure 54). On the recession limb, new water contributions computed using δ^2H and the ions differed by less than 11 % for most of the events. On the rising limb, average new water contributions computed using δ^2H were generally higher, and in some cases much higher, than those computed using EC and major ions. For example,

the average new water contribution in the rising limb based on δ^2H and Ca for event n.7 July 13, 2016 and event n.8 on August 5, 2016 differed by 48 % and 34 %, respectively. These differences in event water contributions on the rising limb were larger for events characterized by dry antecedent conditions and low pre-event streamflow (Figure 55). Differences in average new water contributions computed using δ^2H and EC or major ions in the falling limb were significantly correlated with the streamflow before the events, with a larger difference for events with low pre-event streamflow (Figure 56).

The time series of the differences between the average new water computed using δ^2H and the average new water computed using EC or the major ions during each event (see examples in Figure 57) indicate that the higher new water contribution computed using δ^2H than using EC and major ions peaked before the streamflow peak. This behavior was verified for most of the events. For some events, the difference peaked after the streamflow peak or, in some cases, both before and after the streamflow peak. For example, event n.12 on August 20, 2016 had a peak in the difference in the new water contribution computed using δ^2H and EC and major ions only after the streamflow peak. On the contrary, for events n.1 on September 23, 2015 and n.8 on August 5, 2016 the difference in the new water contribution computed using δ^2H than using EC and major ions peaked both before and after the streamflow peak (Figure 57).

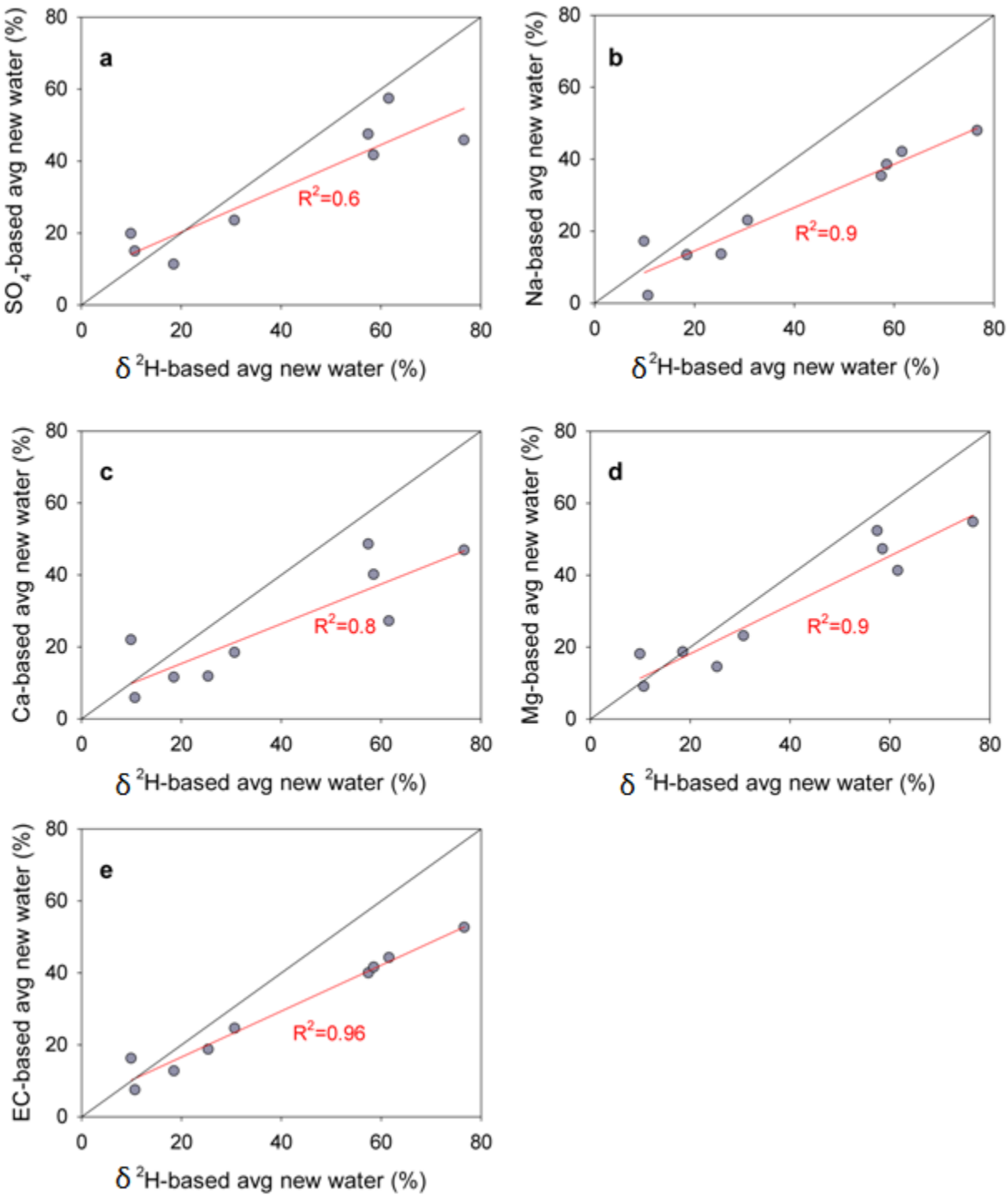

Figure 53: Relation between the average new water contribution computed with δ2H and the average new water contribution computed with SO4 (a), Na (b), Mg (c), Ca (d) and EC (e) for the events sampled between September 2015 and October 2016. The lines indicate the 1:1 line and the regression line.

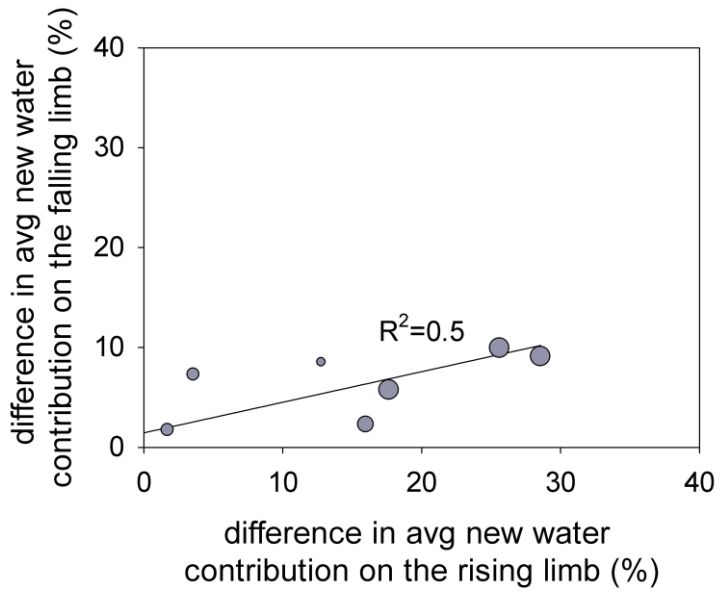

Figure 54: Relation between the difference in the average new waters fraction calculated using δ^2H and the average new water fraction computed using Mg on the rising limb and the difference in the average new water using δ^2H and the average new water using Mg on the falling limb for the events sampled between September 2015 and October 2016. The symbol size increase with increasing time since the last event.

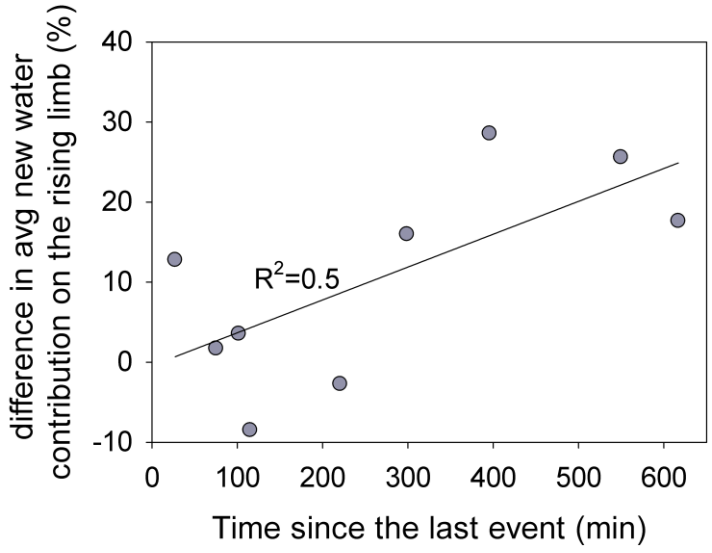

Figure 55: Relation between the time since the last event and the difference in the average new water contribution to streamflow calculated using δ^2H and Mg on the rising limb for the events sampled between September 2015 and October 2016.

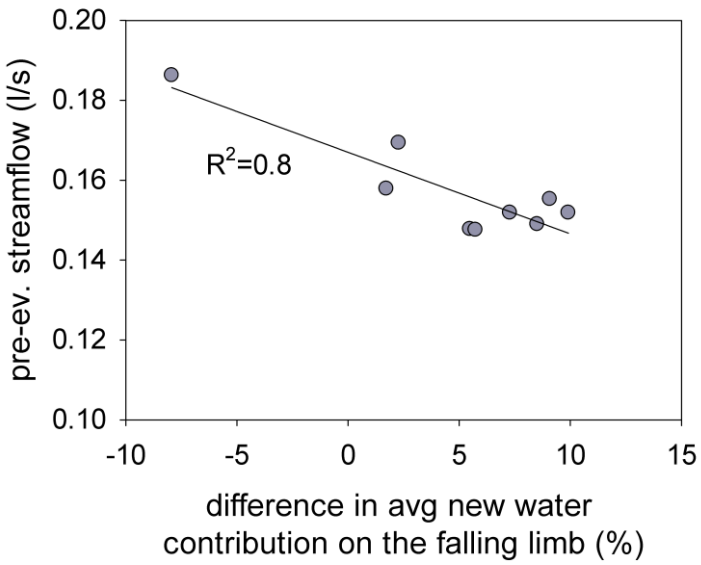

Figure 56: Relation between the streamflow before the event and the difference in the average new water contribution to streamflow calculated using δ^2H and Mg on the falling limb for the events sampled between September 2015 and October 2016.

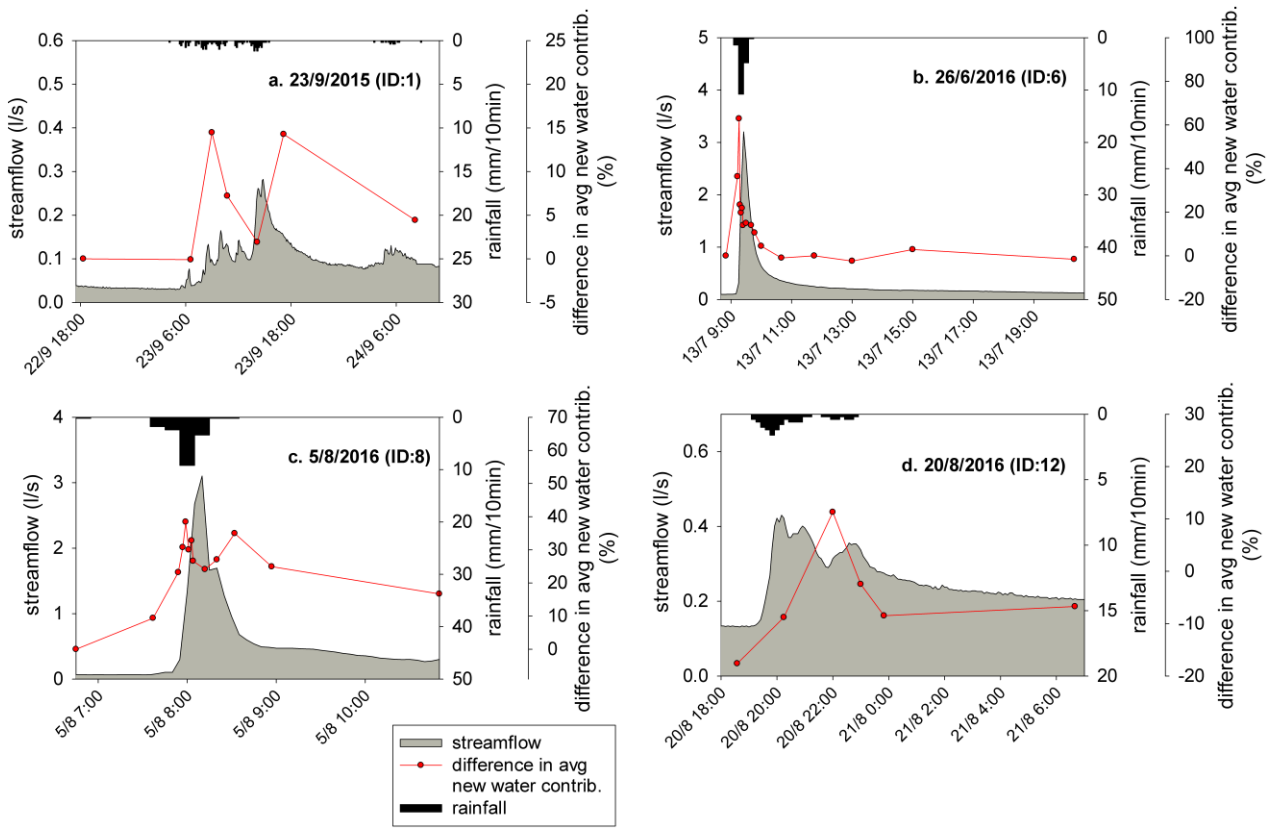

Figure 57: Time series of streamflow and the differences between the average new water contribution determined using δ^2H and the average new water contribution determined using Ca (a), EC (b), Na (c) and SO_4 (d).

3 DISCUSSION

Controls on water table response

Hydrometric data was used together with isotopic and geochemical tracers to investigate runoff generation processes in Ressi catchment. Rainfall and soil moisture showed high temporal variability during the studied period from September 2015 to October 2016, with the alternation of wet and dry periods. Both at surface and subsurface level, the catchment's hydrometric response was quick. The general short lag time for a response to rainfall input can be explained by the small area of the Ressi catchment as found also in Frisbee et al. (2011), but is also affected by the low permeability of the soil profile and the bedrock and the quickly contribution of event water to the stream.

During the dry period, the lag time between the beginning of rainfall and the groundwater or soil water peak was longer than during the wet period. During the wet period, groundwater and soil water peaked before the streamflow peak; the time lag between the streamflow peak and the groundwater or soil water peak was also shorter than during the wet period. This might be due to the fact that in dry period the mesopores and macropores of the soil were dry and needed more time to be filled, while the storage that needed to be filled decreased and the connectivity between the stream and the hillslope increased during wet antecedent conditions (Burns et al. 2001). Similarly, Haught and van Meerveld (2011) found that transient groundwater response changed with increasing antecedent wetness conditions, from a groundwater response after the streamflow peak to a groundwater response before the streamflow peak. Haught and van Meerveld (2011) related the change in groundwater response to the increasing connectivity between the hillslope and stream.

High spatial variability in the lag time in groundwater was observed during all events, indicating that the response of the water table to rainfall input was not uniform. A short time lag between the beginning of the event and the groundwater peak in the hillslope at locations GW5 and GW6 indicated a fast recharge of groundwater in the upper part of the catchment. Groundwater at the bottom of the hillslope at location GW3 had the shortest time lag between the beginning of the event and the streamflow peak. The most logical explanation of this observation is a lateral infiltration of stream water and the consequent rapid change in shallow groundwater in that portion of the catchment. Indeed, in the lower part of the catchment the stream flows on an impermeable rock layer that extends laterally near the

surface level to the bottom of the hillslope. This specific topography facilitates the lateral expansion of the stream and the fast response of the water table but detailed groundwater level measurements or high resolution tracer data are needed to confirm this flow-direction. Groundwater in the lower part of the catchment near the outlet (GW1, GW2 and GW4), had longer response time than groundwater in the upper part of the catchment. This might be due to the fact that riparian groundwater was recharged by a larger area comprising the whole catchment and the smaller permeability of the porous material in the lower part of the catchment. Other studies highlight high spatial variability in groundwater response, among them Fannin et al. (2000), that examined the variation in groundwater response of 12 piezometers in gravelly, sandy soils in the Carnation Creek catchment in British Columbia, and Bachmair and Weiler (2012) investigate the main factors controlling the water table response to precipitation input at hillslope scale in a catchment at the foot of the Black Forest in southwestern Germany. The high spatial variability in groundwater response was also observed by Penna et al. (2014) in a study conduced at hillslope scale in the alpine Bridge Creek Catchment, Northern Italy. In this study, Penna et al. (2014) showed that groundwater response was variable across the catchment and that groundwater in the upper hillslope peaked earlier than groundwater in the lower part of the catchment. This observation was related to the influence of soil depth, with deeper in the lower part of the catchment.

Direct runoff was related to antecedent soil moisture condition and precipitation (ASI+P) following a threshold behavior, similarity to other studies such as Penna at al. (2015) and Detty and McGuire (2010). During the dry season, low runoff coefficients associated with a rapid response of streamflow during the rising limb and a quick recession, suggest that stormflow was mainly generated by direct channel precipitation, by saturated overland flow in the area very close to the stream and by quickly transport of event water from the hillslope to the stream through preferential flow pathways. These conclusions were also confirmed by the results from two-component hydrograph separation that showed high event water contribution during summer events. On the contrary, high runoff coefficient occurred during events in wet conditions suggesting an increased contribution to stormflow from other part of the catchment as subsurface stormflow. These conclusions were also confirmed by the longer recession for the events in the wet season than the events occurred in the dry season.

Isotopic and chemical variability in stream water

The spatio-temporal variability of isotopic and geochemical (EC and major ions) signature of stream water helped to better understand runoff dynamics of the Ressi catchment during

baseflow and high flow conditions. During high flow conditions, stable isotopes of water (δ^2H and $\delta^{18}O$), EC and major ions (SO_4, Na, Mg, Ca) in stream water changed quickly with precipitation input due to dilution effect of rainfall. Similar results were found by Caissie et al. (1996), Ladouche et al. (2001) and Arreghini et al. (2005).

NO_3 and K tended to increase in concentrations during most of the events. We hypothesize that these solutes are stored on the surface or in the first layers of the soil and are displaced by rainfall during an event. High NO_3 concentrations in the first layers of the soil could be due to the interaction of nitrogen in the atmosphere with rain water and the biological activity of nitrogen-fixing bacteria in the soil. For example, *Frankia alni* is a bacteria living in symbiosis with Alder species (Mueller et al., 2016). Alder is present in the Ressi catchment, so the high concentration of NO_3 in the first layers of the soil could be due to the presence of this bacteria. Nevertheless, other sources of NO_3 could be the atmosphere and the mineralization of soil organic nitrogen (De Vries and Breeuwsma, 1987). The influence of local agricultural activities taking place in an upper conterminous area just outside the catchment (near the rain gauge) might explain the flushing of NO_3 during the rainfall events, but we would then also expect a NO_3 increase in groundwater (Wang et al., 2015, Harter at al., 2002), which we did not observe. Consequently, the increasing NO_3 concentrations in stream water during rainfall events could be associated to mobilization of NO_3 accumulated in the first layers of the soil and their flushing down into the stream through preferential flow pathways.

For most events sampled from September 2015 to October 2016 the NO_3 peak was reached a few hours after the streamflow peak. Similar results were found also in Mueller et al. (2016) in a study carried out in four forested headwater catchment in the Swiss Alps. They found high concentration of NO_3 in stream water during high flow conditions only for the catchment with a large percentage of shrub cover (mainly Alnus viridis (Chaix) DC and Sorbus aucuparia). Similarly to our results, Mueller et al. (2016) also observed that NO_3 peaked several hours after the streamflow peak and this behavior was explained by the mobilization of NO_3 by rainfall from soil layer in area far from the stream where green alder was more abundant. Similarly, high concentrations of NO_3 in the stream associated with near surface lateral flow from hillslope during the recession limb of the hydrographs were observed by Zhang et at. (2011). Rusjan et al. (2008) found a positive correlation between the increase in NO_3 concentration in the stream and the increase in streamflow during 15 rainfall-runoff events monitored in 2006 in a forested catchment in Slovenia, with the NO_3 peaks always being delayed by a few hours with respect to the streamflow peaks. In this study, the main

source of NO_3 was attributed to the symbiotic relationship of black alder with the bacterium *Frankia alni,* and the delay in NO_3 response was attributed to the flow through the top layers during the second part of the event in the riparian zone and on the hillslope.

K concentrations in stream water increased for all rainfall events and peaked before or at the same time as the streamflow peak. Suarez et al. (2015) observed that the main sources of K were the leaves of the plants and the organic material. Indeed, the decomposition of leaves and other plant tissues released large quantities of K. Consequently, the increase in K concentrations in the stream during high flow conditions could be explained by the contact of rainfall with the leaves on the ground surface and the passage of rainfall through the very first layer of the soil where K was high concentrated because the decomposition of organic matter (Kennedy, 1977). Consequently, K was easily washed out by new water and quickly transported into the stream during the first part of the events through overland flow and flow in the first centimeters of the soil. Similarly, Kennedy (1977), Feller and Kimmins (1979), Caissie et al. (1996), and Suarez et al. (2015) found that K concentration in stream water increased during high flow conditions because of the mobilization of K by rainfall from the surface organic layer to the stream. The time lag between the peak concentrations in K and NO_3 suggested different flushing processes during the rainfall-runoff events. In the first part of the events, we suppose that rainfall reached the stream very quickly through overland flow and flow in the first centimeters of the soil, transporting high quantities of K. The increase in NO_3 concentration in stream water after the streamflow peak, suggested that shallow subsurface flow paths (in the first layer of the soil below the near surface layers) were activated in the second part of the events.

Cl concentration in the stream increased at the beginning of the rainfall-runoff events. After this initial positive peak, Cl concentrations decreased following the rainfall signal. This behavior occurred during events with low streamflow before the event and was also observed for Ca, Mg and Na for events with high rainfall intensity. This observation can be explained by the accumulation of ions when the ephemeral portion of the stream bed that is active only during rainfall-runoff events and the near stream areas dry up. We suppose that between two different rainfall-runoff events some of the water accumulated in the ephemeral part of the stream evaporates leaving a deposition of ions on the rocks and the organic material. Similarly, evaporation from near stream areas also result in an accumulation of ions. These accumulated ions tend to be immediately washed away at the beginning of the

following rainfall-runoff event when rainfall falls on the ephemeral portion of the stream and flow is activated again.

Isotopic and chemical variability of the water sources

Analysis of mixing plots showed that rainfall, shallow groundwater and riparian soil water were the major contributors to streamflow. High spatial variability of isotopic and geochemical composition of shallow groundwater was observed in Ressi catchment. High spatial variability of shallow groundwater indicates a complex hydrochemical behaviour of groundwater, even at a small spatial scale, suggest that different groundwater from different parts of the catchment contributes to stormflow during rainfall-runoff events. During baseflow conditions, riparian shallow groundwater was the main source of stream runoff because it was isotopically and geochemically similar to stream water. Similar results were found by many other studies, such as Inamdar and Mitchell (2007), Wenninger et al. (2004) and Inamdar et al. (2013). Riparian shallow groundwater did not change significantly in isotopic composition, EC and major ions concentrations during most of the events. This suggests that riparian groundwater is a large storage and that the amount of recharge is small compared to the amount of water in the storage. However, it is not one well-mixed storage but is rather a collection of different storages filled with water coming from different parts of the catchment. Riparian groundwater contribution to streamflow during baseflow conditions was affected by seasonality. During the dry season, GW1 and GW4 were statistically different in major ions. The projection of GW1 and GW4 in the mixing space showed that the two riparian groundwater sources were far each other and that GW1 was the dominant source of streamflow during baseflow conditions. During wet periods, GW1 and GW4 were isotopically and geochemically similar. These results suggested an expansion of riparian groundwater during wet conditions, with a consequently mixing of the two riparian groundwater that both contributed to streamflow during baseflow conditions. Groundwater at the bottom of the hillslope (GW3) was characterized by high temporal variability during most events, with an isotopic composition and geochemical concentrations close to streamflow at the end of the events. Also soil water in the riparian zone at 20 cm depth (SOWR) was located in the middle of the mixing space, close to stream water samples. Because GW3 and SOWR were located very close to the stream (about 50 cm), a lateral expansion of the stream during large rainfall-runoff events could cause mixing between groundwater and stream water and between soil water and stream water. Soil water on the hillslope was different from riparian groundwater and had low concentrations, suggesting a

mix between rainfall and soil water in the first layer of the soil. Shallow groundwater in the upper part of the catchment at location GW5 and GW6 was statistically different from riparian groundwater and also had lower concentrations for most of major ions.

In the first part of the events, stream water changed towards rainfall, suggesting a consistent event water contribution on the rising limb of the hydrograph. During the recession limb of most of the events, stream water changed towards soil water and shallow groundwater on the hillslope in the upper part of the catchment (GW5 and GW6), suggesting the development of subsurface connectivity during the events. At the end of the events, stream water returned to pre-event conditions with a chemical composition similar to riparian groundwater. The shift of stream water toward rainfall at the beginning of the event and to soil water during the second part of the event is in agreement with the results obtained by Inamdar et al. (2013), Penna et al. (2015) and Rice and Hornberger (1998). Inamdar et al. (2013) conducted a study on 42 storm events in a small forested catchment in USA and observed that stream water moved from riparian groundwater and deep groundwater to surficial sources (among them precipitation, throughfall, stemflow and litter leachate) on the rising limb of the hydrograph, and water moved to soil water and shallow groundwater on the falling limb of the hydrograph. Similarly, Penna et al. (2015) found that riparian groundwater, rainfall and soil water were the main contributors to storm event runoff with contributions in that order during the events. A similar conceptual model for the dynamics of different contributors to runoff was developed by Rice and Hornberger (1998) in a study of two years in a small forested catchment in north-central Maryland. Rice and Hornberger (1998) monitored 10 rainfall events using different tracers (δ^2H, $\delta^{18}O$, Cl, Si, Na) and concluded that streamflow is supported by groundwater during baseflow conditions as in the initial phase of the event precipitation and throughfall contribute to stormflow and changed stream water chemistry. During the event, soil water starts to contribute to streamflow because the percolation of event water through the soil column. When it stopped raining, event water and soil water contributions decreased and stream water returned to a pre-event water composition. On the contrary, Barthold et al. (2016) investigated the origin of stormflow in a headwater catchment dominated by subsurface flow and did not found a dominant source of stormflow during the event. They concluded that both event water, consisting in overland flow, and pre-event water, consisting in return flow, were similarly important for stormflow generation and highlighted the important role of pipe flow to discharge pre-event water from the shallow subsurface into the stream via surface flow paths.

Interpretation of two-component hydrograph separation results

Two-component hydrograph separation was applied at 15 rainfall-runoff events sampled from September 2015 to October 2016 in Ressi catchment. For most of the events, runoff was mainly dominated by pre-event water. This is in agreement with other studies conducted in mountain areas by Wenninger et al. (2004), McDonnell (1990), Peters et al. (1995), Hinton (1994), Marc et al. (2001) and Soulsby et al. (1998). During some summer events, the contribution of pre-event water was lower than for events in the wet periods, with average values of pre-event water contribution in summer events reaching approximately 25 %. Similar values were also found by Muñoz-Villers and McDonnell (2012) in a study in a forested mountain catchment on volcanic substrate in Mexico, with on average percentage of new water above 70% for some events in the dry season.

Event water contributions to the stream was higher on the rising limb of the hydrograph than the recession limb. After streamflow peak, event water contribution progressively decreased and the percentage of old water contribution coming from other water sources in the catchment, mainly riparian groundwater and soil water, increased. These results are similar to the findings of Inamdar and Mitchell (2007) who conducted a study in the Point Peter Brook watershed, a glaciated, forested, watershed in Western New York, USA. They monitored 10 storm events with different characteristics and antecedent conditions and observed that stream water during baseflow conditions was mainly composed by deep groundwater. During the event, throughfall mainly contributed to runoff on the rising limb of the hydrograph as the recession limb was dominated by riparian groundwater contributions. The large variability in event and pre-event water fractions for the events sampled in Ressi catchment highlight the influence exerted by different hydrological conditions on the catchment response (Hinton, 1994). The results of the two-component hydrograph separation applied to the 15 rainfall events showed that average new water contributions to stormflow increased with rainfall amount, rainfall intensity and streamflow peak. Kvaerner and Klove (2006) showed a dominant contribution of event water during autumn events characterized by high rainfall intensity and high streamflow. Correa et al. (2017) did not found seasonal variation in event water contribution to streamflow and observed high prevent water contribution both in the drier and wetter season (94 % and 84 %, respectively). Fischer et al. (2016) carried out a study in a pre-alpine catchment in Switzerland where he showed increasing new water contributions with increasing event size and rainfall intensity. High event water contributions associated with large storm events and high rainfall intensity

were also reported by James and Roulet (2009) and Pellerin et al. (2008). The increase in average new water contribution with increasing rainfall amount and rainfall intensity was also observed in a previous study conducted in Ressi catchment (Penna et al., 2015). However, in the study conducted by Penna et al (2015) it was not possible to investigate the influence of rainfall amount and average rainfall intensity separately because these two event characteristics were significantly correlated (R^2=0.5, n=16, p<0.05; Penna et al., 2015). For the events sampled between September 2015 and October 2016 in Ressi catchment, rainfall amount was not significantly correlated with the average rainfall intensity, which allowed a better understand of streamflow generation dynamics at event scale in the catchment. The results of this study highlight that rainfall intensity influenced the average new water contribution during the whole event. Conversely, rainfall amount played a central role in the determination of the average new water contribution in the second part of the event, with higher average contributions of new water on the falling limb than on the rising limb for large events. At the beginning of the event, the event water contribution to the stream mainly depended on antecedent soil moisture conditions and riparian groundwater level before the event, with higher average contributions of new water on the rising limb than on the falling limb in case of lower antecedent wetness conditions and lower groundwater levels. Maximum event water contributions for the 15 rainfall events sampled in Ressi catchment occurred close to the streamflow peak for most of the events, with values above the 50% for events with dry antecedent conditions characterized by high rainfall intensity and large events occurred with wet antecedent conditions. Values of new water at the peak flow higher than 50% found for events sampled in Ressi catchment were in contrast with the limit of 50% found by Buttle (1994) for different forest catchments around the world.

Two hypothesis were formulated to explain the high average event water contributions on the rising limb of the hydrograph during events with dry antecedent conditions and the high new water contribution near the peak flow during events with high rainfall intensity. The first hypothesis is that the upper layers of the soil were less permeable in dry conditions. This condition that exceed infiltration capacity during summer events favored overland flow and the quickly transport of event water to the stream during high rainfall intensity. These mechanisms might explain the fast response of streamflow to precipitation input and the high event water contributions to streamflow during summer events in Ressi catchment. Differences in runoff dynamics from dry to wet season were explained by Blume et al., (2008) by hydrophobicity. In this contest, hydrophobicity is the property of the soil to repel water and can be measured as the time takes for a water drop to be absorbed by the soil (Dekker

and Ritsema, 1994). Blume et al. (2007) analyzed the effect of hydrophobicity on the hydrological response of the catchment. They observed little reaction of soil moisture in the first 10 cm of the soil during events in dry conditions and high rainfall intensity. Deeper soil layers, below the hydrophobic layer, had a larger response to precipitation input probably due to lateral event water infiltration from areas less subject to hydrophobicity. Some other studies investigated the effect of hydrophobicity on different flow patterns during different seasons. For example, Muñoz-Villers and McDonnell (2012) explained the rapid decrease in the percentage of new water as antecedent wetness condition increased and a consequent increased in groundwater contribution especially in the final part of the event by hydrophobicity. Since there was no evidence of overland flow on the hillslope during the events, the hypothesis of hydrophobicity processes in Ressi catchment will need future investigations.

The second hypothesis, to explain the high average new water in the rising limb and the high new water contribution at the peak flow during summer events occurring in dry conditions, is that event water contributed to stream runoff through direct channel precipitation and saturated overland flow in the area close to the stream. At the same time, most of rainfall that felt in the hillslope infiltrated into the soil because the soil was dry and it had more storage capacity. This second hypothesis, that event water contribution was mainly generated by channel precipitation and saturated overland flow on the near-channel zones, was confirmed by the low runoff coefficient and the extremely short response time of streamflow for events in summer. In literature, many studies reported the relation between the catchment conditions prior the events and the percentage of event and pre-event water to storm runoff. For example, Cey et al. (1998), Muñoz-Villers and McDonnell (2012) and Ocampo et al. (2006) found decreasing event water contributions with more wet antecedent conditions. On the contrary, Casper et al. (2003), James and Roulet (2009) and Pellerin et al. (2008) reported the lowest event water contributions during wet periods and vice versa. Moreover, extremely high (higher than 50%) contributions of new water at the peak flow during high rainfall intensity events with dry antecedent conditions can be a consequence of the small size of Ressi catchment. Brown et al. (1999) observed higher contributions of event water at the peak flow for small catchments than bigger catchments, especially for events with high rainfall intensity. Brown et al. (1999) associated this behavior to the smaller groundwater storage in the area near the stream and the greater influence of shallow subsurface flow to transfer event water from the hillslope to the stream in catchments with small size.

Contributions of new water at the peak flow higher than 50%, as well as high average event water contributions during the recession limb of the hydrograph for large events during wet antecedent conditions, might be due to the greater expansion of the saturated area near the stream. In Ressi catchment, groundwater levels during baseflow conditions are higher with increasing wetness conditions. In this context with high soil moisture content and high riparian groundwater level before the event, groundwater level quickly increased in response to rainfall signal and connectivity between riparian groundwater and the steam increased, representing the main runoff sources in the initial phase of the event. This mechanism might explain the lower contribution of new water in the very initial phase of the hydrograph of big events with wet antecedent conditions, where groundwater was well connected to the stream in the riparian zone and was the main contributor to the stream. It could be hypothesized that after storage capacity of the soil was filled as a results of the high rainfall during events in early fall (event on October 12, 2015 and event on October 14, 2016), the saturated area near the stream progressively expanded until the footslope, with a maximum expansion near the streamflow peak and in the final part of the event. Consequently, we can hypothesized that the fraction of event water contribution progressively increased during the event characterized by high rainfall amount and high pre-event groundwater level because the direct precipitation on the saturated riparian area (Pionke et al., 1988). A similar sketch was presented by Correa et al. (2017) in a study conduced in a small tropical headwater catchment in South Ecuador who showed that the saturated conditions of the riparian zone cause the low infiltration of the event water in their system and most of rainfall fraction flows above the saturated area and feed the stream. Moreover, a high percentage of new water in runoff during events in wet conditions characterized by high rainfall amount, might has partially originated from the hillslope at surface and subsurface level. In fact, when rainfall amounts become greater than the water storage capacity of the soil, the formation of saturated area in the hillslope might have supported the lateral transport of rainfall from the hillslope directly to the stream during the second part of the events (Kvaerner and Klove, 2006). In addition, the increase of the subsurface connectivity of the catchment in wet conditions favored the movement of rainfall through preferential flow pathways in the near surface layers. Since there was no evidence of overland flow in the hillslope during the events, we need future investigations to test the hypothesis of event water transport from the hillslope to the stream at the surface level. Other studies investigated the relation between high contribution of new water on the recession limb of the hydrograph and the wetness conditions before the event. Cey et al. (1998) carried out a study in a small

agricultural catchment in Ontario, Canada, to investigate the interaction between riparian groundwater and streamflow during baseflow and event conditions. They concluded that pre-event water was the dominant water source to streamflow during baseflow. During the event, event water contributions to stream were higher for events with high antecedent soil moisture conditions, high groundwater level and high streamflow. Similarly, McCartney et al (1998) conducted a study in a dambo (seasonally saturated wetland) catchment and they concluded that old water mainly contributed to stormflow in the first phases of the hydrograph prior to saturation of ground surface. Once ground water reached the surface, event water was the dominant water sources to stormflow.

Differences between δ^2H-based and EC-based and major ions-based hydrograph separation

Differences in the average new water contribution computed using δ^2H and using EC or major ions were mostly larger for the rising limb than the falling limb of the hydrographs, but there were differences in the average new water contribution computed using δ^2H and using EC or major ions on the falling limb of the hydrograph for events with dry antecedent soil moisture conditions and low streamflow before the event. Three hypotheses were tested to explain this observation.

The first hypothesis is that soil water was different from groundwater in terms of EC and major ions but not in terms of its isotopic composition, and a lot of soil water contributed to streamflow during the later part of the event. In this case, there should be an overestimation of new water contribution computed with EC and major ions. This hypothesis could be explained starting from the assumption that the solution of the steady-state mass balance equation, used to estimate new water and old water contribution to the stream runoff during rainfall or snowmelt events, must underpin the criteria that the components that constitute old water (in our case soil water and groundwater) have the same tracer concentrations or that one component that constitute old water can be considered negligible (Sklash and Farvolden, 1979). When the components constituting old water differ in concentrations, this results in an overestimation or an underestimation of the calculated new water fraction using EC and major ions. There is an overestimation of new water using EC and major ions when a component (for example soil water) has lower concentrations than another component constituting old water (for example groundwater). For this study, the two components constituting old water were not chemically the same because soil water was generally less

enriched in ions than groundwater. For example, pre-event EC was 300 µS/cm, 282 µS/cm, 295 µS/cm in riparian groundwater at location GW1 and 190 µS/cm, 169 µS/cm, 67 µS/cm in riparian soil water at location SOWR for events n.1, n.8 and n.12, respectively. Nevertheless, despite this difference between soil water and groundwater chemistry, most of the events resulted in an underestimation of the new water contribution computed using EC and major ions. This means that the first hypothesis was not valid for these events. Only for some events, for example event on June 14, 2016 with high antecedent soil moisture conditions, there was an overestimation of new water contribution computed using EC and major ions. For these event, there was a large soil water contribution during the event, as indicated by the high NO_3 concentrations in stream water.

The second hypothesis is that groundwater got diluted during the event by soil water coming from the upper soil or by rainfall and diluted groundwater contributed to streamflow during the event. This could be the case for groundwater at the bottom of the hillslope (GW3) for which EC and major ions concentrations decreased during most of the events, especially for large events. For the same principles described above, the second hypothesis was not verified for events where new water contributions computed using EC and major ions were lower than the new water contribution computed using δ^2H. The second hypothesis could be valid for the event on June 14, 2016 that results in an overestimation of the calculated new water fraction using EC and major ions. For this event can be hypothesized a significant contribution of groundwater at the bottom of the hillslope (GW3) to the streamflow.

The third hypothesis is that rainfall become enriched in ions when it moved over the near stream channel and the hillslope as saturated overland flow. Consequently, the ionic enrichment of rainfall caused an underestimation of the new water contribution computed using EC and major ions compared to using δ^2H. This especially explains the lower new water contribution determined with major ions-based and EC-based hydrograph separation than for δ^2H-based hydrograph separation on the rising limb for most of the events. For events where δ^2H-based hydrograph separation gave higher contribution of new water than EC-based and major ions-based hydrograph separation at the beginning of the rising limb of the hydrograph, it was hypothesized that the rain dissolved ions quickly in the ephemeral portion of the stream due to accumulation after evaporation and drying of the stream since the last event. Consequently, an increase in solutes content in rain water led to an underestimation of the new water contribution using EC and major ions. This hypothesis was also confirm by the fact that events with higher new water contributions on the rising

limb based on δ^2H than EC and major ions hydrograph separation were characterized by a long time since the last event and low streamflow before the events. Lower streamflow before the event also mean a shorter flowing stream section and thus a longer dry stream section where solutes may have accumulated. A longer time since the last event implies that more ions could have accumulated on the soil surface because a larger surface near the stream was more exposed to evaporation processes for a longer period.

The fact that higher new water fractions based on δ^2H also occurred on the falling limb of the hydrograph for rainfall-runoff events characterized by a lower riparian water table before the event and lower antecedent soil moisture conditions, supports as well the third hypothesis. Indeed, for dry antecedent conditions, there was an accumulation of ions on the surface and in the very top layers of the soil (leaves and top layers of the organic material) in the riparian zone and on the hillslope and the mobilization of these ions in areas further away from the stream during events due to saturated overland flow and shallow subsurface flow .These processes where also mentioned by Nolan and Hill (1990) who found an underestimation of new water contribution computed using EC, K, and Si compared to δ^2H only for the recession limb of the hydrograph. They concluded that the differences in new water contribution were likely due to chemical reaction as a result of the expansion of runoff contributing areas, as well as the transport of solutes from the soil layers rich in organic matter to the stream. Other studies have also found differences in new water contribution computed using δ^2H, EC and major ions. For example, Meriano et al. (2011) applied two-component hydrograph separation using $\delta^{18}O$ and EC to estimate event and pre-event fractions to runoff for midsummer rainfall events in a urbanized catchment in Canada and found that new water contributions computed using $\delta^{18}O$ were larger than using major ions and EC. Similarly, Wels (1991) report a larger pre-event water contribution computed using Si than using stable isotopes of water. Laudon and Slaymaker (1997) applied hydrograph separation using isotopes (δ^2H and $\delta^{18}O$), EC and Si in two nested alpine/subalpine basins in the Coast Mountains (British Columbia) and found that pre-event water contributions computed using EC and Si were smaller than using isotopes. On the contrary, other studies did not found any significant difference between hydrograph separation estimated by isotopes and EC or major ions. Pellerin et al. (2008) found similar event water contributions computed using δ^2H and using EC or Si. Non-significant differences in new water fractions were also observed by Suarez et al. (2015) using isotopes (δ^2H and $\delta^{18}O$), EC and Mg. Richey et al. (1998) compared the results of two-component hydrograph separation computed using isotopes and chemical tracers from 11 studies around the world (New

Zeland, North America and Europe) and reported similar percentage of pre-event contribution using the two types of tracers (isotopes and major ions) for most of the examined rainfall events, with differences lower than 10%. Of the 23 events under examination, only 4 events had differences in the old water contribution larger than 10% and these differences were mainly attributed to analytical uncertainty.

Although electrical conductivity and major ions are widely used as chemical tracers to investigate hydrological processes (Ladouche et al., 2001; Hoeg et al., 2000, Suarez et al., 2015), contradictory results in many different studies highlight the importance to verify hydrological and lithological conditions before using these non conventional tracers for hydrograph separation (Laudon and Slaymaker, 1997). EC and major ions generally result in uncertainty because they are subject to reaction with mineral material. Consequently, their behavior is strictly correlated with the specific characteristics of each catchment (Laudon and Slaymaker, 1997). The results of this study in Ressi catchment suggest that stable isotopes of water are suitable tracers to investigate water sources to runoff because of their conservative nature. On the other hand, ions and EC result in a higher degree of uncertainty in the computation of pre-event and event water fractions but these differences are instructive in understanding hydrological processes. Pre-event water contributions computed with EC and ions were affected by the catchment conditions prior to the event, resulting in on underestimation of the new water contribution during dry antecedent conditions and an overestimation during wet antecedent conditions. For these reasons, it was not possible to perform a three component hydrograph separation. Inconclusive results from three-component hydrograph separation because of similar reasons were also found by Rice and Hornberger (1998) and Hoeg et al. (2000). On the other hand, EC and major ions were more useful to trace water movement and solute flushing in Ressi catchment. In particular the combination of isotopes, chemical tracers and hydrometric measurements resulted in an ideal approach to investigate the hydrological dynamics of the catchment in different seasons and rainfall-runoff events.

Conceptual model of runoff generation

A conceptual model of runoff generation in Ressi catchment can be developed based on our findings (Figure 58).

Riparian shallow groundwater is a large pool filled by a vast area comprising the whole catchment. It represents the main source of stream during baseflow conditions. In particular during wet conditions, there is an expansion of the riparian groundwater area. Consequently, there is a mixing of groundwater from different locations in the lower part of the catchment that sustain streamflow.

During the events, the hydrological response of Ressi catchment to precipitation input is affected by seasonality.
Events in dry season with high rainfall intensity are characterized by a fast response of the stream. Streamflow is mainly generated by direct channel precipitation, saturated overland flow on the near-channel zone and quickly transport of event water from the hillslope to the stream through preferential flow pathways. Riparian groundwater and soil water only partially participate to streamflow in the initial phase of the event, and their contribution increases after the discharge peak. Water from the hillslope barely contributes to streamflow during the entire event, underlining the low connectivity of the catchment during dry conditions.
During the wet season, the connectivity between the stream and the hillslope increases and groundwater response to precipitation input is different compared to groundwater response in dry season. Since the beginning of the event, riparian groundwater and soil water are well connected to the stream and they mostly contribute to stormflow. During the event, an expansion of the contributing area occurs and groundwater in the hillslope increases its importance in runoff generation, confirming a high connection of the hillslope with the riparian zone. Only in the second part of big events with wet antecedent conditions, the fraction of event water in streamflow progressively increases and becomes the more important source to runoff generation. This because the expansion of the saturated area near the stream until the footslope. Consequently, runoff is mainly generated by the direct precipitation on the saturated riparian area.

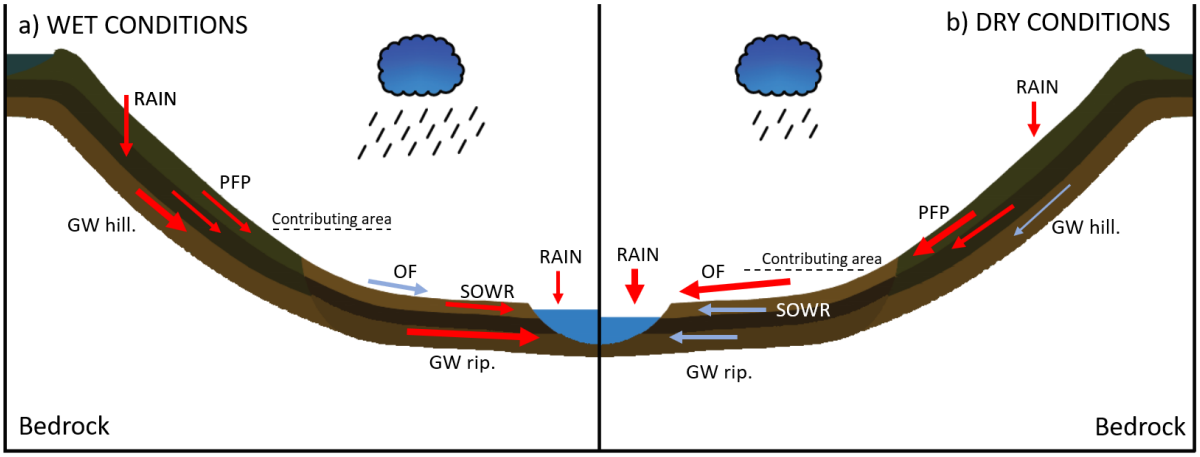

Figure 58: Conceptual model of runoff generation in Ressi catchment. Arrows indicate the relative contributions of the main water sources of runoff generation for the events in (a) wet season and (b) dry season. Red arrows refers to the water sources that mostly contribute to stream in the initial phase of the event; blue arrows refers to the water sources that mostly contribute to stream in the second part of the event. Dotted black line represents the expansion of the contributing area. RAIN is rainfall; GW hill. is groundwater in the hillslope; GW rip. is riparian groundwater; SOWR is riparian soil water; OF is saturated overland flow; PFP are preferential flow paths.

CONCLUSIONS

Identifying the main streamflow components and assessing their spatio-temporal variability is pivotal for a thorough comprehension of runoff generation mechanisms in humid mountain catchments. In this study, data on stable isotopes of water and major ions were paired with hydrometric measurements to analyze runoff generation in a small forested catchment, Ressi catchment, located in the Italian pre-Alps.

In order to answer at the three specific questions of this research, the following analyzes were made: (1) the analysis of the hydrometric data and the spatio-temporal variability of isotopic and geochemical (EC and major ions) signature of stream water and the main water sources, as well as the analysis of mixing plots was made to identify the main contributors to stream runoff and to investigate the spatial and temporal variability of runoff generation dynamics during baseflow and high flow conditions; (2) hydrograph separation was used to study how the different runoff components vary with rainfall intensity and antecedent soil moisture conditions; (3) a comparison of two-component hydrograph separation results using isotopes and major ions was carried out in order to test the effect of the tracer choice on the estimated event water contribution to streamflow and to shed new light on runoff generation processes and solute transport during rainfall-runoff events.

The results are summarized, moving top down in scales.

The analysis of hydrometric data collected during events in Ressi catchment show a general fast hydrometric response of the catchment. For wet conditions and large rainfall events, soil moisture and groundwater level respond faster and runoff rations are larger than for dry conditions. The response to precipitation input of riparian groundwater is consistently slower than for groundwater at the bottom of the hillslope and in the upper part of the catchment.

Analysis of mixing plots reveals that rainfall, shallow groundwater and riparian soil water are the main contributors to streamflow during the events. Isotopic and geochemical data highlight the high spatio-temporal variability in the hydrochemical composition of shallow groundwater. The high spatial variability in isotopic composition, EC and major ion concentrations in shallow groundwater suggests that different groundwater from different parts of the catchment contribute to stream runoff during rainfall-runoff events. Groundwater in the riparian zone has a similar hydrochemical composition as pre-event streamflow, indicating that riparian groundwater in the lower part of the catchment sustains streamflow during baseflow conditions. During events, stream water becomes more similar to soil water

and shallow groundwater on the hillslope in the upper part of the catchment. The concentration of major ions in shallow groundwater at the bottom of the hillslope changes rapidly during the events, suggesting a lateral expansion of the stream and mixing between groundwater and stream water. Furthermore, there is an accumulation of Cl when the ephemeral portion of the stream and the near stream areas dry up. The accumulated Cl is washed away when rainfall starts, increasing Cl concentrations in the stream at the beginning of the event.

Two-component hydrograph separation showed that the event water fraction is higher on the rising limb than on the falling limb of the hydrograph for most of the events, suggesting an increasing contribution of pre-event water (which is a mix of shallow groundwater and soil water) during the later stages of the events. However, the high variability in the event and pre-event water contribution to streamflow for the events sampled during the study period highlight that antecedent conditions and rainfall characteristics control the runoff response to precipitation input. The event water contribution in the initial phase of the events, is strongly correlated with the antecedent wetness conditions of the catchment. High event water fractions were observed for events with high rainfall intensity in dry periods, indicating that for these events streamflow is mainly generated by direct channel precipitation and saturated overland flow on the near-channel zone. Increasing contributions of the pre-event water component in streamflow during events during the fall season reflect the increasing stream-riparian-hillslope subsurface connectivity. Nevertheless, an important contribution of the event water fraction on the falling limb of the hydrograph was observed for large events in wet periods due to more widespread saturation overland flow and flow through shallow soil layers.

There were significant differences in the computed event water fractions for δ^2H-based, EC-based or major ions-based two-component hydrograph separation. During dry antecedent conditions these differences were most pronounced and δ^2H-based hydrograph separation resulted in a higher new water contribution to runoff than EC-based and major ions-based hydrograph separation. For these events it is hypothesized that rainfall became enriched in ions when it moved through the near stream channel and over the hillslope as saturated overland flow, resulting in an underestimation of the new water fraction in streamflow using EC and major ions. For events where the event water fraction computed using δ^2H is underestimated with respect to that ones computed using EC and major ions, it is hypothesized that the pre-event water fraction is mainly generated either by soil water

because soil water is less concentrated in ions than groundwater, or by groundwater that became diluted during the event by soil water from the upper soil or by rainfall flushing the shallow soil layers.

Because the results of the two-component hydrograph separation using EC and major ions were different and were affected by the catchment conditions prior to the events, it is demonstrated that geochemical tracers (EC and major ions) in Ressi catchment violate the assumptions of hydrograph separation that the source components to runoff must be spatially and temporally constant at the catchment scale. However, the results of this study also highlight the usefulness of using EC and major ions to understand solute transport and hydrological dynamics across the catchment. Stable isotopes of water are the ideal tracer to investigate the contribution of different water sources to runoff due to their conservative nature. Therefore, the integrated use of isotopic and geochemical tracers combined with hydrometric data proved to be a powerful method to enhance our knowledge on runoff generation processes in a small mountain catchment.

REFERENCES

AA.VV., 1981. Stable Isotope Hydrology, Deuterium and Oxygen in the Water Cycle. International Atomic Energy Agency, Vienna, 337.

Almasri M.N. and Kaluarachchi J.J., 2004. Assessment and management of long-term nitrate pollution of ground water in agriculture-dominated watersheds. Journal of Hydrology, 295: 225–245, DOI: 10.1016/j.jhydrol.2004.03.013.

Amerman C. R., 1965. The use of unit-source watershed data for runoff prediction. Water Resources Researches, 14: 499–507, DOI: 10.1029/WR001i004p00499.

Anderson M. G. and Burt T. P., 1978. The role of topography in controlling throughflow generation. Earth Surf Processes Landforms, 3: 331-344, DOI: 10.1002/esp.3290030402.

Arnett R. R., 1974. Environmental factors affecting speed and volume of topsoil interflow. In Fluvial Processes in Instrumented Watersheds, edited by Gregory K. J. and Walling D. E., 7-22, Institute of British Geographers.

ARPAV, 2005. Carta dei suoli del Veneto. ARPAV - Osservatorio Regionale Suolo, Castelfranco Veneto (TV).

Arreghini S., de Cabo L., Seoane R., Tomazin N., Serafíni R. and de Iorio A.F., 2005. Influence of rainfall on the discharge, nutrient concentrations and loads of a stream of the “Pampa Ondulada” (Buenos Aires, Argentina). Limnetica, Asociación Española de Limnología, Madrid, Spain, 24(3-4): 225-236.

Ator S.W. and Ferrari M.J., 1997. Nitrate and selected pesticides in ground water of the Mid-Atlantic Region. US Geological Survey, Water-Resources Investigation Report, 97-4139.

Aubertin G. M., 1971. Nature and extent of macropores in forest soils and their influence on subsurface water movement. Forest Serv. Pap. NE (US), 192: 33.

Bachmair S. and Weiler M., 2012. Hillslope characteristics as controls of subsurface flow variability. Hydrology Earth System Sciences, 16: 3699–3715, DOI: 10.5194/hess-16-3699-2012.

Bansah S. and Ali G., 2017. Evaluating the effects of tracer choice and end-member definitions on hydrograph separation results across nested, seasonally cold watersheds. Water Resources Research, 53: 8851-8871, DOI: 10.1002/2016WR020252.

Barthold F.K., Wu J., Vache’ K.B., Schneider K., Frede H.G. and Breuer L., 2010. Identification of geographic runoff sources in a data sparse region: hydrological processes and the limitations of tracer-based approaches. Hydrological Processes, 24: 2313–2327, DOI: 10.1002/hyp.7678.

Barthold F. K., Turner B. L., Elsenbeer H. and Zimmermann A., 2016. A hydrochemical approach to quantify the role of return flow in a surface flow-dominated catchment. Hydrological Processes, DOI: 10.1002/hyp.11083.

Beasly R. S., 1976. Contribution of subsurface flow from the upper slopes of forested watersheds to channel flow. Soil Science Society of America Journal, 40: 955-957.

Betson R.P. and Marius J.B., 1969. Source areas of storm runoff. Water Resources Research, 5: 574–582, DOI: 10.1029/WR005i003p00574.

Betson R.P., 1964. What Is Watershed Runoff? Journal of Geophysical Research, 69: 1541-1552, DOI: 10.1029/JZ069i008p01541.

Beven K. and Germann P., 1982. Macropores and water flow in soils. Water Resources Research, 18(5): 1311–1325, DOI: 10.1029/WR018i005p01311.

Beven K., 1978. The hydrological response of headwater and sideslope areas. Hydrological Sciences Bulletin, 23: 419-437.

Blume T., Zehe E. and Bronstert A., 2007. Rainfall-runoff response, event-based runoff coefficients and hydrograph separation. Hydrological Sciences Journal, 52(5): 843–862, DOI:10.1623/hysj.52.5.843.

Blume T., Zehe E. and Bronstert A., 2007. Use of soil moisture dynamics and patterns for the investigation of runoff generation processes with emphasis on preferential flow. Hydrology and Earth System Sciences, 4: 2587–2624.

Blume T., Zehe E., Reusser D. E., Iroume A. and Bronstert A., 2008. Investigation of runoff generation in a pristine, poorly gauged catchment in the Chilean Andes I: A multi-method experimental study. Hydrological Processes, 22(18): 3661 – 3675, DOI:10.1002/hyp.6971.

Bonell M. and Gilmour D. A., 1978. The development of overland flow in a tropical rainforest catchment. Journal of Hydrology, 39: 365-382, DOI: 10.1016/0022-1694(78)90012-4.

Bonell M., Gilmour D. A. and Sinclair D. F., 1981. Soil hydraulic properties and their effect on surface and subsurface water transfer in a tropical rain forest catchment. Hydrological Sciences Bulletin, 26: 1-18.

Brown V.A., McDonnell J.J., Burns D.A. and Kendall C., 1999. The role of event water, a rapid shallow flow component, and catchment size in summer stormflow. Journal of Hydrology, 217: 171–190, DOI: 10.1016/S0022-1694(98)00247-9.

Burns D. A., Plummer L. N., McDonnell J. J., Busenberg E., Casile G. C., Kendall C., Hooper R. P., Freer J. E., Peters N. E., Beven K. J. and Schlosser P., 2003. The geochemical evolution of riparian ground water in a forested piedmont catchment. Ground Water, 41(7): 913–925, DOI: 10.1111/j.1745-6584.2003.tb02434.x.

Burns D.A. and McDonnell J.J., 1998. Effects of a beaver pond on runoff processes: comparison of two headwater catchments. Journal of Hydrology, 205: 248–264, DOI: 10.1016/S0022-1694(98)00081-X.

Burns D.A., McDonnell J.J., Hooper R.P., Peters N.E., Freer J.E., Kendall C. and Beven K., 2001. Quantifying contributions to storm runoff through end-member mixing analysis and hydrologic measurements at the Panola Mountain Research Watershed (Georgia, USA). Hydrological Processes, 15: 1903-1924, DOI: 10.1002/hyp.246.

Buttle J.M. and McDonald D.J., 2002. Coupled vertical and lateral preferential flow on a forested slope. Water Resources Research, 38(5): 1060, DOI:10.1029/2001WR000773.

Buttle J.M., 1994. Isotope hydrograph separations and rapid delivery of pre-event water from drainage basins. Progress in Physical Geography, 18: 16–41, DOI: 10.1177/030913339401800102.

Caissie D., Pollock T.L. and Cunjak R.A., 1996. Variation in stream water chemistry and hydrograph separation in a small drainage basin. Journal of Hydrology, 178: 137-157, DOI: 10.1016/0022-1694(95)02806-4.

Casper M. C., Volkmann H. N., Waldenmeyer G. and Plate E. J., 2003: The separation of flow pathways in a sandstone catchment of the northern Black Forest using DOC and a nested approach. Physics and chemistry of the earth, 28(6-7): 269–275, DOI: 10.1016/S1474-7065(03)00037-8.

Cervi F., Ronchetti F., Martinelli G., Bogaard T. A. and Corsini A., 2012. Origin and assessment of deep groundwater inflow in the Ca' Lita landslide using hydrochemistry and in situ monitoring. Hydrology and Earth System. Sciences, 16: 4205–4221, DOI: 10.5194/hess-16-4205-2012.

Cey E.E., Rudolph D.L., Parkin G.W. and Aravena R., 1998. Quantifying groundwater discharge to a small perennial stream in southern Ontario, Canada. Journal of Hydrology, 210 (1–4): 21–37, DOI: 10.1016/S0022-1694(98)00172-3.

Chang S.C. and Matzner E., 2000. The effect of beech stemflow on spatial patterns of soil solution chemistry and seepage fluxes in a mixed beech/oak stand. Hydrological processes, 14(1): 135-144, DOI: 10.1002/(SICI)1099-1085(200001)14:1<135::AID-HYP915>3.0.CO;2-R.

Chen J., Liu X., Wang C., Rao W., Tan H., Dong H., Sun X., Wang Y. and Su Z., 2011. Isotopic constraints on the origin of groundwater in the Ordos Basin of northern China. Environmental Earth Sciences, 66: 505–517.

Christophersen N. and Hooper R.P., 1992. Multivariate analysis of stream water chemical data: The use of principal components analysis for the end-member mixing problem. Water Resources Research, 28(1): 99-107, DOI: 10.1029/91WR02518.

Christophersen N., Neal C., Hooper R.P., Vogt R.D. and Andersen S., 1990. Modelling streamwater chemistry as a mixture of soilwater endmembers - a step towards second generation acidification models. Journal of Hydrology, 116: 307–320, DOI: 10.1016/0022-1694(90)90130-P.

Cook P. G. and Herczeg A. L., 1999. Environmental tracers in subsurface hydrology. Kluwer, Dordrecht.

Correa A., Windhorst D., Tetzlaff D., Crespo P., Celleri R., Feyen J. and Breuer L., 2017. Temporal dynamics in dominant runoff sources and flow paths in the Andean Paramo. Water Resources Research, 53: 5998–6017, DOI:10.1002/2016WR020187.

Creed I.F., Band L.E., Foster N.W., Morisson I.K., Nicolson J.A., Semkin R.S. and Jeffries D.S., 1996. Regulation of nitrate N release from temperate forests: a test of the N flushing hypothesis. Water Resources Research, 32(11): 3337–3354, DOI: 10.1029/96WR02399.

Crouzet E., Hubert P., Olive P., Siwertz E. and Marce A., 1970. Le tritium dans les mesures d'hydrologie de surface: Determination experimentale du coefficient de ruisselement. Journal of Hydrology, 11: 217-229, DOI: 10.1016/0022-1694(70)90063-6.

Dansgaard W., 1964. Stable isotopes in precipitation. Tellus, 16: 436-468, DOI: 10.1111/j.2153-3490.1964.tb00181.x.

De Vries J. J. and Simmers I., 2002. Groundwater recharge: an overview of processes and challenges: Hydrogeology Journal, 10: 5–17, DOI: 10.1007/s10040-001-0171-7.

De Vries W. and Breeuwsma A., 1987. The relation between soil acidification and element cycling. Water, Air, and Soil Pollution, 35(3–4): 293–310, DOI: 10.1007/bf00290937.

Dekker L. W. and Ritsema C. J., 1994. How Water Moves in a Water Repellent Sandy Soil .1. Potential and Actual Water Repellency. Water Resources Research, 30: 2507–2517, DOI: 10.1029/94WR00749.

Detty J.M. and McGuire K.J., 2010. Threshold changes in storm runoff generation at a till-mantled headwater catchment. Water Resources Research, 46: W07525, DOI: 10.1029/2009WR008102.

Dunne T. and Black R. D., 1970. Partial area contributions to storm runoff in a small New England watershed. Water Resources Research, 6: 1296-1311, DOI: 10.1029/WR006i005p01296.

Dunne T. and Black R. D., 1970. An experimental investigation of runoff production in permeable soils. Water Resources Research, 6: 478-490, DOI: 10.1029/WR006i002p00478.

Dunne, T., Moore T. R. and Taylor C. H., 1975. Recognition and prediction of runoff producing zones in humid regions. Hydrological Sciences Bulletin, 20: 305-327.

Ehleringer J.R. and Dawson T.E., 1992. Water uptake by plant perspective from stable isotope composition: commissione review. Plant Cell Environment, 15: 1073-1082.

Elsenbeer H., Lorieri D. and Bonell M., 1995. Mixing model approaches to estimate storm flow sources in an overland flow-dominated tropical rain-forest catchment. Water Resources Research, 31(9): 2267–2278, DOI:10.1029/95WR01651.

Fannin R.J., Jaakkola J., Wilkinson M.T. and Hetherington E.D., 2000. Hydrologic response of soils to precipitation at Carnation Creek, British Columbia, Canada. Water Resources Research, 36: 1481–1494, DOI: 10.1029/2000WR900027.

Feller M.C. and Kimmins J.P., 1979. Chemical characteristics of small streams near Haney in Southwestern British Columbia. Water Resources Research, 15: 247-258, DOI: 10.1029/WR015i002p00247.

Fischer B.M.C., Rinderer M., Schneider P., Ewen T. and Seibert J., 2015. Contributing sources to base flow in pre-alpine headwaters using spatial snapshot sampling. Hydrological Processes, 29: 5321–5336, DOI: 10.1002/hyp.10529.

Fischer B.M.C., Stähli M. and Seibert J., 2016. Pre-event water contributions to runoff events of different magnitude in pre-alpine headwaters. Hydrology Research, 48(1): 28-47, DOI: 10.2166/nh.2016.176.

Freeze R. A., 1974. Streamflow generation. Reviews of Geophysics and Space, 12: 627–647, DOI: 10.1029/RG012i004p00627.

Frisbee M.D., Phillips F.M., Campbell A.R., Liu F. and Sanchez S.A., 2011. Streamflow generation in a large, alpine watershed in the southern Rocky Mountains of Colorado: Is streamflow generation simply the aggregation of hillslope runoff responses. Water Resources Research, 47: W06512, DOI: 10.1029/2010WR009391.

Fritz P., JCherry. A., Weyer K. U. and Sklash M., 1976. Storm runoff analyses using environmental isotopes and major ions. In Interpretation of Environmental Isotope and Hydrochemical Data in Groundwater Hydrology, 111-130, IAEA, Vienna.

Garvelmann J., Külls C. and Weiler M., 2012. A porewater-based stable isotope approach for the investigation of subsurface hydrological processes. Hydrology and Earth System Sciences, 16: 631–640, DOI: 10.5194/hess-16-631-2012.

Gat J.R., 1970. Environmental isotope balance of Lake Tiberias. Isotope Hydrology. International Atomic Energy Agency, Vienna, 109–127.

Genereux D., 1998. Quantifying uncertainty in tracer-based hydrograph separations. Water Resources Research, 34(4): 915 – 919, DOI: 10.1029/98WR00010.

Gonfiantini R.,1986. Environmental isotopes in lake studies. In Handbook of Environmental Isotope Geochemistry, edited by Fritz P. and Fontes J. C.,New York Elsevier.

Haga H., Matsumoto Y., Matsutani J., Fujita M., Nishida K. and Sakamoto Y., 2005. Flow paths, rainfall properties, and antecedent soil moisture controlling lags to peak discharge in a granitic unchanneled catchment. Water Resources Research, 41: W12410, DOI: 10.1029/ 2005WR004236

Hallberg G.R. and Keeney D.R., 1993. Nitrate. In Regional ground-water quality, edited by Alley W.M., 297-322., New York, N.Y., Van Nostrand Reinhold.

Hamed Y. and Dhahri F., 2013. Hydro-geochemical and isotopic composition of groundwater, with emphasis on sources of salinity, in the aquifer system in Northwestern Tunisia. Journal of African Earth Sciences, 83: 10–24, DOI: 10.1016/j.jafrearsci.2013.02.004.

Harris D.M., McDonnell J.J. and Rodhe A., 1995. Hydrograph separation using continuous open system isotope mixing. Water Resources Research, 31: 157–171, DOI: 10.1029/94WR01966.

Harter T., Davis H., Mathews M. and Meyer R., 2002. Shallow ground water quality on dairy farms with irrigated forage crops. Journal of Contaminant Hydrology, 55: 287–315, DOI: 10.1016/S0169-7722(01)00189-9.

Haught D. R. W. and van Meerveld H. J., 2011. Spatial variation in transient water table responses: differences between an upper and lower hillslope zone. Hydrological Processes, 25: 3866–3877, DOI: 10.1002/hyp.8354.

Hewlett J. D. and Hibbert A. R., 1963. Moisture and energy conditions within a sloping soil mass during drainage. Journal of Geophysical Research, 68: 1081-1087, DOI: 10.1029/JZ068i004p01081.

Hewlett J. D. and Hibbert A. R., 1967. Factors affecting the response of small watersheds to precipitation in humid areas. In International Symposium on Forest Hydrology, edited by Sopper W. E. and Lull H. W., 275-290, Pergamon, New York.

Hewlett J. D. and Nutter W. L., 1970. The varying source area of streamflow from upland basins. In Proceedings of the Symposium on Interdisciplinary Aspects of Watershed Management, 65-83, American Society of Civil Engineers, New York.

Hewlett J.D., 1961. Watershed management in report for 1961 Southeastern Forest Experiment Station. US Forest Service, Asheville, North Carolina.

Hill A.R. and Waddington J.M., 1993. Analysis of storm run-off sources using oxygen-18 in a headwater swamp. Hydrological Processes, 7: 305–316, DOI: 10.1002/hyp.3360070308.

Hinton M.J., Schiff S. L. and English M.C., 1994. Examining the contributions of glacial till water to storm runoff using two- and three- component hydrograph separations. Water Resources Research, 30: 983-993, DOI: 10.1029/93WR03246.

Hoeg S., Uhlenbrook S. and Leibundgut Ch., 2000. Hydrograph separation in a mountainous catchment combining hydrochemical and isotopic tracers. Hydrological Processes, 14(7): 1199-1216, DOI: 10.1002/(SICI)1099-1085(200005)14:7<1199::AID-HYP35>3.0.CO;2-K.

Hooper R. P., 2003. Diagnostic tools for mixing models of stream water chemistry. Water Resources Researches, 39(3): 1055, DOI:10.1029/2002WR001528.

Hooper R.P., 2001. Applying the scientific method to small catchment studies: a review of the Panola Mountain experience. Hydrological Processes, 15: 2039–2050, DOI: 10.1002/hyp.255.

Hooper R.P., Christopherson N. and Peters N.E, 1990. Modelling streamwater chemistry as a mixture of soilwater end-members-an application to the Panola Mountain catchment, Georgia, USA. Journal of Hydrology, 116: 321-343, DOI: 10.1016/0022-1694(90)90131-G.

Horton R. E., 1933. The role of infiltration in the hydrologic cycle. Transactions, American Geophysical Union, 14: 446–460, DOI: 10.1029/TR014i001p00446.

Hsueh-Yu Lu, 2014. Application of water chemistry as a hydrological tracer in a volcano catchment area: A case study of the Tatun Volcano Group, North Taiwan. Journal of Hydrology, 511: 825-837, DOI: 10.1016/j.jhydrol.2014.02.036.

Inamdar S. P. and Mitchell M. J., 2007. Contributions of riparian and hillslope waters to storm runoff across multiple catchments and storm events in a glaciated forested watershed. Journal of Hydrology, 341: 116–130, DOI: 10.1016/j.jhydrol.2007.05.007.

Inamdar S., Dhillon G., Singh S., Dutta S., Levia D., Scott D., Mitchell M., Stan J. and McHale P., 2013. Temporal variation in end member chemistry and its influence on runoff mixing patterns in a forested, Piedmont catchment. Water resources researches, 49: 1828–1844, DOI:10.1002/wrcr.20158.

Inamdar S.P., Christopher S. and Mitchell M.J., 2004. Export mechanisms for dissolved organic carbon and nitrate during summer storm events in a glaciated forested catchment in New York, USA. Hydrological Processes, 18(14): 2651– 2661, DOI: 10.1002/hyp.5572.

Iovino F., Borghetti M. and Veltri A., 2009. Foreste e ciclo dell'acqua. Forest@, 6: 256-273.

James A.L. and Roulet N.T., 2009. Antecedent moisture conditions and catchment morphology as controls on spatial patterns of runoff generation in small forest catchments. Journal of Hydrology, 377(3-4): 351–366, DOI: 10.1016/j.jhydrol.2009.08.039.

Johnson M.S. and Lehmann J., 2006. Double-funneling of trees: Stemflow and root-induced preferential flow. Ecoscience, 13 (3): 324-333, DOI: 10.2980/i1195-6860-13-3-324.1.

Jones J.A.A., 2010. Soil piping and catchment response. Hydrological Processes, 24: 1548–1566, DOI: 10.1002/hyp.7634.

Kamdee K., Srisuk K., Lorphensri O., Chitradon R., Noipow N., Laoharojanaphand S. and Chantarachot W., 2013. Use of isotope hydrology for groundwater resources study in Upper Chi river basin. Journal of Radioanalytical and Nuclear Chemistry, 297: 405–418, DOI: 10.1007/s10967-012-2401-y.

Katsuyama M., Ohte N. and Kobash S., 2001. A three-component end-member analysis of stream water hydrochemistry in a small Japanese forested headwater catchment. Hydrological Processes, 15: 249–260, DOI: 10.1002/hyp.155.

Kendall C. and McDonnell J.J., 1998. Isotope Tracers in Catchment Hydrology. Elsevier Science Limited, Amsterdam.

Kendall C., McDonnell J.J. and Gu W., 2001. A look inside black box hydrograph separation models: a study at the Hydrohill catchment. Hydrological Processes, 15: 1877–1902, DOI: 10.1002/hyp.245.

Kennedy V.C., Kendall C., Zellweger G.W., Wyerman T.A. and Avanzino R.J., 1986. Determination of the components of stormflow using water chemistry and environmental isotopes, Mattole river basin, California. Journal of Hydrology, 84: 107–140, DOI:10.1016/0022-1694(86)90047-8.

Kennedy V.C., 1977. Geochemistry of the Mattole river of northern California. Unite States Department of the Interior Geological Survey.

Kirkby, M.J. and R.J. Chorley, 1967. Overland flow, throughflow, and erosion. International Association of Scientific Hydrology Bulletin, 7, DOI: 10.1080/02626666709493533.

Kvaerner J. and Klove B., 2006. Tracing sources of summer stream flow in boreal headwaters using isotopic signatures and water geochemical components. Journal of Hydrology, 331: 186–204, DOI: 10.1016/j. jhydrol.2006.05.008.

Ladouche B., Probst A., Viville D., Idir S., Baque C., Loubet M., Probst J.L. and Bariac T., 2001. Hydrograph separation using isotopic, chemical and hydrological approaches (streng- bach catchement, France). Journal of Hydrology, 242: 255–274, DOI:10.1016/S0022-1694(00)00391-7.

Laudon H. and Slaymaker O., 1997. Hydrograph separation using stable isotopes, silica and electrical conductivity: an alpine example. Journal of Hydrology, 201: 82–101, DOI: 10.1016/S0022-1694(97)00030-9.

Lee K., Kim J., Lee D., Kim Y. and Lee D., 2007. Analysis of water movement through an unsaturated soil zone in Jeju Island, Korea using stable oxygen and hydrogen isotopes. Journal of Hydrology, 345: 199–211, DOI: 10.1016/j.jhydrol.2007.08.006.

Li X.Y., Liu L.Y., Gao S.Y., Ma Y.J. and Yang Z.P., 2008. Stemflow in three shrubs and its effect on soil water enhancement in semiarid loess region of China. Agricultural and Forest Meteorolgy, 148: 1501-1507, DOI: 10.1016/j.agrformet.2008.05.003.

Liang W.L., Kosugi K. and Mizuyama T., 2011. Soil water dynamics around a tree on a hillslope with or without rainwater supplied by stemflow. Water Resources Research, 47, DOI: 10.1029/2010WR009856.

Liu F.J., Parmenter R., Brooks P.D., Conklin M.H and Bales R.C, 2008. Seasonal and interannual variation of streamflow pathways and biogeochemical implications in semi-arid, forested catchments in Valles Caldera, New Mexico. Ecohydrology, 1: 239–252, DOI:10.1002/eco.22.

Machavaram M.V., Whittemore D.O., Conrad M.E. and Miller N.L., 2006. Precipitation induced stream flow: An event based chemical and isotopic study of a small stream in the Great Plains region of the USA. Journal of Hydrology, 330: 470-480, DOI: 10.1016/j.jhydrol.2006.04.004.

Marc V., Didon-Lescot J.F. and Michael C., 2001. Investigation of the hydrological processes using chemical and isotopic tracers in a small Mediterranean forested catchment during autumn recharge. Journal of Hydrology, 247(3-4): 215–229, DOI: 10.1016/S0022-1694(01)00386-9.

Maurya A.S., Shah M., Deshpande R.D., Bhardwaj R.M., Prasad A. and Gupta S.K., 2011. Hydrograph separation and precipitation source identification using stable water isotopes and conductivity: River Ganga at Himalayan foothills. Hydrological Processes, 25: 1521–1530, DOI: 10.1002/hyp.7912.

McCartney M.P., Neal C. and Neal M., 1998. Use of deuterium to understand runoff generation in a headwater catchment containing a dambo. Hydrology Earth System Sciences, 2(1): 65–76.

McDonnell J.J., 1990. A rationale for old water discharge through macropores in a steep, humid catchment. Water Resources Research, 26: 2821–2832, DOI: 10.1029/WR026i011p02821.

McKinney C.R., McCrea J.M., Epstein S., Allen H.A. and Urey H.C., 1950. Improvements in mass spectrometers for the measurement of small differences in isotope abundance ratios. Review of Scientific Instrument, 21: 724-730, DOI: 0.1063/1.1745698.

Meriano M., Howard K.W.F. and Eyles N., 2011. The role of midsummer urban aquifer recharge in stormflow generation using isotopic and chemical hydrograph separation techniques. Journal of Hydrology, 396(1–2): 82–93, DOI: 10.1016/j.jhydrol.2010.10.041.

Mohanty B. P., Bowman R. S., Hendrickx J. M. H., Simunek J. and Van Genuchten M. T., 1998. Preferential transport of nitrate to a tile drain in an intermittent-flood-irrigated field: Model development and experimental evaluation. Water Resources Research, 34: 1061–1076, DOI: 10.1029/98WR00294.

Mosley M.P., 1979. Streamflow generation in a forested watershed, New Zealand. Water Resources Research, 15: 795-806, DOI: 10.1029/WR015i004p00795.

Mosley M.P., 1982. Subsurface flow velocities through selected forest soils, South Island, New Zealand. Journal of Hydrology, 55: 65–92, DOI: 10.1016/0022-1694(82)90121-4.

Mueller M.H., Alaoui A. and Alewell C., 2016. Water and solute dynamics during rainfall events in headwater catchments in the Central Swiss Alps under the influence of green alder shrubs and wetland soils. Ecohydrology, 9: 950–963, DOI: 10.1002/eco.1692.

Muñoz-Villers L.E. and McDonnell J.J., 2012. Runoff generation in a steep, tropical montane cloud forest catchment on permeable volcanic substrate. Water Resources Research, 48: W09528, DOI: 10.1029/ 2011WR011316.

Muraoka K. and Hirata T., 1988. Streamwater chemistry during rainfall events in a forested basin. Journal of Hydrology, 102(1-4): 235-253, DOI: 10.1016/0022-1694(88)90100-X.

Nolan K.M. and Hill B.R., 1990. Storm-runoff generation in the Permanente Creek drainage basin, west central California: an example of flood wave effects on runoff composition. Journal of Hydrology, 113: 343–367, DOI: 10.1016/0022-1694(90)90183-X.

Norbiato D., Borga M., Merz R., Blöschl G. and Carton A., 2009. Controls on event runoff coefficients in the eastern Italian Alps. Journal of Hydrology, 375: 312–325, DOI: 10.1016/j.jhydrol.2009.06.044.

Ocampo C.J., Oldham C.E., Sivapalan M. and Turner J.V., 2006. Hydrological versus biogeochemical controls on catchment nitrate export: a test of the flushing mechanism. Hydrological Processes, 20(20): 4269–4286, DOI: 10.1002/hyp.6311.

Pearce A. J., Stewart M. K. and Sklash M. G., 1986. Storm Runoff Generation in Humid Headwater Catchments: Where Does the Water Come From? Water Resources Research, 22(8): 1263-1272, DOI: 10.1029/WR022i008p01263.

Pellerin B.A., Wollheim W.M., Feng X. and Charles J.V., 2008. The application of electrical conductivity as a tracer for hydrograph separation in urban catchments. Hydrological Processes, 22: 1810–1818, DOI: 10.1002/hyp.6786.

Penna D., Mantese N., Hopp L., Dalla Fontana G. and M. Borga, 2014. Spatio-temporal variability of piezometric response on two steep alpine hillslopes. Hydrologcal Processes, 29: 198-2011, DOI: 10.1002/hyp.10140.

Penna D., Tromp-van Meerveld H.J., Gobbi A., Borga M. and Dalla Fontana G., 2011. The influence of soil moisture on threshold runoff generation processes in an alpine headwater catchment. Hydrology and Earth System Sciences, 15: 689–702, DOI: 10.5194/hess-15-689-2011.

Penna D., van Meerveld H.J., Oliviero O., Zuecco G., Assendelft R.S., Dalla Fontana G. and Borga M., 2015. Seasonal changes in runoff generation in a small forested mountain catchment. Hydrological processes, 29: 2027–2042, DOI: 10.1002/hyp.10347.

Peters D.L., Buttle J.M., Taylor C.H. and LaZerte B.D., 1995. Runoff production in a forested, shallow soil, Canadian Shield basin. Water Resources Research, 31: 1291–1304, DOI: 10.1029/94WR03286.

Pilgrim D. H., 1966. Radioactive tracing of storm runoff on a small catchment, I, Experimental technique. Journal of Hydrology, 4: 209-305, DOI: 10.1016/0022-1694(66)90094-1.

Pilgrim D. H., 1966. Radioactive tracing of storm runoff on a small catchment, II, Discussion of results. Journal of Hydrology, 4: 306-326, DOI: 10.1016/0022-1694(66)90095-3.

Pilgrim D. H., 1976. Travel times and nonlinearity of flood runoff from tracer measurements on a small watershed. Water Resources Research, 12: 487-496, DOI: 10.1029/WR012i003p00487.

Pilgrim D. H., 1983. Some problems in transferring hydrological relationships between small and large drainage basins and between regions. Journal of Hydrology, 65: 49-72, DOI: 10.1016/0022-1694(83)90210-X.

Pilgrim D. H., Huff D. D. and Steele T. D., 1978. A field evaluation of surface and subsurface runoff, II, Runoff processes. Journal of Hydrology, 38: 319-341, DOI: 10.1016/0022-1694(78)90077-X.

Pinder G. F. and Jones J. F., 1969. Determination of the groundwater component of peak discharge from the chemistry of total runoff water. Water Resources Researches, 5(2): 438-445, DOI: 10.1029/WR005i002p00438.

Pionke H.B., Hoover J.R., Schnabel R.R., Gburek W.J., Urban J.B. and Rogowski A.S., 1988. Chemical–hydrologic interactions in the near-stream zone. Water Resources Research, 24: 1101–1110, DOI: 10.1029/WR024i007p01101.

Ragan R. M., 1968. An experimental investigation of partial area contributions. In: Hydrological Aspects of the Utilization of Water, Reports and Discussions (Proc. IAHS Assembly at Bern), 241–251, IAHS Publ. 76.

Rice K. C. and Hornberger G. M., 1998. Comparison of hydrochemical tracers to estimate source contributions to peak flow in a small, forested headwater catchment. Water Resources Research, 34: 1755–1766, DOI: 10.1029/98WR00917.

Richey D.G., McDonnell J.J., Erbe M.W. and Hurd T.M., 1998. Hydrograph separations based on chemical and isotopic concentrations: a critical appraisal of published studies from New Zealand, North America and Europe. Hydrological Processes, 37: 95–111.

Rinderer M., van Meerveld H.I., Manfred Stähli M. and Seibert J., 2016. Is groundwater response timing in a pre-alpine catchment controlled more by topography or by rainfall? Hydrological Processes, 30: 1036–1051, DOI: 10.1002/hyp.10634.

Rusjan S., Brilly M. and Mikos M., 2008. Flushing of nitrate from a forested watershed: an insight into hydrological nitrate mobilization mechanisms through seasonal high-frequency stream nitrate dynamics. Journal of Hydrology, 354(1–4): 187–202, DOI: 10.1016/j.jhydrol.2008.03.009.

Schellekens J., Scatena F. N., Bruijnzeel L. A., van Dijk A., Groen M. M. A. and van Hogezand R. J. P., 2004. Stormflow generation in a small rainforest catchment in the Luquillo experimental forest, Puerto Rico. Hydrological Processes, 18(3): 505–530, DOI:10.1002/hyp.1335.

Sedea R., Di Lallo E. and De Vecchi G., 1986. Carta Geologica Dell'area Di Valli Del Pasubio - Posina – Laghi. 1:20.000. Consiglio Nazionale Delle Ricerche and Universita' Di Padova, Italy.

Segura C., James A.L., Lazzati D. and Roulet N.T., 2012. Scaling relationships for event water contributions and transit times in small-forested catchments in Eastern Quebec. Water Resources Research, 48: W07502, DOI: 10.1029/2012WR011890.

Sidle R.C., Kitahara H., Terajima T. and Nakai Y., 1995. Experimental studies on the effects of pipeflow on throughflow partitioning. Journal of Hydrology, 165: 207–219, DOI: 10.1029/98WR00917.

Sklash M.G. and Farvolden R.N., 1979. The role of groundwater in storm runoff. Journal of Hydrology, 43: 45–65, DOI: 10.1016/0022-1694(79)90164-1.

Sklash M.G., Farvolden R.N. and Fritz P. A, 1976. Conceptual model of watershed response to rainfall developed through the use of oxygen-18 as a natural tracer. Canadian Journal of Earth Science, 13: 271-283.

Soulsby C., Chen M., Ferrier R.C., Helliwell R.C., Jenkins A. and Harriman R., 1998. Hydrogeochemistry of shallow groundwater in an upland Scottish catchment. Hydrological Processes, 12: 1111–1127, DOI: 10.1002/(SICI)1099-1085.

Suarez V.V.C., Okello A. M. L.S., Wenninger J. W. and Uhlenbrook S., 2015. Understanding runoff processes in a semi-arid environment through isotope and hydrochemical hydrograph separations. Hydrology Earth System Sciences, 19: 4183–4199, DOI: 10.5194/hess-19-4183-2015.

Sukhija B. S., Reddy D. V., Nagabhushanam P. and Syed Hussain, 2003. Recharge processes: Piston flow vs preferential flow in semi-arid aquifers of India. Hydrogeology Journal, 11(3): 387-395, DOI: 10.1007/s10040-002-0243-3indican.

Taniguchi M., Tsujimura M. and Tanaka T., 1996. Significance of stemflow in groundwater recharge. 1: Evaluation of the stemflow contribution to recharge using a mass balance approach. Hydrological Processes, 10: 71-80, DOI: 10.1002/(SICI)1099-1085(199601)10:1<71::AID-HYP301>3.0.CO;2-Q.

Tarboton D., 2003. Rainfall-runoff processes. Utah State University, 1:2.

Tetzlaff D. and Soulsby C., 2008. Sources of baseflow in large catchments—using tracers to develop a holistic understanding of runoff generation. Journal of Hydrology, 359: 287–302, DOI: 10.1016/j.jhydrol.2008.07.008.

Troendle C. A. and Hofmeyer J. W., 1971. Storm flow related to measured physical parameters on small forested watersheds in West Virginia. Eos Transactions AGU, 52: 204, DOI: 10.1029/WR022i008p01263.

Tsukamoto Y., 1961. An experiment on subsurface flow. Journal of the Japanese Forestry Society, 43: 61-68.

Turner J.V., Macpherson D.K. and Stokes R.A., 1987. The mechanisms of catchment flow processes using natural variations in deuterium and oxygen-18. Journal of Hydrology, 94: 143–162, DOI: 10.1016/0022-1694(87)90037-0.

U.S. Forest Service, 1961. Watershed management: Some ideas about storm runoff and base flow, annual report, 61-66, Southeast Forest Exp. Sta., Asheville, N. C..

Van Der Velde Y., De Rooij G. H., Rozemeijer J. C., van Geer,F. C. and Broers H. P., 2010. Nitrate response of a lowland catchment: On the relation between stream concentration and travel time distribution dynamics. Water Resources Research, 46: W11534, DOI: 10.1029/2010wr009105.

Wang H., Gao J.E., Li X.H., Zhang S.I. and Wang H.J., 2015. Nitrate accumulation and leaching in surface and ground water based on simulated rainfall experiments. PLoS One, 10(8): e0136274, DOI:10.1371/journal.pone.0136274.

Weiler M., McDonnell J.J., Tromp-Van Meerveld I. and Uchida T., 2005. Subsurface stormflow. In Encyclopedia of Hydrological Sciences, edited by Anderson M., Wiley J. and Sons Ltd.

Wels C., Cornett R.J. and Lazerte B.D., 1991. Hydrograph separation: a comparison of geochemical and isotopic tracers. Journal of Hydrology, 122(1): 253–274, DOI: 10.1016/0022-1694(91)90181-G.

Wenninger J., Uhlenbrook S., Tilch N. and Leibundgut Ch., 2004. Experimental evidence of fast groundwater responses in a hillslope/floodplain area in the Black Forest Mountains, Germany. Hydrological Processes, 18: 3305–3322, DOI: 10.1002/hyp.5686.

Weyman D. R., 1970. Throughflow on hillslopes and its relation to the stream hydrograph. International Association of Hydrological Sciences Bulletin, 15: 25-33.

Whipkey R. Z., 1965. Subsurface flow on forested slopes. International Association of Hydrological Sciences Bulletin, 10: 74-85.

Whipkey R. Z., 1967. Theory and mechanics of subsurface stormflow. In International Symposium of Forest Hydrology, edited by Sopper W. E. and Lull H. W., 255-260, Pergamon, New York.

Yang L., Song X., Zhang Y., Han D., Zhang B. and Long D., 2012. Characterizing interactions between surface water and groundwater in the Jialu River basin using major ion chemistry and stable isotopes. Hydrology and Earth System Sciences, 16: 4265–4277, DOI: 10.5194/hess-16-4265-2012.

Yuko A., Uchida T. and Ohte N., 2002. Residence times and flow paths of water in steep unchannelled catchments, Tanakami, Japan. Journal of Hydrology, 261: 173–192, DOI: 10.1016/S0022-1694(02)00005-7.

Zhang B., Tang J.L., Gao Ch. and Zepp H., 2011. Subsurface lateral flow from hillslope and its contribution to nitrate loading in streams through an agricultural catchment during subtropical rainstorm events. Hydrology and Earth System Sciences, 15: 3153–3170, DOI:10.5194/hess-15-3153-2011.

APPENDIX

		NTP_{Tstart}										
		soil moisture (SM)				groundwater (GW)						
Event	Date	SM 1	SM 2	SM 3	SM 4	GW1	GW2	GW3	GW4	GW5	GW6	Wetness conditions
1	23/09/2015	580	610	2250	780	2630		625	990			Dry
2	04/10/2015	165	175	265	175	340	295	180	385	205	180	Wet
3	12/10/2015	4850	4860	4880	4860	4895	4930	4860	5060	4880	4865	Wet
4	28/10/2015	605	695	705	695	725	1165	700	770	650	715	Wet
5	14/06/2016	105	115	325	145	360	210	110	380	215	355	Wet
6	26/06/2016	115	135	665	255	475	310	140	400			Dry
7	13/07/2016	35	35	315	25	375		40	315		40	Dry
8	05/08/2016	95	135	85	85	105	105	105	295	105	105	Dry
9	05/08/2016	155	205	465	195		760	205	475	430	175	Dry
10	09/08/2016					655	640	610	710	630	655	Wet
11	17/08/2016	45	45	195	35	405	240	40	330	70	110	Dry
12	20/08/2016	200	230	750	290	1605	995	230	630	815	1115	Dry
13	15/09/2016	55	55		65		865	115	840			Dry
14	16/09/2016	135	150	205	145		200	145	370	160	185	Dry
15	14/10/2016	970	980	980	980	1010	995	985	1075	985	975	Wet

Table 8: Time lag between the time of the start of the rainfall input and the time of peak soil moisture at four locations (SM 1-4) and groundwater at six locations (GW1-GW6). Data are shown for 15 rainfall events between September 2015 and October 2016. Time to peak is when the 90% of the total rise is reached. Grey font refers to events in the wet season, white font refers to events in the dry season.

		NTP_{Qpeak}										
		soil moisture				groundwater						
Event	Date	SM 1	SM 2	SM 3	SM 4	GW1	GW2	GW3	GW4	GW5	GW6	Wetness conditions
1	23/09/2015	-20	10	1650	180	2030		25	390			Dry
2	04/10/2015	-5	5	95	5	170	125	10	215	35	10	Wet
3	12/10/2015	-125	-115	-95	-115	-80	-45	-115	85	-95	-110	Wet
4	28/10/2015	-95	-5	5	-5	25	465	0	70	-50	15	Wet
5	14/06/2016	5	15	225	45	260	110	10	280	115	255	Wet
6	26/06/2016	85	105	635	225	445	280	110	370			Dry
7	13/07/2016	15	15	295	5	355		20	295		20	Dry
8	05/08/2016	10	50	0	0	20	20	20	210	20	20	Dry
9	05/08/2016	-35	15	275	5		570	15	285	240	-15	Dry
10	09/08/2016					45	30	0	100	20	45	Wet
11	17/08/2016	20	20	170	10	380	215	15	305	45	85	Dry
12	20/08/2016	140	170	690	230	1545	935	170	570	755	1055	Dry
13	15/09/2016	5	5		15		815	65	790			Dry
14	16/09/2016	-5	10	65	5		60	5	230	20	45	Dry
15	14/10/2016	-70	-60	-60	-60	-30	-45	-55	35	-55	-65	Wet

Table 9: Time lag between the time of peak soil moisture at four locations (SM 1-4) and groundwater at six locations (GW1-GW6) and the time of peak streamflow. Data are shown for 15 rainfall events between September 2015 and October 2016. Time to peak is when the 90% of the total rise is reached. Pre-event is the time of the beginning of the rainfall input. All occasions where soil moisture or groundwater peaked before streamflow are highlighted in grey.

		STW	GW1	GW2	GW3	GW4	GW5	GW6	SOWR	SOWR3	SOW-LH10	SOW-LH30	SOW-UH30	RAIN
Cl (ppm)	N	273	37	12	34	36	11	10	32	13	6	6	4	57
	Mean	0,6	0,5	0,5	0,6	0,6	1,2	0,9	0,5	1,4	0,8	1,5	1,3	0,4
	Std.dev.	0,4	0,1	0,3	0,3	0,2	0,3	0,3	0,4	0,9	0,5	1,0	0,6	0,5
	Min	0,2	0,4	0,3	0,4	0,5	0,6	0,5	0,2	0,2	0,3	0,4	0,7	0,1
	Max	4,4	0,8	1,5	2,0	1,0	1,6	1,6	2,3	3,3	1,7	2,9	1,8	2,3
NO_3 (ppm)	N	272	36	12	33	35	11	10	29	13	5	6	3	55
	Mean	5,3	1,8	1,7	3,1	1,9	2,6	1,1	1,0	3,6	16,1	9,0	7,3	1,2
	Std.dev.	3,2	0,9	1,1	3,0	1,9	5,0	0,6	1,6	7,1	15,6	11,8	6,1	1,0
	Min	0,1	0,2	0,1	0,5	0,5	0,2	0,3	0,1	0,1	0,4	1,2	0,6	0,1
	Max	14,4	3,5	3,7	17,2	10,4	17,6	2,3	8,9	26,9	35,2	32,2	12,4	5,3
SO_4 (ppm)	N	277	36	12	33	35	11	10	29	13	5	6	3	55
	Mean	2,7	3,1	1,8	3,1	2,1	4,7	4,3	2,5	0,7	3,3	2,9	2,4	0,5
	Std.dev.	0,7	0,4	1,0	1,1	0,5	3,3	2,1	0,8	2,4	2,2	1,6	0,9	0,8
	Min	0,4	1,9	0,8	1,4	1,1	~0	1,8	1,1	~0	1,3	0,4	1,2	~0
	Max	5,3	3,9	4,5	5,7	3,2	9,1	7,9	5,6	5,7	7,7	5,0	3,3	3,5
Na (ppm)	N	279	37	11	34	36	9	10	31	10	6	3	3	59
	Mean	4,5	6,0	2,4	3,8	2,0	5,7	5,0	4,7	3,1	1,5	1,6	1,3	0,2
	Std.dev.	1,1	0,5	0,4	1,7	0,2	6,7	1,7	2,0	1,5	0,8	0,6	0,5	0,3
	Min	0,7	3,9	1,7	1,2	1,7	2,7	2,6	0,5	0,6	0,6	0,9	0,9	~0
	Max	6,4	6,7	3,1	6,2	2,4	23,6	7,1	8,4	5,7	3,0	2,0	1,9	1,4
Mg (ppm)	N	279	37	11	34	36	9	10	31	10	6	3	3	57
	Mean	10,9	16,6	6,8	10,6	22,2	6,1	3,3	8,8	24,3	3,4	4,1	3,4	0,6
	Std.dev.	3,1	1,3	2,4	5,2	2,9	4,3	1,1	2,0	12,9	2,4	3,2	1,5	0,9
	Min	1,8	11,7	2,4	2,2	16,1	2,9	1,9	0,3	3,8	0,6	1,2	2,5	~0
	Max	17,8	19,7	9,8	17,5	27,7	17,1	5,4	12,0	44,3	7,3	7,5	5,1	6,6
Ca (ppm)	N	277	37	11	34	36	9	10	31	10	6	3	3	59
	Mean	26,0	37,0	19,2	25,3	43,7	18,7	11,4	19,1	50,3	8,4	8,5	6,3	2,1
	Std.dev.	6,4	3,9	6,9	12,2	6,9	9,6	5,4	4,1	27,6	3,3	5,6	4,3	2,1
	Min	3,7	24,8	9,6	5,0	27,1	9,6	5,5	4,7	7,4	2,3	3,3	3,2	~0
	Max	41,0	43,5	30,8	43,7	59,4	37,6	23,0	29,4	92,9	11,3	14,5	11,2	14,7
EC (µS/cm)	N	280	37	11	34	36	9	10	31	10	5	2	2	59
	Mean	202,6	283,1	117,6	184,8	299,7	107,6	68,1	164,5	392,6	60,8	53,9	36,6	12,2
	Std.dev.	49,7	26,1	33,9	87,0	54,2	19,3	22,9	37,1	191,5	28,4	33,7	16,1	8,5
	Min	88,5	167,1	51,5	47,1	33,0	79,0	28,0	67,2	128,0	15,8	30,0	25,2	0,8
	Max	309,0	315,0	152,8	309,0	334,0	134,0	106,3	320,0	694,0	88,5	77,7	48,0	46,0
δ^2H (‰)	N	279	36	11	34	36	11	10	34	12	7	7	5	59
	Mean	-49,7	-55,7	-48,4	-52,1	-57,8	-50,8	-46,9	-49,3	-50,6	-54,6	-44,1	-56,1	-51,3
	Std.dev.	7,0	1,6	5,4	5,4	2,2	4,8	8,2	10,5	10,3	15,8	6,6	8,7	22,2
	Min	-66,7	-58,8	-57,5	-59,9	-63,6	-58,2	-62,9	-61,6	-64,5	-78,8	-52,7	-63,0	-104,2
	Max	-26,7	-53,2	-41,1	-40,0	-53,2	-44,0	-38,8	0,0	-31,3	-40,2	-36,3	-41,4	-12,7
$\delta^{18}O$ (‰)	N	279	37	12	34	36	11	10	34	13	7	7	5	59
	Mean	-8,1	-8,5	-7,1	-8,2	-9,0	-8,1	-7,7	-7,9	-7,3	-8,0	-6,8	-8,0	-8,3
	Std.dev.	0,8	1,5	2,3	0,6	0,4	0,6	0,9	1,5	2,4	1,8	0,7	0,9	2,8
	Min	-9,7	-9,5	-8,8	-9,5	-10,4	-9,0	-9,2	-9,6	-8,8	-10,9	-7,7	-9,3	-14,1
	Max	-5,5	0,0	0,0	-6,9	-8,2	-7,3	-6,6	0,0	0,0	-6,2	-5,9	-6,7	-2,3

Table 10: Number of the samples (N), mean (Mean) and standard deviation (Std. dev.), minimum value (Min), maximum value (Max) of stream water (STW) groundwater at different locations (GW1 to GW5), soil water in the riparian zone (SOWR and SOWR3), soil water in the hillslope (SOW-LH10, SOW-LH30, SOW-UH30) of the major ions, EC, δ2H and δ18O of the samples collected during the sampled events (pre-event, during the event and post event) from September 2015 to October 2016.

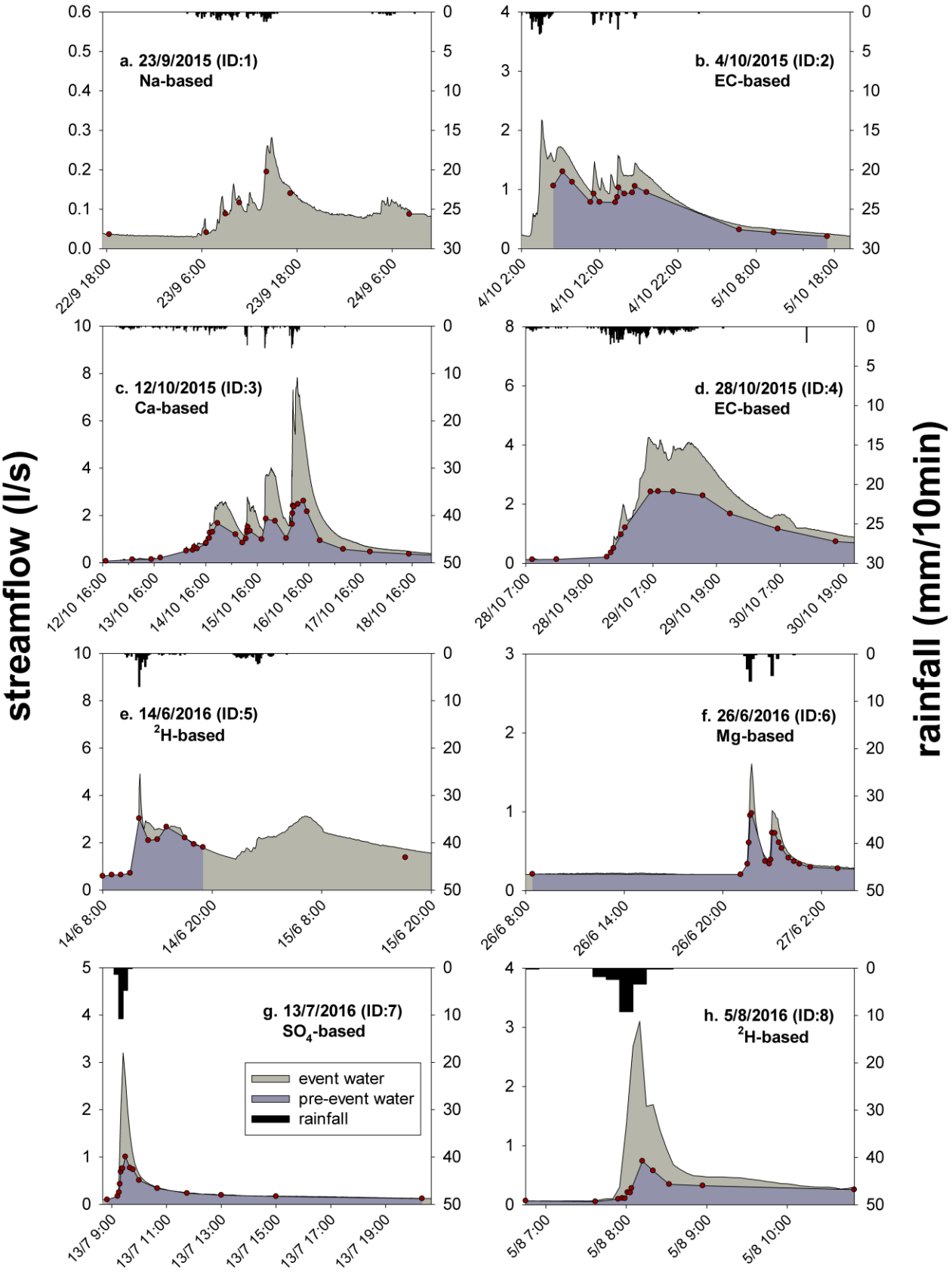

Figure 59: Results from two-component hydrograph separation computed using δ^2H, EC and major ions for events sampled from September 2015 to August 2016 (from event n.1 to n.8). Dark dots indicate the sampling times. Note the difference in the scale of the y-axis for the eight events. The tracer used to represent the result from two-component hydrograph separation for each event was randomly selected among the tracers showing significant results from two-component hydrograph separation for that event.

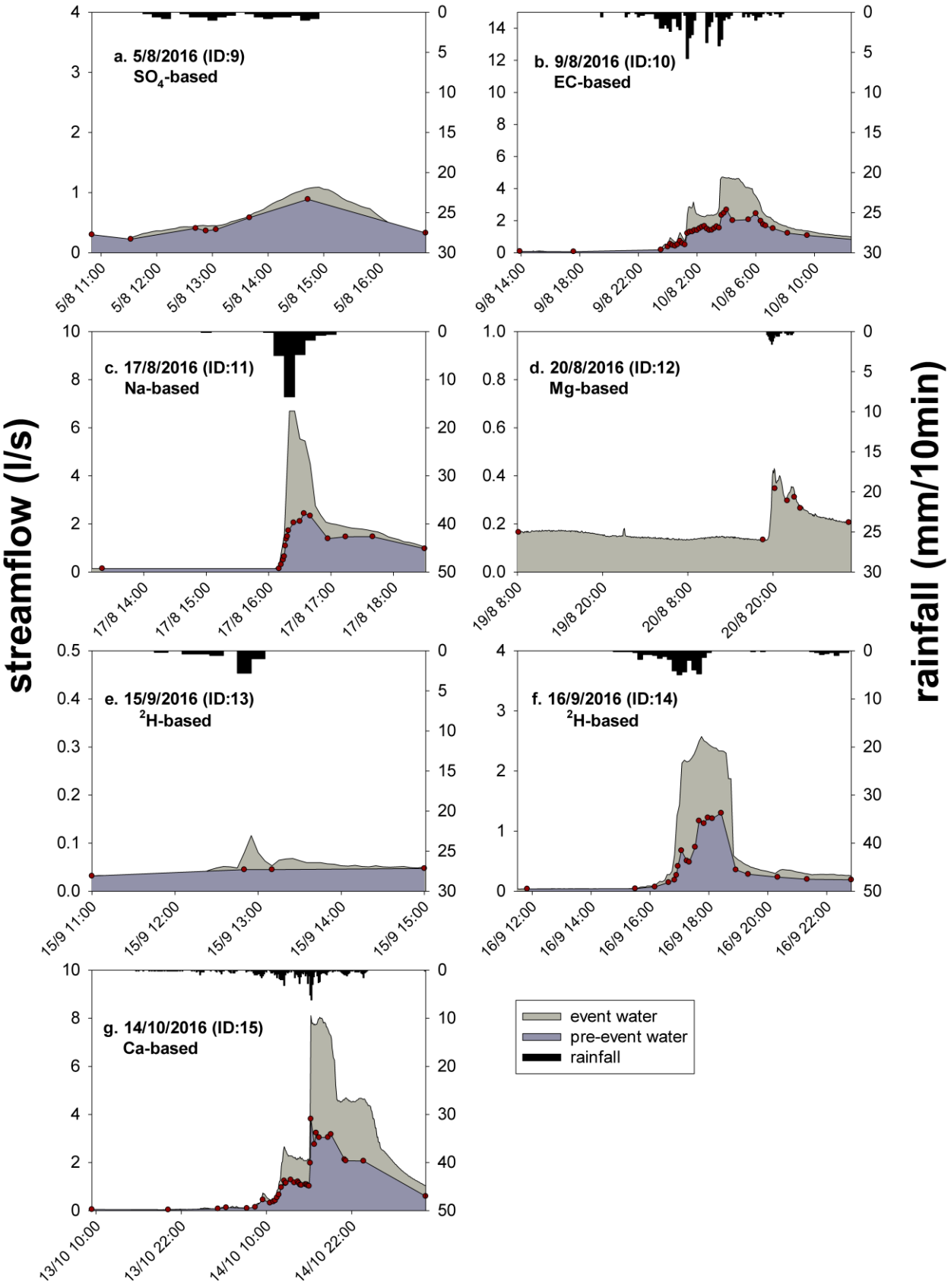

Figure 60: Results from two-component hydrograph separation computed using δ^2H, EC and major ions for events sampled from August 2016 to October 2016 (from event n.9 to n.15). Dark dots indicate the sampling times. Note the difference in the scale of the y-axis for the seven events. The tracer used to represent the result from two-component hydrograph separation for each event was randomly selected among the tracers showing significant results from two-component hydrograph separation.

		δ^2H (‰)	EC (µS/cm)	Cl (ppm)	SO_4 (ppm)	Na (ppm)	Mg (ppm)	Ca (ppm)
Event 1	avg %	18,6	12,7	15,2	11,3	13,4	18,6	11,5
22/09/2015	rising limb only	19,5	15,8	18,4	16,4	15,5	22,2	14,1
	falling limb only	16,7	6,3	8,4	0,6	8,9	11,2	6,2
	max	25,8	24,5	23,3	26,9	22,7	31,9	23,9
	near streamflow peak	25,8	24,5	23,3	26,9	22,7	31,9	23,9
Event 2	avg %		16,7		9,9	6,3	20,0	17,0
03/10/2015	rising limb only		17,3		11,5	7,7	22,0	13,9
	falling limb only		16,6		9,6	6,0	19,6	17,7
	max		25,6		20,1	13,0	29,4	26,4
	near streamflow peak		15,0		6,9	3,2	22,6	7,5
Event 3	avg %		43,4			36,3	50,7	47,3
12/10/2015	rising limb only		41,3			32,1	47,5	44,3
	falling limb only		47,6			44,7	57,1	53,1
	max		62,0			60,0	68,1	66,6
	near streamflow peak		62,0			60,0	66,8	66,6
Event 4	avg %		34,9		28,2	18,2	40,6	32,9
27/10/2015	rising limb only		35,3		29,1	18,6	40,5	31,9
	falling limb only		34,7		27,7	18,1	40,7	33,4
	max		42,1		33,3	23,2	46,1	37,4
	near streamflow peak		42,1		30,0	20,4	45,7	37,0
ID: 5	avg %	10,0	16,2	21,5	19,8	17,1	18,0	21,9
14/06/2016	rising limb only	19,5	26,6	24,6	28,6	26,2	27,9	30,0
	falling limb only	6,8	12,7	20,2	16,9	14,1	14,7	19,2
	max	30,1	38,4	49,4	40,5	37,6	39,6	40,6
	near streamflow peak	30,1	38,4	38,0	40,5	37,6	39,6	40,6
Event 6	avg %	30,7	24,6		23,5	23,0	23,1	18,4
26/06/2016	rising limb only	46,2	36,0		35,0	35,9	30,2	21,9
	falling limb only	20,9	17,3		16,2	14,8	18,6	16,2
	max	52,3	43,2		47,1	41,4	39,1	31,2
	near streamflow peak	48,5	43,2		47,1	41,4	39,1	31,2
Event 7	avg %	61,6	44,2		57,4	42,1	41,2	27,1
13/07/2016	rising limb only	72,9	50,6		68,6	51,7	44,3	24,7
	falling limb only	46,0	35,4		41,8	28,7	37,0	30,6
	max	76,4	58,2		74,5	60,9	52,0	41,2
	near streamflow peak	72,2	58,2		74,5	60,9	52,0	34,5
Event 8	avg %	76,7	52,6		45,8	47,9	54,7	46,8
05/08/2016	rising limb only	83,4	57,5		50,5	54,3	57,8	49,0
	falling limb only	54,7	36,6		30,2	26,9	44,8	39,9
	max	90,5	63,2		62,0	61,8	64,3	56,7
	near streamflow peak	70,7	56,5		43,2	46,6	62,7	56,7
Event 9	avg %		10,8		11,9	6,8	11,7	12,5
05/08/2016	rising limb only		11,8		12,8	7,5	12,2	13,3
	falling limb only		0,8		3,6	0,1	7,1	5,0
	max		16,5		18,9	11,2	18,8	18,3
	near streamflow peak		16,5		16,9	10,7	18,8	18,3

Event 10 09/08/2016	avg %	57,5	39,9			35,3	52,3	48,5
	rising limb only	55,7	41,7			36,6	52,1	48,5
	falling limb only	59,8	37,7			33,6	52,5	48,6
	max	80,3	56,1			89,5	96,2	97,4
	near streamflow peak	79,4	50,3			39,4	59,6	56,6
Event 11 17/08/2016	avg %		61,8		61,7	58,3	58,5	47,0
	rising limb only		66,1		69,7	66,5	59,2	43,8
	falling limb only		57,9		56,0	50,7	57,8	50,0
	max		73,0		77,0	73,7	66,3	58,7
	near streamflow peak		70,8		77,0	73,7	62,8	42,9
ID: 12 19/08/2016	avg %	10,8	7,4		14,9	2,1	9,0	5,8
	rising limb only	15,3	13,2		26,2	6,5	13,6	9,7
	falling limb only	8,5	4,6		9,4	0	6,8	3,9
	max	21,5	17,7		30,3	10,7	19,1	14,1
	near streamflow peak	21,5	17,7		30,3	10,7	19,1	14,1
Event 13 15/09/2016	avg %	25,4	18,7			13,6	14,5	11,8
	rising limb only	43,9	37,5			25,9	26,3	23,2
	falling limb only	11,1	4,2			4,0	5,3	3,0
	max	43,9	37,5			25,9	26,3	23,2
	near streamflow peak	43,9	37,5			25,9	26,3	23,2
Event 14 16/09/2016	avg %	58,6	41,5		41,7	38,5	47,3	40,1
	rising limb only	65,9	47,5		51,3	47,2	53,1	43,4
	falling limb only	44,8	30,2		23,4	22,1	36,3	33,8
	max	77,6	55,5		72,3	60,4	56,6	50,1
	near streamflow peak	54,9	46,0		47,9	41,7	54,1	48,5
Event 15 13/10/2016	avg %		48,9		27,8	39,3	53,7	48,6
	rising limb only		46,6		25,4	36,7	48,9	43,0
	falling limb only		51,1		30,0	41,6	58,1	53,8
	max		59,2		45,5	55,1	64,5	62,5
	near streamflow peak		59,2		45,	54,3	64,59	62,5

Table 11: The average new water contribution during the entire event, the rising limb, and the falling limb; the maximum new water contribution; and the new water contribution close the streamflow peak (all in %) for each event sampled between September 2015 and October 2016. The results are shown for the different tracers: δ2H, EC, Cl, SO4, Na, Mg, Ca.

		δ^2H-EC (%)	δ^2H-Cl (%)	δ^2H-SO_4 (%)	δ^2H-Na (%)	δ^2H-Mg (%)	δ^2H-Ca (%)	Time since last event (minutes)	ASI (mm)
event 1 **22/09/2015**	avg %	5,9	3,4	7,3	5,2	-0,1	7,0	13240	59,7
	rising limb only	3,7	1,0	3,1	4,0	-2,7	5,4		
	falling limb only	10,4	8,3	16,1	7,7	5,5	10,5		
	max	1,3	2,5	-1,1	3,1	-6,1	1,9		
	near discharge peak	1,3	2,5	-1,1	3,1	-6,1	1,9		
event 2 **03/10/2015**	avg %							15655	70,4
	rising limb only								
	falling limb only								
	max								
	near discharge peak								
event 3 **12/10/2015**	avg %							12835	65,8
	rising limb only								
	falling limb only								
	max								
	near discharge peak								
event 4 **27/10/2015**	avg %							22735	68,5
	rising limb only								
	falling limb only								
	max								
	near discharge peak								
event 5 **14/06/2016**	avg %	-6,2	-11,5	-9,8	-7,1	-8,1	-11,9	6905	67,7
	rising limb only	-7,1	-5,1	-9,1	-6,8	-8,5	-10,5		
	falling limb only	-5,9	-13,5	-10,1	-7,3	-7,9	-12,4		
	max	-8,3	-19,3	-10,4	-7,5	-9,6	-10,5		
	near discharge peak	-8,3	-7,9	-10,4	-7,5	-9,6	-10,5		
event 6 **26/06/2016**	avg %	6,2		7,2	7,7	7,6	12,3	17930	59,4
	rising limb only	10,2		11,2	10,3	16,0	24,3		
	falling limb only	3,6		4,7	6,1	2,3	4,7		
	max	9,1		5,2	10,8	13,2	21,0		
	near discharge peak	5,3		1,4	7,0	9,4	17,2		
event 7 **13/07/2016**	avg %	17,4		4,3	19,6	20,4	34,5	23750	52,3
	rising limb only	22,3		4,3	21,2	28,6	48,2		
	falling limb only	10,7		4,2	17,3	9,1	15,5		
	max	18,2		2,0	15,5	24,4	35,2		
	near discharge peak	14,0		-2,2	11,3	20,2	37,8		
event 8 **05/08/2016**	avg %	24,1		30,9	28,8	21,9	29,9	32980	55,4
	rising limb only	25,9		32,9	29,1	25,6	34,4		

	falling limb only	18,1		24,5	27,8	9,9	14,9		
	max	27,4		28,5	28,7	26,3	33,8		
	near discharge peak	14,2		27,5	24,1	8,1	14,0		
event 9 **05/08/2016**	avg %							300	65,1
	rising limb only								
	falling limb only								
	max								
	near discharge peak								
event 10 **09/08/2016**	avg %	17,6		10,1	22,2	5,2	9,0	6110	55,5
	rising limb only	13,9		4,9	19,1	3,6	7,2		
	falling limb only	22,1		16,9	26,2	7,3	11,2		
	max	24,2		-32,3	-9,2	-15,9	-17,1		
	near discharge peak	29,1		27,6	40,0	19,8	22,8		
event 11 **17/08/2016**	avg %							11420	57,9
	rising limb only								
	falling limb only								
	max								
	near discharge peak								
event 12 **19/08/2016**	avg %	3,3		-4,2	8,7	1,7	4,9	4515	62,0
	rising limb only	2,1		-10,9	8,8	1,7	5,6		
	falling limb only	3,9		-0,9	8,5	1,7	4,6		
	max	3,8		-8,8	10,9	2,4	7,5		
	near discharge peak	3,8		-8,8	10,9	2,4	7,5		
event 13 **15/09/2016**	avg %	6,7			11,8	10,9	13,6	37015	44,1
	rising limb only	6,5			18,0	17,7	20,8		
	falling limb only	6,9			7,1	5,7	8,1		
	max	6,5			18,0	17,7	20,8		
	near discharge peak	6,5			18,0	17,7	20,8		
event 14 **16/09/2016**	avg %	17,0		16,9	20,1	11,3	18,5	1640	46,1
	rising limb only	18,3		14,5	18,7	12,8	22,5		
	falling limb only	14,5		21,4	22,7	8,5	11,0		
	max	22,0		5,3	17,2	21,0	27,5		
	near discharge peak	8,9		7,0	13,2	0,8	6,5		
event 15 **13/10/2016**	avg %							39405	54,1
	rising limb only								
	falling limb only								
	max								
	near discharge peak								

Table 12: The difference in the average percentage of new water contribution calculated using δ^2H and EC and major ions (Cl, SO_4, Na, Mg, Ca) for the entire event, the rising limb only, the falling limb only; the maximum new water contribution; the new water contribution near the streamflow peak. Negative differences indicating higher new water contribution calculated using EC and major ions than δ^2H are highlighted in grey.